NOTE TO USERS

Page(s) not included in the original manuscript and are unavailable from the author or university. The manuscript was microfilmed as received.

35

This reproduction is the best copy available.

UMI

University of Alberta

PARTIALLY SCALED SAGD-TYPE EXPERIMENTS OF HEAVY OIL RESERVOIRS IN A LOW-PRESSURE PHYSICAL MODEL

BY

HASHEM A. ABDELMOTTLEB

A THESIS
SUBMITTED TO THE FACULTY OF GRADUATE STUDIES AND RESEARCH IN
PARATIAL FULFILLMENT OF THE REQUIREMENT FOR THE DEGREE OF

MASTER OF SCIENCE

IN

PETROLEUM ENGINEERING

DEPARTMENT OF CIVIL AND ENVIORMENTAL ENGINEERING

EDMONTON, ALBERTA
Spring, 2000

National Library of Canada
Acquisitions and Bibliographic Services
395 Wellington Street
Ottawa ON K1A 0N4
Canada

Bibliothèque nationale du Canada
Acquisitions et services bibliographiques
395, rue Wellington
Ottawa ON K1A 0N4
Canada

Your file Votre référence

Our file Notre référence

The author has granted a non-exclusive licence allowing the National Library of Canada to reproduce, loan, distribute or sell copies of this thesis in microform, paper or electronic formats.

L'auteur a accordé une licence non exclusive permettant à la Bibliothèque nationale du Canada de reproduire, prêter, distribuer ou vendre des copies de cette thèse sous la forme de microfiche/film, de reproduction sur papier ou sur format électronique.

The author retains ownership of the copyright in this thesis. Neither the thesis nor substantial extracts from it may be printed or otherwise reproduced without the author's permission.

L'auteur conserve la propriété du droit d'auteur qui protège cette thèse. Ni la thèse ni des extraits substantiels de celle-ci ne doivent être imprimés ou autrement reproduits sans son autorisation.

0-612-60086-6

Canada

University of Alberta
Library Release Form

Name of Author	Hashem Abosief Abdelmottleb
Title of Thesis	Partially Scaled SAGD-Type Experiments of Heavy Oil Reservoirs in a Low-Pressure Physical Model
Degree:	Master of Science
Year this Degree Granted:	2000

Permission is hereby granted to the University of Alberta Library to reproduce single copies of this thesis and to lend or sell such copies for private, scholarly, or scientific research purposes only.

The author reserves all other publication and other rights in association with the copyright in the thesis, and except as hereinbefore provided, neither the thesis nor any substantial portion thereof may be printed or otherwise reproduced in any material form whatever without the authors written permission.

(SIGNED) 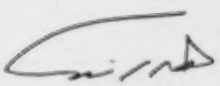

PERMANENT ADDRESS:

Engineering Planning. Dept.
Zueitina Oil Company
P.O. BOX 2134
Tripoli-Libya

DATED: Dec. 8, 1999

UNIVERSITY OF ALBERTA

FACULTY OF GRADUATE STUDIES AND RESEARCH

The undersigned certify that they have read, and recommend to the Faculty of Graduate Studies and Research for acceptance, a thesis entitled PARTIALLY SCALED SAGD-TYPE EXPERIMENTS OF HEAVY OIL RESERVOIRS IN A LOW-PRESSURE PHYSICAL MODEL submitted by HASHEM A. ABDELMOTTLEB in partial fulfillment of the requirements for the degree of MASTER OF SCIENCE in PETROLEUM ENGINEERING.

Professor Q. Doan (Supevisor)

Professor S.M. Farouq Ali (Co-Supevisor)

Professor B. Lepski (Committee Chair)

Professor Z. Xu (External Examiner)

Date: Oct. 22, 99

Abstract

In this study, a visual model and a subatmospheric scaled physical model were used to perform the various experiments of the Steam-Assisted Gravity Drainage (SAGD) process. The visual model experiments were conducted to visualize the growth of the steam chamber and the oil drainage process. Using the scaled physical model, SAGD experiments were conducted to test the performance of three different well configurations. Also, experiments in which hot water was injected were performed to determine the influence of intermittent steam injection on oil recovery.

Theoretical analyses including heat balance calculations, and steam zone volumes were performed on one of the base case experiments.

The well configuration in which the injector is in the upper position and the producer is in the lower position gave the highest oil recovery and highest cumulative oil-steam ratio.

The breakthrough time was a function of the volume of the reservoir lying above the horizontal producer; the larger the volume, the later the breakthrough time.

The vertical position of the horizontal injector has an effect on the recovery performance when implementing a hot waterflood either before or after the SAGD process.

To My Parents for Their Boundless Support and Encouragement
To My Wife for Being Understanding Most of the Time

The heat balance calculations revealed that the heat lost to the overburden and the underburden was much less than had been thought, and represents only 20% of the total heat injected.

Acknowledgment

The author wishes to express his sincere gratitude to Dr. S.M. Farouq Ali and Dr. Quang T. Doan for their generous guidance, and support throughout the course of this study.

The author wishes to extend special thanks to Mr. Nasser Albartamani for his support and encouragement during the whole period of his M.Sc. studies. The voluntary help from Mr. John Czuroski is highly appreciated. The valuable instructions on how to operate the apparatus given by Mr. Bob Smith were very important in the progressing of this project.

Finally, special thanks to the Canadian staff and the Libyan representatives who are responsible for the Libyan Educational Program at the Canadian Bureau for International Education for their support and services throughout the author's M.Sc. studies.

Table of Contents

Chapter		Page
1.	Introduction	1
2.	Statement of the Problem	2
	2.1 Experimental Objective	2
	2.1 Theoretical Objectives	2
3.	Literature Review	3
	3.1 Overview	3
	3.2 Thermal Drive Processes	3
	3.3 The Application of Horizontal Wells to Heavy Oil Recovery	3
	3.4 Steam-Assisted Gravity Drainage (SAGD)	4
	3.4.1 Theoretical Studies of SAGD Process	4
	3.4.2 Experimental Studies of SAGD Process	7
	3.4.3 Numerical Studies of the SAGD Process	9
	3.4.4 Field Pilots of the SAGD Process	10
	3.5 Predictive Models for steam Zone Volumes	11
	3.5.1 Marx-Langenheim Model	11
	3.5.2 Neuman's Model	12
4.	Scaling Parameters and Calculations	13
	4.1 Development of Scaling Parameters for the Low Pressure Model	13
	4.1.1 Uscaled Parameters	13
	4.1.2 Scaling Procedure	13
	4.2 Designing the Low Pressure Model of the Kern "A" Reservoir	17
	4.2.1 Length Scaling	17
	4.2.2 Model Production Pressure Scaling	19
	4.2.3 Model Temperature Scaling	19
	4.2.4 Calculation of the Required steam Quality	20
	4.2.5 Scaling of the Model Oil Viscosity	21
	4.2.6 Calculation of the time Scale Factor	21
	4.2.7 Calculation of the Permeability of the Model	23
	4.2.8 Calculation of the Model Injection and production Rate	23
5.	Experimental Apparatus and procedure	25
	5.1 Experimental Apparatus	25
	5.1.1 Scaled Physical Model	25
	5.1.2 Visual Model	25
	5.1.3 Porous Media	27
	5.1.4 Model Fluids	27

5.1.5 Model Cart, Rail System, and Cold Storage Compartment 27
5.1.6 Production System 27
5.1.7 Injection System 30
5.1.8 Data Acquisition System 30
5.2 Preparation of the Scaled physical Model for an Experiment 30
5.2.1 Packing Procedure 30
5.2.2 Saturation Process 31
5.2.3 Packing and Saturating the Visual Model 31
5.3 Conducting the Experiments 31
5.4 Data Analysis 32
6. Experimental Results and Discussion 34
6.1 Presentation of Results 34
6.2 Steam Chamber Volumes 37
6.3 Heat Balance 37
6.4 Base Case Experiments 39
6.4.1 A Base case Experiment 39
6.4.2 Comparison of the Base Case Experiments 42
6.5 A Hot Waterflood Prior to the SAGD Process 49
6.6 SAGD Followed by a Hot Waterflood 54
6.7 The Visual Model Experiments 67
6.8 The Development of the Steam Chamber 68
6.9 The Dominant Driving Force in the Reservoir 68
6.10 Scaling Up of the Experimental Results to the Prototype 75
7. Conclusions 78
8. Recommendations 79
References 80
Appendix A 84
Appendix B 89

List of Tables

Table		Page
Table 4.1	Scaling Parameters for steam Processes	14
Table 4.2	Scaling Parameters for the prototype and Model reservoir	18
Table 4.3	Prototype and Model Scaling Values	22
Table 5.1	Sieve Analysis of the Glass Beads Used in the Experiments	28
Table 6.1	Summary of the Experiments Conducted	36
Table 6.2	Experimental Results of Run 115	41
Table 6.3	Experimental Results of Run 107	46
Table 6.4	Experimental Results of Run 108	48
Table 6.5	Experimental Results of Run 110	52
Table 6.6	Experimental Results of Run 116	56
Table 6.7	Experimental Results of Run 114	61
Table 6.8	Experimental Results of Run 117	64
Table A1	Steam Zone Volumes Calculated using Marx-Langenhiem Model, Neuman's Model, and Experimental Data	87
Table B1	Heat Lost Through the overburden after the Injection of 1.00 PV of Steam, Run 115	91
Table B2	Heat Lost to the Underburden after the Injection of 1.00 PV of Steam, Run 115	92
Table B3	Heat Produced after the Injection of 1.00 PV of Steam, Run 115	94
Table B4	Heat Accumulated in the Model after the Injection of 1.00 PV of Steam, Run 115	96

List of Figures

Figure		Page
Figure 5.1	Schematic Diagram of the Apparatus	26
Figure 5.2	The Prototype Oil and the Model Oil Viscosity-Temperature Relationship	29
Figure 6.1	Overview of the Experiments Reported	35
Figure 6.2	Comparison of the Experimental and the Theoretical Volumes of the Steam Zone	38
Figure 6.3	Production History of a Base Case Experiment (Run 115); SAGD, Injector/Producer in Middle/Lower Position	40
Figure 6.4	Pressure/Temperature of the Injector and the Producer for a Typical Experiment (Run 115); SAGD, Injector/Producer in the Middle/Lower Position	43
Figure 6.5	The Cumulative Oil Recovery vs. Pore Volume Injected for the Base case Runs (Run 107, Run 108, and Run 115)	44
Figure 6.6	Production History of Run 107, Base Case Run, Injector/Producer in Upper/Middle Position	45
Figure 6.7	Production History of Run 108, Base Case Run, Injector/Producer in Upper/Lower Position	47
Figure 6.8	Cumulative Oil-Steam Ratio vs. Cumulative Pore Volume (CWE) Injected for the Base Case Runs (Run 107, Run 108, and Run 115)	50
Figure 6.9	Production History of Run 110, Hot Waterflood followed by SAGD, Injector/Producer in Upper/Lower position	51
Figure 6.10	Cumulative Oil Recovery vs. Cumulative Pore Volume (CWE) Injected for Run 110 and It's Corresponding Base Case (Run 108)	53
Figure 6.11	Production History of Run 116; Hot Waterflood followed by	

SAGD, Injector/Producer in Middle/Lower Position 55

Figure 6.12 Cumulative Oil Recovery vs. Cumulative Pore Volume (CWE) Injected for Run 110 and Run 116 57

Figure 6.13 Cumulative Oil Recovery vs. Cumulative Pore Volume (CWE) Injected for Run 116 and It's Corresponding Base Case (Run 115) 58

Figure 6.14 Production History of Run 114, SAGD followed by a Hot Waterflood, Injector/Producer in Upper/Lower Position 60

Figure 6.15 Cumulative Oil Recovery vs. Cumulative Pore Volume (CWE) Injected for Run 114 and Its Corresponding Base Case (Run 108) 62

Figure 6.16 Production History of Run 117; SAGD followed by a Hot Waterfllood, Injector/Producer in Middle/Lower Position 63

Figure 6.17 Cumulative Oil Recovery vs. Cumulative Pore Volume (CWE) Injected for Run 117 and It's Corresponding Base Case (Run 115) 65

Figure 6.18 Cumulative Oil Recovery vs. Cumulative Pore Volume (CWE) Injected for Runs 117 and 114. 66

Figure 6.19A Front View, of the Temperature Distribution of the First Half of the Model after the Injection of: a) 0.25, b) 0.50, c) 1.00, and d) 1.50 PV CWE of Steam, for Run 107: SAGD, Injector/Producer in Upper/Middle Position 69

Figure 6.19B Front View, of the Temperature Distribution of the Second Half of the Model after the Injection of: a) 0.25, b) 0.50, c) 1.00, and d) 1.50 PV CWE of Steam, for Run 107: SAGD, Injector/Producer in Upper/Middle Position 70

Figure 6.20A Front View, of the Temperature Distribution of the First Half of the Model after the Injection of: a) 0.25, b) 0.50, c) 1.00, and d) 1.50 PV CWE of Steam, for Run 108: SAGD, Injector/Producer in Upper/Lower Position 71

Figure 6.20B Front View, of the Temperature Distribution of the Second Half of the Model after the Injection of: a) 0.25, b) 0.50, c) 1.00, and d) 1.50 PV CWE of Steam, for Run 108: SAGD, Injector/Producer in Upper/Lower Position 72

Figure 6.21A Front View, of the Temperature Distribution of the First Half the Model after the Injection of: a) 0.25, b) 0.50, c) 1.00, and 1.50 PV CWE of Steam, for Run 115: SAGD, Injector/Producer in Middle/Lower Position 73

Figure 6.21B Front View, of the Temperature Distribution of the Second Half the Model after the Injection of: a) 0.25, b) 0.50, c) 1.00, and 1.50 PV CWE of Steam, for Run 115: SAGD, Injector/Producer in Middle/Lower Position 74

Figure 6.22 Pressure Gradient and Gravity Gradient vs. Cumulative Pore Volume (CWE) Injected; Run 115, Base Case Experiment. 76

Figure 6.23 Scaling-Up of the Experimental Oil Rate to the Prototype Reservoir; Run 115, Base Case Experiment. 77

Figure A1 Steam Zone Volumes Calculated Using Marx-Langenheim Model, Neuman's Model, and Experimental Data 88

Nomenclature

C	Specific heat, $[L^2t^{-2}T^{-1}]$
f_b	the amount of the injected heat that has been produced, dimensionless
f_d	the steam quality downhole, dimensionless
f_s	steam quality, dimensionless
g	acceleration due to gravity, $[Lt^{-2}]$
h	enthalpy per unit mass, $[L^2t^{-2}]$
i	steam injection rate $[L^3s^{-1}]$
k	permeability, $[L^2]$
k_h	thermal conductivity, $[MLt^{-3}T^{-1}]$
k_r	relative permeability, dimensionless
L	length, $[L]$
L_v	latent enthalpy per unit mass, $[L^2t^{-2}]$
m	arbitrary variable,
M	volumetric heat capacity, $[ML^{-1}t^{-2}T^{-1}]$
P	pressure, $[ML^{-1}t^{-2}]$
Q	heat, $[kJ]$
$\vec{q}$	conductive heat flux, $[M/t^{-3}]$
S	saturation, mass fraction
T	Temperature, $[T]$
t	time, $[t]$
$\vec{u}$	volumetric flux (Darcy velocity), $[L/t]$
W	mass flow rate,

Greek Symbols

α	thermal diffusivity, $[L^2t^{-1}]$
ΔP	pressure drop, $[ML^{-1}t^{-2}]$
ϕ	porosity, dimensionless
μ	viscosity, $[ML^{-1}t^{-1}]$
ρ	density, $[ML^{-3}]$
∇	del operator

Subscripts

D	dimensionless
Form	formation
inj	injected
j	phase (oil, water or steam)
loss	loss to the cap and base rock
o	oleic phase
ob	overburden
P	prototype
prod	production
R	reference variable used to obtain a dimensionless quantity
res	reservoir
s	steam
w	water (unless otherwise specified)

1. Introduction

For more than two decades (since 1980), the SAGD process has been investigated using theoretical, numerical, and experimental studies. Most of these studies have concentrated on the application of the SAGD process to the oil sand reservoirs. In these reservoirs the bitumen has a very high viscosity (in the range of 100,000 centipoise (cp)) and is immobile at the reservoir conditions. Unlike bitumen, heavy oils have viscosity (in the range of 1000-10,000 cp) and are mobile at the reservoir conditions. Thus a study, which is specifically focused on the application of the SAGD process to the conventional heavy oil reservoirs, needed to be conducted.

Due to the limitation on the grid size, the majority of the numerical studies of SAGD Process were 2-dimensional ones. In addition, most of the experimental investigations on the SAGD process have used 2-Dimensional physical models. In this study a 3-dimensional physical scaled model was used to study the performance of the SAGD process in the conventional heavy oil reservoirs. Using a 3-dimensional model will be helpful in seeing the 3-dimensional phenomena like the variation of the steam quality along the horizontal injector.

Thermal projects reach a stage where the recovered oil would not cover the cost of the injected steam, and as a consequence, these projects will be shut-in. Heat scavenging techniques could recover additional oil and extend the life of the project. Testing the viability of scavenging the available heat after a SAGD process needed to be conducted.

2. Statement of the Problem

The broad aim of this study was to test the performance of the SAGD process in conventional heavy oil reservoirs. In order to understand the performance of the SAGD process, experiments using a 2-dimensional visual model and a 3-dimensional scaled physical model were carried out. Prior to conducting the planned experiments, the following modifications were made to the visual model and the scaled model.

i. Modifying the wells configuration in the visual model into a SAGD configuration.

ii. Placing thermocouples into the visual model, in an attempt to obtain better understanding of steam chamber growth.

iii. Redistributing the thermocouple positions of the scaled physical model in order to make more effective use of temperature distribution in following the growth of the steam chamber.

In this research there were experimental as well as theoretical objectives, as listed in the following:

2.1 Experimental Objectives

1) Testing saturating the model with oil from the updip end to maintain density and gravity saturation front.

2) Conducting a series of base case experiments, which could be used to compare with other experiments.

3) Investigating the performance of various wells configuration in SAGD.

4) Examining the effectiveness of implementing a hot waterflood prior to SAGD process.

5) Testing the effectiveness of having hot waterflood after SAGD process.

2.2 Theoretical Objectives

1) Performing the model heat balance calculations.

2) Confirming the experimental steam chamber volumes by comparing it to those obtained from Marx-Langenhiem frontal model and Neuman's override model.

3. Literature Review

3.1 Overview

Basically, there are two classes of thermal recovery processes: displacement (or drive) processes and stimulation processes. In a drive process, a fluid is injected to displace reservoir fluids to an adjacent well, as in waterflood. In thermal drive processes, heat is injected to reduce oil viscosity, thus enhancing the efficiency of the displacement process. The fluid may carry heat generated at the surface, as in the case of steam and hot water, or the heat may be generated within the reservoir, as with in situ combustion. In thermal stimulation process, only a limited region around a producing well is heated to reduce oil viscosity and to improve near-wellbore permeability. Steam stimulation involves periodic injection of steam into a producing well (Boberg, 1988.)

3.2 Thermal Drive Processes

The simplest of the all thermal drive processes and the closest to a conventional waterflood is the hot water injection. In this process hot water is injected into the reservoir to raise the temperature of the oil, and as a consequence, improving its mobility relative to that for water. (Boberg, 1988.) Implementation of hot water injection to recover heavy oils has been limited. Hot water is not as effective in displacing oil as steam, because steam can lose all the latent heat and does not suffer a drop in its temperature (Farouq Ali, 1976.) The most widely used thermal drive process is the steamflooding. In the flooding process, steam is injected continuously into one or more wells to drive the oil to separate production wells. Another advantage of using steam as the injected fluid rather than hot water is that more energy can be injected into the formation, and high oil recovery can be obtained. Producing reservoirs with very viscous oils usually require the implementation of steam stimulation prior to the steamflooding. This is to create flow communication between the injector and the producer (Butler, 1991.)

Several steamflood projects that originally started with the attention of displacing oil horizontally have ended up with more attention being paid to the importance of the gravity forces in providing drive. It was recognized that displacing the oil downwards in dipping reservoirs by injecting steam into the top of the reservoir results in high production rates. Recoveries of the order of 50% are achievable using steamflooding (Butler, 1991.)

3.3 Application of Horizontal Wells to Heavy Oil Recovery

One of the prospective areas of using horizontal wells lies in the field of heavy oil recovery, particularly thermal recovery using steam (Butler, 1994). The increase in the direct contact between the wellbores and the formation is an advantage of the horizontal over the vertical ones (Hauang et. al., 1986.) In the case of very thin pay zone areas, vertical drilling would be uneconomical due to insufficient wellbore openings for production. Using horizontal wells in certain thin formations with bottom water table

could defer and reduce water coning due to the low-pressure drop area over a long wellbore.

Thermal recovery usually requires close well spacing. Typically projects have a spacing of 1 to 2 hectares (2.5 to 5 acres) per well and in many cases, these are later filled in to improve recovery. In such circumstances, a single horizontal well can replace a row of as many as ten or more conventional wells. Another important advantage of using horizontal wells in thermal recovery is the possibility of obtaining a high recovery with little steam production (Butler, 1994.)

3.4 Steam-Assisted Gravity Drainage (SAGD)

In the SAGD process, two horizontal wells are implemented; these wells are drilled parallel to each other. The injector is in the upper position while the producer is in the lower position, usually as close as possible to the bottom of the reservoir. The purpose of developing the SAGD process was to take advantage of the gravity, already available in the reservoir, in producing the heavy oil or bitumen in a systematic manner avoiding the differential fingering that occurs when viscous oils are pushed with a less viscous fluid. In this process steam is introduced near the bottom of the reservoir and tends to rise, forming a steam chamber above the horizontal injector; inside the steam chamber the steam flows through the sand within the chamber to the interface and condenses. The heat released due to condensation is conducted into the colder oil sand. This heats the oil near the condensation front, lowering its viscosity and making it more mobile; the heated oil and the condensate drain by gravity to the production well, which is positioned parallel to and below the injection well. As the oil is removed from the reservoir through the producer, the steam chamber grows upwards and sideways. The horizontal injector can be replaced by a number of vertical injectors. In cases where the reservoir oil is mobile, the injector can be placed higher in the reservoir in order to take advantage of the higher drawdown (Butler, 1991.)

3.4.1 Theoretical Studies of SAGD Process

Butler, McNab, and Lo (1981) introduced the theory for SAGD process. In their derivation of an expression for the oil drainage rate, they had assumed that the heat released due to condensation is transferred into the colder oil sand by conduction only, thus the whole process was localized at the steam-oil interface. In deriving the theory, a material balance was performed on the oil being heated at the interface and the oil being drained by gravity. The authors had arrived at an expression for the total oil drainage rate; this rate was a function of the height of the steam chamber, the viscosity of the oil at the steam temperature, the difference between the initial oil saturation and the residual one, and the thermal diffusivity. Expressions for the X-coordinate and Y-coordinate of the steam chamber interface were developed. Experimental work was conducted for the purpose of testing the derived theory. In this experimental work, a scaled visual model working at atmospheric pressure and a scaled physical model working at high pressures had been used. An expression for the dimensional similarity was established. A comparison between the theoretical rate and the experimental rate from the scaled visual model experiments and the scaled physical model experiments

revealed that the experimental rate was of the same order as that predicted, but slightly lower. It was concluded that the slightly lower experimental rate was due to factors that had not been considered in the derivation of the theory.

Butler and Stephens (1981) modified the above-mentioned theory by eliminating the movement of the interface away from the producer. In addition to that, they generalized the theory of the oil drainage rate by including a series of parallel well pairs instead of only one pair. The authors had developed an expression for determining the time needed for the steam chamber to move horizontally to the no-flow plane between the patterns. The theory does not predict the oil drainage rate during the vertical growth of the steam chamber, because in its derivation it was assumed that from the beginning the steam chamber extends for the whole vertical height. However, the theory predicts a maximum production rate that is close to the one found experimentally. It matched the declining drainage rate during the depletion reasonably well.

Butler, Stephens, and Weiss (1981) performed a study in which they have considered the rising-chamber period, which has not been considered in the above mentioned studies. This assumption had led to a discrepancy in the theoretical oil drainage rate during the rising period of the steam chamber. The authors took in consideration the vertical growth rate and the lateral growth rate while the chamber was moving upwards. It was assumed that the steam chamber has a circular shape with the horizontal well at its center. The rate of growth of the steam chamber was taken as the rate of increase in its radius. An expression representing the height of the steam chamber as a function of time was developed. There was good agreement between the theoretical steam chamber heights calculated using the derived equation and the heights resulted from a scaled experiment.

Butler (1985) took a new approach in modeling the SAGD process by treating the interface of the steam chamber as a number of segments. The main concern with the original theory of oil drainage in the SAGD process was the assumption that the temperature distribution corresponds to the steady state. While this was a reasonable approximation in the central part of the interface, it was not true at the ends. In the new theory, it was assumed that the interface is consisted of a number of straight segments. These segments can move and extend or contract in length as the drainage process proceeds. Oil drainage for each segment is calculated for successive time steps and these rates are used to calculate the displacement of the interface. An approximate differential equation was used for calculating the change in the accumulated heat penetration. Based on the results of the new theory, it was concluded that the new method predicts drainage rates of the same order as those obtained from the earlier methods.

Butler (1987) developed an approximate expression, which predicts the rate of the rise of a steam chamber in a reservoir. In developing this theory, the problem was considered as a 2-D problem. The theoretical analysis in this study is concerned mainly with the material, pressure, and heat balances in the region where the steam fingers advance into the cooler reservoir. It was found that the upper boundary of the steam fingers has a parabola shape and that the rise rates of the fingers are proportional to the

permeability of the reservoir, and are strong functions of the steam temperature and oil viscosity.

Ferguson and Butler (1988) developed a new calculation procedure by which the effects of varying steam injection rates, pressures, and the duration of injection cycles on the recovery of heavy oil can be determined. The model used an approximate mathematical method to determine the heat transferred to the receding oil bank and to the cap and base rock. The pressure and the temperature of the steam chamber were changed based on the surplus or deficiencies of the balancing of the total heat injected against the total losses from the system. The new method had been used to test the effect of steam cycle duration, the effect of injection pressure, and the effect of multiple injection cycles on three types of reservoirs. It was found that a considerable increase in the cumulative oil-steam ratio could be gained when the steam injection is stopped before the recoverable reserves have been completely produced. In addition, it was found that higher injection pressures and rates accelerate the production and do not reduce the cumulative oil-steam ratio significantly.

Vikas and Kamath (1992) developed a 2-dimensional analytical model for the process. The effect of porosity, effective permeability, pay zone thickness, well spacing, and the length of the horizontal well on the production performance has been studied. The 2-Dimensional model developed in this study build upon the original concept derived by Butler (1981). In deriving the model, heat balance and fluid flow equations were solved to determine the growth of the chamber, the position of the steam interface and the rate of gravity drainage of oil. The model calculations were divided into two stages: a rising steam chamber stage during which the chamber grows upwards and reaches the top of the reservoir, and a spreading chamber stage during which the chamber grows sideways. The derived model was tested against the results of scaled experiments and numerical simulation results obtained by Chung and Butler (1988.) It was concluded that the model predictions were in good agreement with scaled physical model experiments and numerical simulation results for the Cold Lake oil sand reservoir.

Reis (1992) developed a predictive method for the SAGD process in linear geometry. In developing the new model, the author assumed that the steam chamber has a shape of an inverted triangle with its lower vertex fixed at the producer. He also assumed that the temperature profile declines exponentially with distance away from the interface, independently of the position on the interface. An energy balance approach was used to determine the latent heat injection rate of the steam to expand the steam chamber, preheat the reservoir ahead of the chamber, and supply the heat losses to the overburden. The model was validated by testing it against the experimental data of Chung and Butler (1988). A good agreement was found when the effect of the relative permeability considered. In addition, the author compared his model to the other published models and found that his model gave the closest match the experimental data.

Butler (1997) has showed that it is not necessary that the entire steam chamber to be at a uniform high temperature. In conventional SAGD process large steam quan-

tities are needed to maintain the whole steam chamber at the saturation temperature corresponding to the reservoir pressure, and to supply the heat losses to the overburden and the underburden. High temperatures in the upper part of the reservoir are crucial to the viability of the SAGD process, especially in thin reservoirs due to the high heat losses to the overburden. In this study, a modification of the original SAGD process was proposed in which a non-condensable gas is injected with the steam; the gas will accumulate in the chamber above the injector, and lower the temperature in the upper part of the chamber. In one example, it has been shown that heat stored in the chamber per cubic meter of produced oil was only 62% of that of conventional SAGD.

3.4.2 Experimental Studies of SAGD Process

Butler, McNab and Lo (1981) carried out the earliest experiments on SAGD process, in Esso Canada's Laboratory. These experiments were carried out in a low-pressure scaled visual model, and in a high pressure scaled model. These experiments were scaled based on scaling criteria developed by the authors. The purpose of this experimental work was to test their SAGD theory. The various stages of the growth of the steam chamber were photographed from the visual model experiments. It was found that the experimental oil drainage rate was of the same order as the one predicted by the theory.

Griffin and Trofimenkoff (1984) performed an experimental study to test several factors, including oil viscosity, and injection temperature on oil production in SAGD as observed in scaled laboratory experiments and to extend the SAGD theory to examine steam injection from a vertical well situated above the horizontal producer. In this study two types of models were used: 1) atmospheric pressure, 2-dimensional visual model, and 2) 3 dimensional high-pressure model. Two configurations of the visual model were used; one, which had a horizontal injector and a horizontal producer and the other, had a vertical injector and a horizontal producer. From the visual model experiments, good agreement between the theoretical and the experimental oil production rates was found, and it was found that the highest oil rate occurred when the steam chamber reached the top of the reservoir. The results of both the visual model and the physical model agreed well with the theory. The authors concluded that steam override and subsequent overburden heat loss was not as large as had been expected by the SAGD theory, and that the oil rate increased as the injection pressure increased, due to temperature increase and oil viscosity decrease.

Joshi and Threlkeld (1985) conducted an experimental study to compare the production performance of the following three SAGD configurations: 1) a horizontal well pair, 2) a vertical injector and a horizontal producer, and 3) a vertical well pair. In addition, the effect of the existence of different configurations of fractures in the reservoir on the production performance had been tested. Most of the experiments were conducted using light oil, while bitumen was used in some experiments. It was found that the horizontal well pair recovered more oil than the other two configurations. The horizontal well pair configuration heated and drained the reservoir more effectively. It was also found that vertical fractures improve the performance of the SAGD process,

especially at the beginning when the fracture scheme gave a higher oil-steam ratio than the uniform permeability pack.

Chung and Butler (1988) conducted an experimental study to investigate the in situ emulsification of oil and water during the SAGD process. The authors investigated how the change in well configuration in the SAGD process effects the amount of water-oil emulsion in the produced fluids. The well configurations tested were: 1) a steam injector slightly above a producer; 2) a producer at the base of the formation and a vertical circulating steam injector which was perforated near the top of the formation. The results showed that the water-oil emulsion in the produced fluids was higher during the upward growing stage than during the sideways growing stage of the steam chamber. This is because during the upward growing stage of the chamber there was a meandering and counter-current flow of steam and heated oil, while during the sideways growing stage the flow was a two-phase (oil and steam).

Sugianto and Butler (1990) tested the performance of the SAGD process in reservoirs containing a bottom water. Experiments were conducted in a scaled, 2-dimensional reservoir model containing an active aquifer system. The study investigated the mechanism, the process, and the effect of steam injection pressure, bottom water thickness and the location of the production well. It was found that the SAGD process could economically produce heavy oils from reservoirs having bottom water aquifers. The ultimate oil recovery varied from 87% for the no bottom water case to 48% where the bottom water aquifer represented 41% of the total reservoir volume. It was desirable that the steam injection pressure to be comparable to the aquifer pressure in reservoirs having a bottom water aquifer. Although in most of the conducted experiments the producer was above the water-oil contact, it was found that excellent recovery could be obtained with the producer was located below the water-oil contact.

Sasaki, et al (1996) carried out experiments on the initial stage of the SAGD process. The main aim of this study was to shorten the leading time to generate a steam chamber in near breakthrough conditions between two horizontal wells. A 2-dimensional physical model was used. The steam chamber was visualized using video and thermal-video cameras. In order to modify the initial stage of the original SAGD process, the authors decided to study the effect of some factors on this process. It was found that the time of the steam breakthrough increased as the drawdown decreased. Also, it was noticed that the width of the steam chamber at the steam breakthrough decreased as the drawdown increased; however, the difference in the chamber shape became gradually small during the rising stage of the chamber. The authors noticed that the larger the distance between the injector and the producer the better the rate of recovery especially after the breakthrough time. Based on the above results, it has been decided that the initial stage of the original SAGD process can be modified by injecting steam intermittently from the producer in addition to the continuously steam injection from the injector.

Nasr, et al (1996) performed an experimental and numerical study of the SAGD process. The experiments were conducted to verify the numerical model. Four experi-

ments were conducted in this study. The first and the second experiments were performed using paraffinic wax, and designed to investigate the effect of enthalpy control on the SAGD process (the first experiment was injection controlled and the second one was enthalpy controlled). In the third experiment, Cold Lake oil was used and enthalpy control was applied, this experiment was used to validate the numerical model. The fourth experiment was used to evaluate the effect of wellbore dynamics on the development of the steam chamber. In addition, the effect of permeability on the source/sink simulation was investigated. The size of the steam chamber was larger in the case of the enthalpy controlled than in case of the rate controlled. It was also found that the duration of the initialization phase of the SAGD process increased as the permeability decreased.

3.4.3 Numerical Studies of the SAGD Process

Kamath, et al (1993) performed a simulation study of SAGD process in Ugnu Tar Sand Reservoir. Because the SAGD analytical models were developed for a homogeneous, isotropic reservoirs, the authors decided to develop a 2-dimensional numerical model in which the effect of heterogeneity and anisotropy on the performance of the SAGD Process were considered. The effect of heterogeneity was considered by implementing a model, which was consisted of N layers, with each layer having different porosity, permeability, initial oil and water saturations, but same relative permeability. A base case run was established for comparison in which the reservoir was considered homogeneous, and an average value for each reservoir property was selected. The tested parameters were the porosity, absolute permeability, initial mobile water saturation, Dykstra Parsons permeability variation, ratio of vertical to horizontal permeability, steam temperature, steam quality, steam injection rate, horizontal well length, injector-producer spacing, lateral well spacing, and shale barriers. The performance of the SAGD process improves significantly with high steam injectivities, higher steam quality, low mobile water saturation near the producer, absence of continuous shale barriers, high vertical to horizontal permeability ratio and optimum injector-producer vertical spacing.

Kisman and Yeung (1995) tested the performance of the SAGD process in the Burnt Lake Oil Sands Lease using a 2-dimensional numerical model. Due to the limitations on the grid size, each 100-m of the 500 m long well pair was represented by a separate 2-dimensional model, and then the performance of the entire well was determined by combining results of all the 2-dimensional models. A base case model was prepared for comparison. These parameters were not known accurately. The comparison was done by comparing the recovery performance after 4 and 8 years of each sensitivity run to the base case run. The tested parameters were: vertical permeability, live oil viscosity as a function of temperature, flow barriers, thermal conductivity, solution gas, relative permeability, well placement, and operating pressure. The base case model predicted a favorable recovery performance, and that the oil viscosity and the relative permeability in the region surrounding the steam chamber had more effect on recovery performance than corresponding properties within the steam chamber. It was also found

that placing the producer at the base of the reservoir where the permeability was poor had a significant effect on the SAGD performance in Burnt Lake Oil Sands Lease.

Ito and Suzuki (1996) performed a simulation study of the SAGD process applied to the Hanginstone Oil Sands Reservoir. The study was conducted to forecast the recovery performance and to further understand the oil production mechanism. Thus, the authors decided to review in detail the flow behavior of steam, water, and oil as well as the mechanism by which heat is transferred from the steam chamber to the surrounding reservoir. It was found that the peak oil flow appeared to be at 2 to 3 meters away from the steam chamber interface; this area was between the temperature contours of 160°C and 210°C, which was 50-100°C lower than the steam saturation temperature. Steam condensate therefore played a role in displacing the oil from the reservoir. This disagrees with what had been believed about the mechanism of oil displacement of the SAGD process.

3.4.4 Field Pilots of the SAGD Process

Phase A of the UTF project was the first field pilot of the SAGD process. The purpose of this pilot was to test the performance of the SAGD process in the field. Phase A project consisted of three pairs of horizontal wells, each pair had a producer completed low in the pay zone and an injector located parallel to and 5 meters above the producer. The well pairs were spaced 25 meters apart, and the effective length of the completion was 55 meters. The pattern also contained 26 observation wells, to monitor temperature, pressure and geotechnical effects. The production was controlled by setting the wellhead temperature at a value below the boiling point of water on the basis of the wellhead flowing pressure. This steam-trap control maintains correct drawdowns because no steam can be produced and production cannot be accumulated at the chamber bottom. Based on the performance of Phase A of the UTF Project, the original SAGD concepts had been confirmed, and that the conventional numerical models accurately predicted the process performance, with sufficient knowledge of formation permeability and sufficient grid resolution. It was also concluded that a commercially viable combination of recovery, production rate, and steam-oil ratio would be obtained from full-scale operations, and that significant advances in completions design and production engineering were demonstrated (Edmunds et al., 1994.)

Edmunds and Gittins (1993) reviewed the effective application of SAGD process of bitumen to long horizontal well pairs. After the success of Phase A of the UTF project it was decided to design Phase B in which 500-m wells (commercial length) will be implemented. Based on the review, it was concluded that the start up of the SAGD process could be achieved with thermal conduction and gravity alone.

The main objectives of Phase B of the UTF Project were to demonstrate that the encouraging Phase A productivities can be scaled up in proportion to the lengths of the wells, and can be sustained for a producing life proportional to the pattern spacing. Thirty-one wells were implemented for the purpose of monitoring the temperature, pressure, and geotechnical effects in Phase B project. Prior to the start of the Phase B project, a simulation study was performed to predict the performance. These forecasts

were used later on for comparison with the actual performance of the project after one-third of the pattern life has elapsed. It was concluded that the overall Phase B performance was very close to the predicted one and that SAGD performance can be scaled directly to the lengths of the horizontal wells when the wellbore hydraulic effects are small (Mukherjee et al., 1995.)

3.5 Predictive Models for Steam Zone Volumes

Over the years many predictive models have been developed for the purpose of predicting the growth of the steam zone during a steamflooding. Each model has its limitations. In this study two different theoretical models have been used to confirm the experimental steam zone volumes. These two models will be discussed here in detail.

3.5.1 Marx-Langenheim Model

Marx and Langenheim (1959) considered the ideal situation of steamflooding where the steam is introduced at a constant rate into a steam zone, which spreads laterally over the entire thickness of the reservoir, i.e., there is no gravity segregation. The model assumes that the steam zone is at a constant temperature, T_s, extending from the injection end to the point where the temperature abruptly drops from T_s to T_R, the reservoir temperature (Farouq Ali, 1976). Heat is transferred from the steam zone to its surroundings, including the overburden and the underburden by conduction. There is no heat flow from the steam zone into liquid zone ahead of the condensation front. This assumption is realistic if the latent heat supplied in the injected steam is enough to supply all the heat losses, i.e., there is still latent heat arriving at the front (Butler, 1990). The following expression was derived for the steam zone volume:

$$V_s = \frac{Q_i M_s h_t^{\,2} F1}{4k_{hob} M_{ob} (T_s - T_R)} \qquad \text{(3.1)}$$

F_1 can be defined by the following expression:

$$F_1 = e^{t_D}\, erfc\sqrt{t_D} + 2\sqrt{t_D/\pi} - 1 \qquad \text{(3.2)}$$

F_1 can be determined from a plot of F_1 vs. t_D or can be approximated using the following expression:

$$F_1 = \frac{t_D}{1 + 0.85\sqrt{t_D}} \qquad \text{(3.3)}$$

3.5.2 Neuman's Model

Neuman (1985) developed a model for predicting the steam zone volume; in this model the gravity override of the steam had been taken into consideration. In deriving this model it was assumed that: the steam rises quickly to the top of the reservoir, the vertical pressure gradient is much higher than the horizontal pressure gradient, and the water and oil saturations remain constant throughout the steam zone. Once the steam zone risen to the top of the reservoir, which happens in a short time compared to the time needed to heat the whole reservoir, the steam zone starts in growing downwards, from the top to the bottom of the reservoir. Expressions were developed for calculating the steam zone thickness, the areal growth of the steam zone, the volume of the steam zone. The following expression were derived for determining the steam zone thickness:

$$h = \frac{4k_h C_w \Delta T_s}{M_s L_v} \sqrt{\frac{(t-\pi)}{\pi a}} \qquad \text{(3.4)}$$

The areal growth of the steam zone can be calculated using the following equation:

$$A = \left[\frac{f_d(1-f_p)i\rho_w L_v}{k_h \Delta T_s}\right] \sqrt{\frac{at}{\pi}} \qquad \text{(3.5)}$$

The volume of the steam zone can be determined using the following equation:

$$V_s = \frac{f_d(1-f_p)i\rho_w C_w t}{M_s} \qquad \text{(3.6)}$$

4. Scaling Parameters and Calculations

Physical models have been widely used to study fluid flow through porous media phenomena, especially those not well described mathematically, they also have been used to design or assist in the operation of steamflooding projects. From scaling point of view, physical models can be described by three categories: unscaled, partially scaled, and fully scaled models. Depending on the type of the study, one of the three categories will be chosen. In order to apply the laboratory results to the field, the model must be scaled using scaling groups. The scaling criteria proposed by Stegemeier et al. (1980) have been used in this study to scale-up the physical model to the prototype reservoir (Kern "A" reservoir). In this study the implementation of the above mentioned scaling criteria is illustrated, including example calculations.

4.1 Development of Scaling Parameters for the Low Pressure Model

4.1.1 Unscaled Parameters

In reality it's not possible to satisfy all the scaling groups due to the unavailability of materials and fluids having physical properties that satisfy all the scaling requirements and also because several of the scaling groups are not compatible with each other. Thus some approximations and simplifications have to be made, which will lead to a reduced number of scaling parameters. In this study, the following parameters were unscaled between the model and the prototype reservoir.

1. Capillary pressure and relative permeability.
2. Thermal expansion and compression of the reservoir fluids and matrix.
3. Steam distillation of the crude oil.
4. The extent of emulsification and its mechanism.
5. Asphaltene flocculation.
6. Specifications corresponding to the injection and production of a horizontal well such as: pressure drop in the vicinity of and within the well-bore, skin factor, and perforations interval.

Although the above mentioned parameters were not scaled, the success of vacuum model studies in simulating the prototype reservoirs performance implies that these parameters have only a second order effect on the process of producing heavy oils using steam injection.

4.1.2 Scaling Procedure

In this study the procedure introduced by Stegemeier et al. (1980) has been used to scale the physical model used in this study. The scaling parameters that have been used in this study are listed in Table 4.1. The first step in the development of the scaling parameters is to drive the governing equations of fluid flow and heat transfer. The governing equations should then be made dimensionless by dividing the dimensional variable (m) by a characteristic reference quantity (m_R).

Thus:

Table 4.1-Scaling Parameters for Steam Processes (Modified from Stegemeier et al 1980)

Number	Scaling Parameter	Name of Scaling Parameter
I	$\frac{P_R}{\rho_R g_R L_R}$	Poiseuille Number divided by Stokes Number
II	$\left(\frac{f_{sR} L_{VR}}{C_R T_R} + 1\right) \times A^*$	Modified Jacob Number +1
III	$\frac{f_{sR} \mu_{sR} \rho_R}{\mu_R \rho_{sR}}$	Ratio of steam pressure gradient to oil pressure gradient
IV	$\frac{k_{hR} t_R}{\phi_R S_R \rho_R C_R L_R^2} A^*$	Fourier Number or Peclet Number^{-1}
V	$\frac{\phi_R S_R \mu_R L_R}{k_R \rho_R g_R t_R}$	Stokes Number
VI	$\frac{W_R t_R}{\rho_R \phi_R S_R L_R^3}$	Poiseuille Number Divided by Modified Poiseuille Number

* When $\phi \Delta S$ is not matched, A takes on a value between unity and $\phi_R S_R (\rho_R C_R / \rho_{cR} C_{cR})$

- If reservoir heating or heat production predominates, use unity.
- If cap and base rock heating predominates, use $\phi_R S_R (\rho_R C_R / \rho_{cR} C_{CR})$.

$$m_D = \frac{m}{m_R} \quad \text{.....(4.1)}$$

Once the governing equations had been dimensionlized, the inspectional analysis was then used to obtain the similarity parameters. Satisfying all of these similarity parameters is almost impossible in most of the physical models due to the reason that has been mentioned above. Therefore these parameters are combined and modified using engineering judgement to generate new set of similarity parameters, which could be matched between the model and the prototype reservoir.

The following assumptions has been made by Stegemeier et al. (1980) in order to drive the scaling criteria for the subatmospheric pressure model:

1. Three phases may exist, and these are the oleic phase, the aqueous phase, and the vapor phase (no volatile hydrocarbon) may exist.
2. There is no partitioning into or out of the oil phase (dead oil assumption).
3. Rock compressibility and thermal expansion are negligible.
4. Darcy's and Fourier's laws are valid.
5. The system is in local thermodynamic equilibrium.
6. Capillary pressure effects are negligible.
7. Kinetic energy, and potential energy, are negligible compared with thermal energy.
8. The enthalpy and internal energy are essentially equal for the oleic phase and aqueous phase, and are linear functions of temperature.
9. The difference between the steam enthalpy and internal energy can be neglected.
10. The time rate of change of the specific steam enthalpy in the steam zone is negligible.
11. The internal energy of the rock is linear function of temperature.
12. The saturated temperature is the maximum temperature at any location.
13. Relative permeability depends exclusively on the saturations.
14. S_w and S_{wc} are constant and uniform throughout the model.
15. Critical saturation for steam flow is assumed to be zero.
16. The change in density of the immobile water and residual oil are negligible.

Taking the above mentioned assumptions into consideration, and applying the conservation of mass balance to the oil phase yields,

$$\phi \frac{\partial(\rho_o S_o)}{\partial t} + \nabla \cdot (\rho_o \vec{u}_o) = 0 \quad \text{.....(4.2)}$$

where the subscript 'o' denotes oil phase.

Applying the conservation of mass to the water phases (liquid and vapor) results in,

$$\phi \frac{\partial(\rho_w S_w)}{\partial t} + \nabla \cdot (\rho_w \vec{u}_w) + \phi \frac{\partial(\rho_s S_s)}{\partial t} + \nabla \cdot (\rho_s \vec{u}_s) = 0 \quad \text{.....(4.3)}$$

where the subscript 'w' signifies the water in the liquid phase and 's' signifies the water in the vapor phase.

Based on the assumption that Darcy's equation applies, thus the following equation can be written for any phase j, where j= o, w, or s,

$$\vec{u}_j = -\frac{kk_\eta}{\mu_j}\left(\nabla P - \rho_j \vec{g}\right) \quad \text{.....(4.4)}$$

The conservation of the energy of the reservoir can be written as follows,

$$\left[(1-\phi)\rho_r C_r + \phi(\rho_o C_o S_o + \rho_w C_w S_w)\right]\frac{\partial T}{\partial t} + L_v\left[\phi\frac{\partial(\rho_s S_s)}{\partial t} + \nabla\cdot\rho_s\vec{u}_s\right] \quad \text{.(4.5)}$$
$$+\left[\rho_o C_o u_o + \rho_w C_w \vec{u}_w\right]\cdot\nabla T + \rho_s\vec{u}_s\cdot\nabla h_s + \nabla\cdot\vec{q} = 0$$

Assuming that the conductive heat influx from the model to the overburden and the underburden is expressed by Fourier's equation,

$$\vec{q} = -k_h\nabla T \quad \text{.....(4.6)}$$

Because it was assumed that there is only three phases, thus the saturation identity becomes,

$$S_o + S_w + S_s = 1 \quad \text{.....(4.7)}$$

The Clausius-Claperyron relationship, which relates the pressure and the temperature at the saturation conditions, is as follows,

$$P_{sat} = P_{sat}(T_{sat}) \quad \text{.....(4.8)}$$

The rest of the relationships needed to describe the system are the constitutive equations, which express the dependence of the reservoir material properties on the thermodynamic-state variables. These equations can be expressed in the functional form,

$$\phi = \phi(x,y,z) \quad \text{.....(4.9)}$$
$$\rho_j = \rho_j(P,T) \quad \text{.....(4.10)}$$
$$k = k(x,y,z) \quad \text{.....(4.11)}$$
$$k_\eta = k_\eta(S) \quad \text{.....(4.12)}$$
$$\mu_j = \mu_j(T) \quad \text{.....(4.13)}$$
$$h_s = h_s(T) \quad \text{.....(4.14)}$$
$$L_v = L_v(T) \quad \text{.....(4.15)}$$
$$k_v = k_h(x,y,z) \quad \text{.....(4.16)}$$
$$\rho_s = \rho_s(x,y,z) \quad \text{.....(4.17)}$$

where s denotes dependence on the phase saturation.

The above mentioned equations constitute a complete set for describing the reservoir behavior.

A fewer number of equations are required in the cap and the base rock due to the fact that there are no movable fluids in these regions. The equations of significance in these regions are the energy equation, which is:

$$\rho_e C_e \frac{\partial T}{\partial t} + \nabla \cdot \vec{q} = 0 \quad \text{.....(4.18)}$$

and the heat-flux equation, which is given by equation (4.6).

In addition to the above equation the initial and boundary conditions had been formulated and then dimensionlized by dividing each variable, parameter, and operator in these equations by a characteristic reference quantity, m_R. Once the governing equations had been put in a dimensionless form, the next step was determining which of these equations are independent. This can be accomplished either by observations or by using the Buckingham Pi theorem. Due to the impossibility of satisfying all of the similarity parameters some of these parameters will be relaxed depending on the materials, fluids, and the working conditions of the model and the prototype reservoir. Appendix A of Stegemier et al. (1980) has a detailed derivation of the scaling parameters.

4.2 Designing the Low Pressure Model of the Kern "A" Resevoir

One-quarter of an imaginary 2-ha (5.4-acre), five-spot steam-displacement pattern was selected in the Kern "A" project (Kern "A" Reservoir) as the prototype for the physical model. The first step in the design of the physical model is selecting the prototype values that would be representative of typical field values of the Kern "A" reservoir (Kern River field). The reservoir properties that have to be specified for the scaling calculations (Table 4.2) were net pay thickness, porosity, permeability, thermal conductivity, heat capacity, movable saturation, oil density, oil viscosity as a function of temperature, injection pressure, and the initial reservoir pressure and temperature.

4.2.1 Length Scaling

Although the length scale of the model is somewhat arbitrary, there are factors, which should be considered in the determination of the length scale, and these are: the physical size of the model, and the temperature-pressure relationships. Stegemeier et al. (1980) suggested in order to match the temperature-pressure relationship for saturated steam while our prototype production pressure is 689 kPa or less, the model should be as large as possible, i.e., the length scale, g(L), should be as small as possible taking into considerations the constraints of space available, leaking, time required to prepare for and to run the experiment.

The prototype length, L_p, for the element of symmetry was 65.5 m (214.9 ft). The model length, L_m, was 0.38 m (15 inches). Therefore, the length scale factor is 172, that is,

$$\frac{L_p}{L_M} = g(L) \quad \text{.....(4.19)}$$

Table 4.2- Scaling Parameters of the Prototype Reservoir

Field Property	Prototype Value	Model Value
Well Spacing	¼ of 2.7 acre, 5-spot pattern	SAGD Configuration
Length	65.5 m	0.38 m
Net Pay Thickness	22.56 m	0.305 m
Porosity	0.35	0.36
Permeability	2.1 darcies	1294 darcies
Thermal Conductivity	0.00277 kW/m.K	0.003266 kW/m.K
Heat Capacity	2.1803 kJ/kg K	2.3824 kj/kg K
Initial Fluid Saturations	$S_o = 44.25\%$ $S_w = 56.1\%$	$S_o = 94.7\%$ $S_w = 5.5\%$
Residual oil Saturation	$S_{or} = 17.0\%$	$S_{or} = 6.0\%$
Oil Density	961.11 kg/m^3	879 kg/m^3
Oil Viscosity	3000 mPa. s at 23.9°C 740 mPa. s at 37.8°C 107 mPa s at 65.6°C 24 mPa s at 93.3°C	270 mPa.s at 22.9°C 238 mPa s at 25.0°C 137 mPa s at 35.0°C 123 mPa s at 37.0°C
Water Viscosity 25.8°C	0.891 m Pa s at 25.8°C	0.891m Pa s at
Initial Reservoir Temperature	35°C	3°C
Initial Reservoir pressure (absolute)	0.345 MPa (absolute)	0.088 MPa
Steam Injection Pressure (absolute)	4.24 MPa (absolute)	0.052 MPa
Steam Injection Rate	20 m^3/D	180 ml/min
Steam Quality	0.7	0.1

4.2.2 Model Production Pressure Scaling

The selection of the model production pressure is some how arbitrary in that the scaling does not dictate the value that has to be chosen. However, scaling the temperature in the model when there is an appreciable pressure drop in the steam zone dictates that the temperature-pressure relationship for saturated steam must be scaled. For prototype pressure as low as 50 Psia and typical length scale of 100 to 200, the temperature pressure relationship at saturation can be matched best if the model production pressure was selected as low as possible (Stegemeier et al 1980). In this study, from the preliminary experiments experience, and due to the dynamics of the experiments the production pressure was 42 kPa (absolute).

Once the model production pressure has been chosen, model pressure scaling is determined from the first scaling parameter in table 4.1 as:

$$\gamma(\Delta P)=\frac{(P-P_p)_p}{(P-P_p)_M}=\frac{\rho_p g_p L_p}{\rho_M g_M L_M} \qquad \text{.....(4.20)}$$

Since the length scale had been calculated previously from Eq. 4.19, the ratio of the gravitational accelerations is essentially unity, and the density ratio, $\frac{\rho_p}{\rho_M}$, is 1.09. Since the production pressure of the model and the prototype are 42 kPa, and 99.9 kPa respectively, therefore based on equation 4.20 the relationship between the model production pressure and the prototype production pressure is as follows:

$$P_M = 0.00531P_p + 0.0415 \qquad \text{.....(4.21)}$$

where P_M and p_p are in MPa.

Based on the above equation Table 4.3 was created, which contains several prototype and model pressures covering the range of scaling along with their corresponding saturated steam temperatures, T_s, the enthalpy of water at steam temperature, and the effective $C_w\Delta T$, where ΔT is the difference between steam temperature and the initial reservoir temperature.

4.2.3 Model Temperature Scaling

The best match between the model and the prototype oil-viscosity can be obtained by having the largest possible temperature range. Having this constraint, the temperature lower limit was set at 3°C, which is slightly above the freezing point of water.

Because that most of the oil will be produced when the temperature is high and due to the difficulty in matching the lower region of the Clausisus-Clapeyron relation for saturated steam. Stegemeier et al. (1980) suggested that it is best to take a value from the middle or the upper regions of the pressure range for finding the temperature

difference ratio. From the preliminary experiments, it was found that the steady-state injection temperature and pressure of the model were 83°C and 52 kPa, respectively. The corresponding values of the injection pressure and the injection temperature of the prototype from Table 4.3 are 214.1°C and 2.07 MPa, respectively. With the above temperatures, the temperature ratio can be calculated as follows:

$$\frac{(\Delta T)_p}{(\Delta T)_M} = \frac{(T_{inj} - T_I)}{(T_{inj} - T_I)} = \frac{(T_{sat} - T_I)_p}{(T_{sat} - T_I)_M} \quad \text{.....(4.22)}$$

From table 4.3, the steam saturation temperature of the model and the prototype are 82.6°C, and 214.1°C, respectively, while the initial temperature of the model and the prototype are 3°C, and 35°C, respectively. Substituting these values in the above equation yields:

$$\frac{(\Delta T)_p}{(\Delta T)_M} = \frac{(214.4 - 35)}{(82.6 - 3)} = 2.25 \quad \text{.....(4.23)}$$

Because the above ratio must be constant over the whole temperature range, thus,

$$\frac{(T_{sat} - 35)_p}{(T_{sat} - 3)_M} = 2.233 \quad \text{.....(4.24)}$$

Therefore the relationship between the model temperature and the reservoir temperature is,

$$T_M = 0.444T_p - 12.555 \quad \text{.....(4.25)}$$

4.2.4 Calculation of the Required Steam Quality

When the temperature distribution is more significant in the cap and the base rock than in the reservoir, which frequently is the case in steam drives where the thermal efficiencies are less than 0.5 (Stegemeier et al. 1980). The model steam quality was calculated from parameter II in table 4.1. Assuming that the heating of the cap and base rock predominates, therefore term A in the scaling parameter II is replaced by $\phi_R S_R (\rho_R C_R / \rho_{cR} C_{cR})$. Thus the model steam quality could be calculated using the following equation.

$$f_{SM} = \left(\frac{C_w \Delta T}{L_v}\right)_M \left\{\left(\frac{f_{st} L_v}{C_w \Delta T} + 1\right) \times \left[\left(\frac{\phi_p \Delta S_p}{\phi_M \Delta S_M}\right)\left(\frac{\rho_p C_p}{\rho_M C_M}\right)\left(\frac{\rho_{CM} C_{CM}}{\rho_{CP} C_{CP}}\right)\right] - 1\right\}$$

.....(4.26)

By substituting the appropriate values of ratios at steady-state steam injection pressure, equation 4.26 yields,

$$f_{SM} = \left(\frac{335.8}{2302.5}\right)\left\{\left(\frac{0.7 \times 1881.5}{774} + 1\right) \times \left[\left(\frac{0.345 \times 0.67}{0.37 \times 0.89}\right)(1)(1)\right] - 1\right\} = 0.1\ldots \quad \text{(4.27)}$$

Column 14 in Table 4.3 constitutes the model steam quality for the whole scaling range.

4.2.5 Scaling of the Model oil viscosity

In order to match the pressure gradient in the steam zone and oil zone, the viscosity of the model oil must be scaled according to parameter III in table 4.1, thus:

$$\frac{\mu_{oM}}{\mu_{oP}} = \left(\frac{f_{sM}}{f_{sP}}\right)\left(\frac{\mu_{sM}}{\mu_{sP}}\right)\left(\frac{\rho_{sP}}{\rho_{sM}}\right)\left(\frac{\rho_{oM}}{\rho_{oP}}\right) \quad \text{.....(4.28)}$$

The values of the variables of equation 4.28 were inserted to yield the corresponding model oil viscosities which,

$$\frac{\mu_{oM}}{\mu_{oP}} = \left(\frac{0.098}{0.7}\right)\left(\frac{0.01114}{0.015773}\right)\left(\frac{7.066}{0.30105}\right)\left(\frac{1}{0.915}\right) = 2.53 \quad \text{.....(4.29)}$$

Column 17 in table 4.2 contains the viscosity ratio of the whole scaling range.

4.2.6 Calculation of the Time Scale Factor

The time scale factor was calculated using parameter IV in table 4.1. Due to the earlier mentioned assumption that the heat in the cap and base rock predominates, therefore the constant A in parameter IV should be equal to $\phi S_R\left(\rho_R C_R / \rho_{oR} C_{oR}\right)$. Thus the time scale factor will be on the following form:

$$\frac{t_M}{t_P} = \left(\frac{k_{hP}}{k_{hM}}\right)\left(\frac{\rho_{oM} C_{oM}}{\rho_{oP} C_{oP}}\right)\left(\frac{L_M}{L_P}\right)^2 \quad \text{.....(4.30)}$$

where

$k_{hM} = 0.003266\ \text{kW/m}\cdot\text{K}$

$k_{hP} = 0.002769\ \text{kW/m}\cdot\text{K}$

$\rho_{oM}C_{oM} = 2.3824\ \text{kJ/kg}\cdot\text{K}$

$\rho_{oP}C_{oP} = 2.1803\ \text{kJ/kg}\cdot\text{K}$

Substituting the above values into equation 4.30, thus the time scale factor can be determined as follows:

$$\frac{t_M}{t_P} = \left(\frac{0.002769}{0.003266}\right)\left(\frac{2.3824}{2.1803}\right)\left(\frac{1}{172}\right)^2 = 3.06\times10^{-5} \quad \text{.....(4.31)}$$

If we take the lab time, t_M, in minutes and the field time, t_P, in years. Thus the $\frac{t_M}{t_P}$ will yield:

$$\frac{t_M}{t_P} = 16.1\ \text{min/yr} \quad \text{.....(4.32)}$$

Table 4.3: Prototype and Model Scaling Values.

Prototype Values							Model Values									
P (MPa)	Ts (C)	hw (KJ/Kg)	CwDT (KJ/Kg)	Lv (KJ/Kg)	ρ (Kg/m3)	μs (CP)	P (MPa)	Ts (C)	Tsc (C)	hw (KJ/Kg)	CWDT (KJ/Kg)	Lv (KJ/Kg)	ρ (Kg/m3)	μs (cp)	fs	μsm/μsp cp/cp
*	*	**	*	***	****	*****	Eq. 4.21	*	Eq. 4.25	**	*	***	****	*****	Eq. 4.26	Eq. 4.28
4.14	252.34	1104.9	958.2	1702.6	20.81	0.01747	0.0635	87.4	93.85	368.52	355.92	2289.95	0.385	0.01137	0.089	2.195
3.45	241.67	1053.21	906.51	1756.1	17.35	0.01719	0.0598	85.9	89.39	362.25	349.65	2293.89	0.365	0.01132	0.099	2.385
2.75	229.22	993.36	846.66	1815.2	13.92	0.01686	0.0561	84.2	84.18	355.14	342.54	2298.34	0.343	0.01126	0.113	2.529
2.07	214.08	921.33	774.63	1881.5	10.49	0.01643	0.0525	82.6	77.85	348.45	335.85	2302.52	0.323	0.01121	0.131	2.586
1.38	194.33	828.98	682.28	1960.4	7.07	0.01577	0.0488	80.7	69.59	340.48	327.88	2307.45	0.301	0.01114	0.158	2.527
0.69	164.34	693.5	546.79	2066.9	3.62	0.01457	0.0452	78.8	57.06	332.51	319.91	2312.37	0.28	0.01108	0.216	2.209
0.35	138.34	581.1	434.4	2148.9	1.87	0.01343	0.0434	77.9	46.19	328.73	316.13	2314.69	0.271	0.01105	0.291	1.817
0.09	99.62	419.37	272.67	2256.2	0.59	0.01182	0.0419	77	30	324.94	312.34	2317	0.262	0.01102	0.508	1.234

* "Engineering Thermodynamics", 2nd Edition, S.I. version by Van Nostrand Reinhold (International) (1988)

** hw=23665.2-366.23ZT+2.2695ZT^2-0.007303T^3+1.30241E-5*T^4-1.22103E-8*T^5+4.70878E-12*T^6, Ref. 48

*** Lv= (7184500+11048.6*T-88.4050*T^2+0.162561*T^3-1.21377E-4*T^4)^1/2 , Ref. 48

**** hp=-93.7072+0.833941*T-0.00320809*T^2+6.57652E-6*T^3-6.93747E-9*T^4+2.97203E-12*T^5, Ref. 48

***** μs=1E3*(-5.46807E-4+6.89490E-6*T-3.39999E-8*T^2+8.29842E-11*T^3-9.97060E-14*T^4+4.71914E-17*T^5), Ref.48

Thus 16.1 minutes of the experiment time is equivalent to one year of the field time.

4.2.7 Calculation of the Permeability of the Model

The model permeability is scaled according to parameter V in table 4.1, which is:

$$\frac{k_M}{k_P} = \left(\frac{\phi_M \Delta S_M}{\phi_P \Delta S_P}\right)\left(\frac{L_M}{L_P}\right)\left(\frac{\mu_M}{\mu_P}\right)\left(\frac{\rho_{oP}}{\rho_{oM}}\right)\left(\frac{t_P}{t_M}\right) \quad \text{.....(4.33)}$$

It is obvious from Equation 4.33 that k_M / k_P is dependent on the temperature as a result of the dependency of the viscosity ratio, μ_M / μ_P, on the temperature. However, the scaling of ratio, k_M / k_P, is not possible if the temperature dependency has been considered, therefore a single value of the viscosity ratio, μ_M / μ_P, must be chosen. Stegemeier et al. suggested that this value should be chosen after the steam breakthrough when the steam pressures tend to be low and as a consequence this value is significant after that time (Stegemeier et al. 1980). Thus the viscosity ratio was taken at the prototype injection pressure of 0.69 MPa. Substituting the value of the ratios in Equation 4.33 yields:

$$\frac{k_M}{k_P} = \left(\frac{0.36 \times 0.86}{0.35 \times 0.67}\right)\left(\frac{1}{172}\right)(2.21)\left(\frac{1}{0.9}\right)\left(\frac{1}{3.06 \times 10^{-5}}\right) = 615.968 \quad \text{.....(4.34)}$$

Since the prototype permeability is 2.1 darcy, and based on the above equation the model permeability will be:

$$k_M = 615.968 \times 2.1 = 1293.53 \text{ darcies} \quad \text{.....(4.35)}$$

4.2.8 Calculation of the Model Injection and Production Rates

The model injection and production rates is calculated based on parameter VI in table 4.1, which is:

$$\frac{W_M}{W_P} = \left(\frac{\rho_{oM}}{\rho_{oP}}\right)\left(\frac{L_M}{L_P}\right)\left(\frac{\phi_M \Delta S_M}{\phi_P \Delta S_P}\right)\left(\frac{t_P}{t_M}\right) \quad \text{.....(4.36)}$$

Substituting the appropriate values in the above equation yields:

$$\frac{W_M}{W_P} = \left(\frac{1}{0.9}\right)\left(\frac{1}{172}\right)^3\left(\frac{0.366 \times 0.86}{0.345 \times 0.67}\right)\left(\frac{1}{3.06 \times 10^{-5}}\right)\left(\frac{110 \text{ cm}^3/\text{min}}{0.15899 \text{ m}^3/\text{D}}\right)$$

$$= 6.72 \frac{\text{cm}^3/\text{min}}{\text{m}^3/\text{D}} \quad \text{.....(4.37)}$$

Since the range of the injection rate for the element of symmetry in the five-spot pattern was between 20 m^3/D, thus the range of the injection rate of the model should be 130 ml/min.

5. Experimental Apparatus and Procedure

5.1 Experimental Apparatus

The following chapter describes the apparatus, materials, and procedures used in this study. Detailed discussion of the experimental procedures involved in packing and saturating the models, as well as those involved in conducting the experiments is also included. Figure 5.1 gives a schematic illustration of the apparatus used in conducting the experiments of this study. The essential components of the apparatus are: the scaled physical model, steam injection system, model cart and rail system, cold storage unit, produced fluids collection system, data acquisition system, and the visual model.

5.1.1 Scaled Physical Model

The scaled physical model used in this study represents one-quarter of an imaginary two-hectare (5.4-acre) five-spot pattern having the dimensions of 65.5 m ×65.5 m× 52.5 m (thick). The model is made of aluminum. The model is open at the top and the bottom in order for two granite blocks, which represent the overburden and the underburden to be in a direct contact with the reservoir. Styrofoam plates are attached to the four sides to prevent heat losses through these sides. The scaled physical model has the following dimensions: 0.38 m× 0.38 m× 0.305 m (thick). Three positions (the upper position, middle position, and lower position) are available for mounting the wells in different vertical levels. Altogether, 36 thermocouples were placed at different positions inside the model to monitor the reservoir temperature during the experiment. The thermocouples were divided into groups; each group is placed along certain vertical level of the sides of the model. Two pressure transducers and two thermocouples were used to monitor the temperature and the pressure at the injection and the production wells.

5.1.2 Visual Model

A visual model, which had been used in previous studies for different purposes, was utilized in this study to visualize the growth of the steam chamber and the mechanism of oil drainage in the SAGD process. In addition, these experiments were meant to be a helpful tool in designing the experiments in the scaled physical model. This visual model is made from Lucite, and its dimensions are: 40.32 cm× 14.61 cm× 40.32 cm (thick).

The visual model has three openings for mounting the wells: one near the top of the model, and one in the middle, while the other near to the bottom of the model. Having three openings was helpful in representing various configurations of the SAGD process. The model can be opened from the top and the bottom for packing and clean-

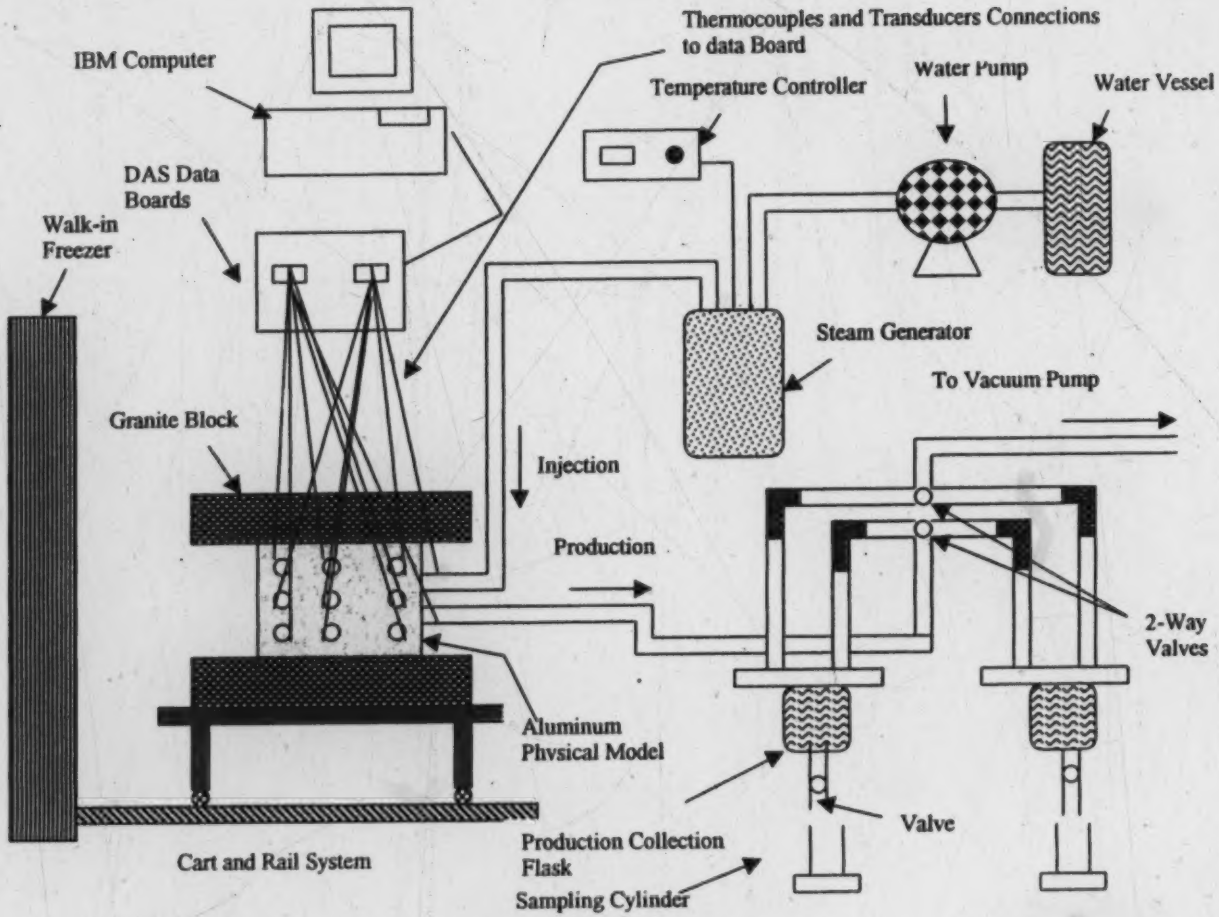

Figure 5.1-The Experimental Apparatus Used in This Study.

ing. Six thermocouples were inserted in pre-existed openings for the purpose of acquiring thermal data.

5.1.3 Porous Media

Based on the scaling criteria the model permeability should be 1293 darcies. To satisfy the scaling requirement, three different sizes of glass beads were used as the porous media in the all experiments of this study, these sizes are listed in Table 5.1.

5.1.4 Model Fluids

Figure 5.2 shows the viscosity-temperature relationship for the model oil (Faxam-100) and the prototype oil. The viscosity-temperature relationship for the model oil was obtained from Matthias (1993), while the viscosity-temperature data for the prototype was obtained from Chu (1975.) It was found that Faxam-100 oil behavior matches closely to that of the prototype oil, and it was selected to represent the prototype oil.

In the visual model experiments, using Faxam-100 oil, which had a yellowish color, did not give a good contrast in visualizing the oil-steam interface. In solving this problem, a blue dye was used to make the oil dark in order to have a sharp contrast between the oil-steam interface. Using the same oil in the visual model experiments as the one used in the scaled physical model was necessary.

5.1.5 Model Cart, Rail System, and Cold Storage Compartment

The scaling criteria dictate that the initial temperature of the scaled physical model had to be 3°C, to accomplish this, a castor-equipped support cart and a rail system were needed. The cart and the rail system made it easy to transport the scaled physical model from the refrigerator to a location near the production system. The support cart was equipped with a gearbox and a rack and pinion system, which allowed the scaled physical model to be tilted to about 45°. This system made it possible to run the experiments, simulating dipping reservoirs, although this subject was not part of this research. Placement, lifting and lowering of the upper granite block from above and onto the top of the scaled physical model was accomplished using a hydraulic hoist system.

5.1.6 Production System

The production collection system consisted of a vacuum pump, a mercury manometer, two plastic vacuum trap collection containers equipped with a fluid level indicator tube, and a pressurized discharge system, to evacuate the produced fluids from the traps. The two traps were designed in a certain way to allow each one to operate independently from the other. The pressurized discharge line was used to inject air into the collection traps in order to shorten the time needed to drain each collection trap.

Table 5.1: The Sieve Analysis for the Glass Beads used in the Experiments of this Study.

Sieve Opening (mm)	Weight of glass beads (gm)	% by Weight
3.35	14.63	4.63
3.35 to 2.36	298.73	94.5
2.36 to 2.00	0.65	0.206
-2	1.95	0.62

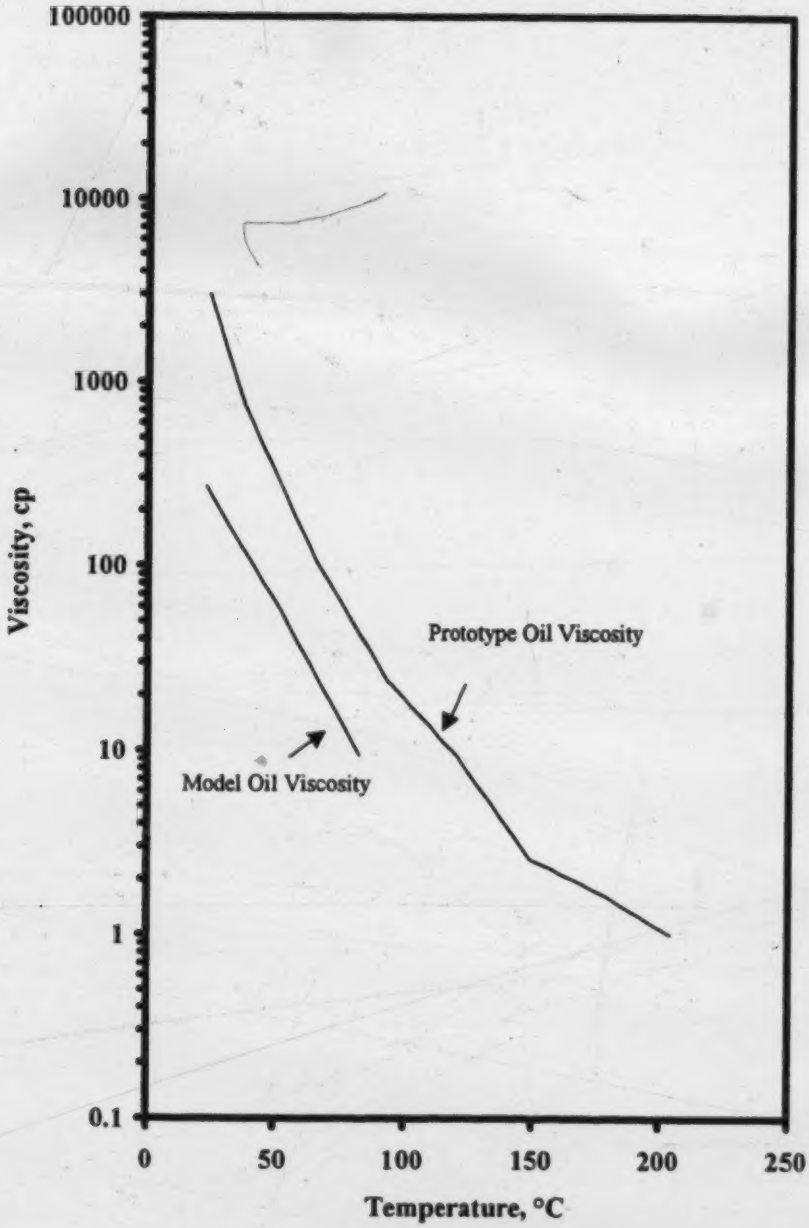

Figure 5.2 -Viscosity-Temperature Relationships for the Prototype Oil and the Model Oil.

5.1.7 Injection System

One of the most important factors in the success of steam injection projects is good control of the injected steam. The steam injection system consisted of one 20-litre vessel containing feed water, one Milroyal controlled volume pumps, a low-pressure boiler. The pump transported room temperature water from the 20-litre vessel to the steam generator, the generated steam moved along the insulated line to the injection point and into the model.

5.1.8 Data Acquisition System

The data acquisition system consisted of a personal computer equipped with a Das-8 card, eight EXP-16 multiplexers, one ten-channel Validyne board and the Labtech Notebook Software. The thermocouples were connected directly into four of the EXP-16 boards. The pressure transducers were connected to a Validyne board. All the EXP-16 boards were connected to the Das-8 card in the computer. The Labtech Notebook Software processed all raw thermocouples and pressure transducers data in millivolts and converted them to a real values of temperatures in (°C), pressure data in (kPa), and time in (seconds). The sampling rate of the raw temperature and the pressure data was every 30 seconds, in order to monitor the change in the temperature profile over a short period of time. The acquired experimental data were stored in ASCII file format, which was read by Lotus 1-2-3, and then analyzed using Surfer ™.

5.2 Preparation of the Scaled Physical Model for an Experiment

5.2.1 Packing Procedure

Due to the large size of the model, it took two weeks to prepare for and to run a single run. At the end of each experiment, the upper granite block was lifted and the unpacking of the model began. All the glass beads had been taken out of the model into the perforated plastic containers. In order to make the cleaning process easier, the model was flipped over and taken aside to clean the bottom granite block. Following this, the O-rings were placed in the grooves along the bottom four flanges, and vacuum grease was spread over them (to help in the sealing).

Then the model was placed on the surface of the bottom granite block. Prior to the start of the packing process, the horizontal wells were mounted in the right positions according to the well configuration of the experiment to be conducted. At this stage the model was ready to be packed. Due to the shape, size, and weight of the model, it was not possible to use either a vibrator or a particle distributor to uniformly and tightly pack the glass beads inside the model. Once the model was filled with glass beads to the top, the extra beads were scraped off until the beads pack was leveled with the sides of the model. Then the O-rings were placed into the grooves of the upper wings and the vacuum grease was spread over them. Finally the upper granite block was lowered on the top of the model.

5.2.2 Saturation Process

Once the model had been packed and the upper granite block lowered on the top of the model, a vacuum was applied to the model. This vacuum was maintained during the whole duration of the saturation, cooling, and conducting the experiments processes. Once we felt a good seal had been established across the contact surface between the model and the granite blocks, a vacuum was applied in order to evacuate the air trapped inside the model.

Water, which was at the atmospheric pressure, was imbibed into the pore spaces inside the model. The pore volume was determined by the difference between the initial volume of the container water and the volume remained.

After finishing saturating the model with water, Faxam-100 oil was injected from the top of the model at a low rate in order to have a stable front, ensuring that all the water but the irreducible be displaced out of the model. The oil displacement continued until a continuous oil phase appeared out of the lower port of the model; at this point, the oil injection was stopped.

In the saturation process, the oil was considered incompressible; therefore the amount of oil in the model was equal to the amount of the displaced water. By knowing the pore volume and irreducible water volume inside the model, the initial oil and water saturations can be determined. Finally, the saturated model was pushed into the cooler and left there for 24 hours in order to lower its temperature to 3°C as dictated by the scaling criteria.

5.2.3 Packing and Saturating the Visual Model

The first step prior to packing the visual model, involved mounting the horizontal wells in the right position as required by the type of the experiment to be conducted. The top cover of the visual model was removed and the glass beads, of the same size of those used in packing the scaled physical model, poured into the model manually. Once the model had been filled to the top, it was shaken carefully in order to have a tight pack. Then the extra glass beads were scrapped off and leveled with the top of the model.

Due to the unavailability of saturation ports in this model and due to the purpose of these experiments, a simpler procedure was used to saturate the model. This was done by vacuuming the model through one of the wells, then the oil was imbibed into the model through the same well from a known-volume container.

5.3 Conducting the Experiments

Once the temperature of all the thermocouples of the model were checked and were 3 °C, some preparations had to be done prior to the start of the experiment. The water vessels were filled with water, and the Milroyal pump should set at the injection

rate required by the scaling criteria, the steam generator had to be set at the required temperature and left running at that temperature for an hour. This was done to stabilize the steam generator output and to let the heat losses, through the injection line, to reach steady-state. Then the model was wheeled out of the cooler, and the connections of the thermocouples and pressure transducers were made. The pressure transducers were calibrated; at the same time the data acquisition program (Labtech Notebook Software) was activated in order to check the consistency of the readings of the temperatures and the pressures. In case there was any inconsistency in the pressure and the temperature readings, changes in the connections had to be made. Once all the readings were consistent, the vacuum production pump was turned on, and the two production traps and the production line were evacuated. When the vacuum pressure of the production pump had reached about 13.8 kPa, the production line was connected to the production well, at the same time the steam injection line was connected to the injection well and the data acquisition program was reactivated. Production sample was collected every 7 minutes.

In the hot water injection experiments the procedure was slightly different. In those experiments, which had a hot water injection at the beginning, the steam generator was set at a low temperature (60°C) in order to have only hot water entering the model. After 0.5 PV of steam (CWE) had been injected, the steam generator setting is raised to the required steam temperature.

In those experiments, which had a hot water injection towards the end, the production and the injection lines were disconnected from the model. Then the steam generator was turned off, and the water feed pump was set at a high rate in order to accelerate the cooling of the steam generator to the required temperature of the hot water. Once the temperature of the steam generator had declined to the hot water temperature, it was turned on again and the production and the injection lines were reconnected to the model, and the experiment was resumed again.

5.4 Data Analysis

The collected samples of oil-water emulsions were left for one week after each experiment to separate. Once the oil and water had been separated, the volumes of each were recorded and copied to a spreadsheet to be used in the production history analysis. The following variables were then plotted as a function of the pore volume injected: cumulative oil recovery as a percent of the original oil in place (OOIP), instantaneous oil production rate, cumulative oil-steam ratio (COSR), and instantaneous water-oil ratio (WOR).

The acquired temperature data during the various experiments were analyzed using a contouring package (SURFER). The SURFER package has powerful features like gridding, contouring, imaging, volume calculations. The first step in creating a contour map is to form a regular spaced grid out of the irregular spaced data using the grid menu of the SURFER Package. Once a grid file had been created, then either a contour map or an image could be formed out of the same grid file using the MAP

Menu in the SURFER Package. SURFER has other useful menus like the VOLUME MENU, which can be used in calculating the volumes of a contoured surface. The volume determination was useful in the heat balance calculations.

6. Experimental Results and Discussion

The objectives of this study were: (1) testing the performance of the different configurations of the SAGD process in conventional heavy oil reservoirs (2) investigating the effectiveness of implementing a hot waterflood either before and/or after a SAGD process (3) testing the suitability of the SAGD process specifically to Kern "A" Reservoir (Kern-River Field). The following experiments were analyzed and discussed: SAGD experiments, experiments in which a hot waterflood was implemented prior to the SAGD, and experiments in which hot waterflood was implemented after the SAGD. Figure 6.1 shows the wells configuration used for the SAGD experiments and they were: injector/producer configurations: injector in the upper position and producer in the middle position, injector in the upper position and the producer in the lower position, and injector in the middle position and producer in the lower position. Those experiments in which a hot waterflood was implemented either at the begging or toward the end of the experiment were conducted only for the first two well configurations.

6.1 Presentation of Results

In this study seventeen experiments were conducted. Three of these runs were conducted in a visual unscaled model, to visualize the growing of the steam chamber and the oil displacement process in the SAGD process and to be as a guidance tool in designing the experiments, to be conducted in a scaled physical model. Three preliminary runs were conducted in the scaled physical model for the purpose of testing the apparatus and to ensure that the operating conditions were according to the ones dictated by the scaling criteria. The rest of the experiments were conducted to test the above mentioned objectives. Figure 6.1 illustrates schematically the experiments performed in this study. Table 6.1 presents a summary of the experimental results and the pertinent initial model properties, such as porosity and initial fluid saturations.

The discussion of the experimental results was based on the analysis of the production and injection data, as well as the thermal data. The data analysis of each run included the preparation of a table showing all of the important experimental parameters and a listing of the production as a function of the volume of the steam (CWE) injected. Plots of the cumulative oil recovery as a percent of the original oil in place (OOIP), the instantaneous oil percent, the cumulative oil-steam ratio (COSR), and the water-oil ratio (WOR) versus the cumulative pore volume of steam (CWE) injected. The thermal data from the thermocouples were used to generate contour maps of the temperature distribution inside the model. Because some of the thermocouples have the same (X, Y) coordinates, they were divided into two groups. Each group was used to generate a contour map for the temperature distribution of the front view of one half of the model (one for the first half and the other for the second half). These contour maps were generated at 0.25, 0.50, 1.00, and 1.50 PV of steam (CWE) injected. The generated contour maps were used to monitor the size and the shape of the steam chamber at various times of the experiment.

6. Experimental Results and Discussion

The objectives of this study were: (1) testing the performance of the different configurations of the SAGD process in conventional heavy oil reservoirs (2) investigating the effectiveness of implementing a hot waterflood either before and/or after a SAGD process (3) testing the suitability of the SAGD process specifically to Kern "A" Reservoir (Kern-River Field). The following experiments were analyzed and discussed: SAGD experiments, experiments in which a hot waterflood was implemented prior to the SAGD, and experiments in which hot waterflood was implemented after the SAGD. Figure 6.1 shows the wells configuration used for the SAGD experiments and they were: injector/producer configurations: injector in the upper position and producer in the middle position, injector in the upper position and the producer in the lower position, and injector in the middle position and producer in the lower position. Those experiments in which a hot waterflood was implemented either at the begging or toward the end of the experiment were conducted only for the first two well configurations.

6.1 Presentation of Results

In this study seventeen experiments were conducted. Three of these runs were conducted in a visual unscaled model, to visualize the growing of the steam chamber and the oil displacement process in the SAGD process and to be as a guidance tool in designing the experiments, to be conducted in a scaled physical model. Three preliminary runs were conducted in the scaled physical model for the purpose of testing the apparatus and to ensure that the operating conditions were according to the ones dictated by the scaling criteria. The rest of the experiments were conducted to test the above mentioned objectives. Figure 6.1 illustrates schematically the experiments performed in this study. Table 6.1 presents a summary of the experimental results and the pertinent initial model properties, such as porosity and initial fluid saturations.

The discussion of the experimental results was based on the analysis of the production and injection data, as well as the thermal data. The data analysis of each run included the preparation of a table showing all of the important experimental parameters and a listing of the production as a function of the volume of the steam (CWE) injected. Plots of the cumulative oil recovery as a percent of the original oil in place (OOIP), the instantaneous oil percent, the cumulative oil-steam ratio (COSR), and the water-oil ratio (WOR) versus the cumulative pore volume of steam (CWE) injected. The thermal data from the thermocouples were used to generate contour maps of the temperature distribution inside the model. Because some of the thermocouples have the same (X, Y) coordinates, they were divided into two groups. Each group was used to generate a contour map for the temperature distribution of the front view of one half of the model (one for the first half and the other for the second half). These contour maps were generated at 0.25, 0.50, 1.00, and 1.50 PV of steam (CWE) injected. The generated contour maps were used to monitor the size and the shape of the steam chamber at various times of the experiment.

NOTE TO USERS

Page(s) not included in the original manuscript and are unavailable from the author or university. The manuscript was microfilmed as received.

35

This reproduction is the best copy available.

UMI

Table 6.1: Summary of the Experiments Conducted in this Study

Run#	Model Type	Run Type	Porosity (%)	Oil Type	Soi (%)	Swi (%)	Oil Rec.	PV inj
101	Visual	I/P in U/L (SAGD)		Faxam-100				
102	Visual	I/P in M/L (SAGD)		Wainwright				
103	Visual	I/P in M/L (SAGD)		Faxam-100				
104	Scaled Model	I/P in U/M (SAGD)		Faxam-100				
105	Scaled Model	I/P in U/L (SAGD)		Faxam-100				
106	Scaled Model	I/P in U/L (SAGD)		Faxam-100				
107	Scaled Model	I/P in U/M (SAGD)	36.6	Faxam-100	95.3	4.7	61	2.00
108	Scaled Model	I/P in U/L (SAGD)	36.3	Faxam-100	94.5	5.5	85	1.96
109	Scaled Model	I/P in U/L (SAGD/HWF)	36.3	Faxam-100	95.3	4.7	74	1.65
110	Scaled Model	I/P in U/L (SAGD/HWF)	36.3	Faxam-100	96.9	3.1	56	1.58
111	Scaled Model	I/P in U/L (SAGD)	36.1	Faxam-100	94.5	5.5	53	1.58
112	Scaled Model	I/P in U/L (SAGD)	36.2	Faxam-100	98.5	1.5	47	1.50
113	Scaled Model	I/P in U/L (SAGD)	37.2	Faxam-100	95.8	4.2	72	1.60
114	Scaled Model	I/P in U/L (SAGD/HWF)	37.1	Faxam-100	92.0	8.0	64	1.62
115	Scaled Model	I/P in M/L (SAGD)	37.2	Faxam-100	91.9	8.1	83	2.00
116	Scaled Model	I/P in M/L (HWF/SAGD)	37.2	Faxam-100	93.6	6.4	59	1.54
117	Scaled Model	I/P in M/L (SAGD/HWF)	36.1	Faxam-100	92.9	7.1	61	1.59

Legend: I/P – Injector/Producer M/L – Middle/Lower SAGD – Steam-Assisted Gravity Drainage
U/L – Upper/Lower U/M – Upper/Middle HWF – Hot Waterflood

6.2 Steam Chamber Volumes

The pressure inside the model was not known with a high degree of certainty; as consequence, the limits of the steam chamber cannot be exactly determined. In Appendix B steam zone calculations using Marx-Langenheim model and Neuman's model are presented. The steam zone volumes resulting from the above models were compared with the experimental steam chamber volumes for confirmation. The Marx-Langenheim model is based on frontal displacement, while Neuman's model is a gravity override model.

The volumes of the various isotherms, as determined by Surfer™ (contouring package) based on assumption of pressure distribution inside the reservoir, were compared with the volumes calculated using Marx-Langenheim's model and Neuman's model. Results from Marx-langenheim's model showed a large discrepancy with those obtained experimentally. This difference is believed to be due to the gravity override of the steam. On the other hand, Neuman's model gave comparable results to the experimental volumes. Figure 6.2 shows a comparison between the theoretical volumes and the experimental ones. It was found that the volume enclosed by the 70°C temperature contour gave the best match to the Neuman's model, as a consequence, the volume enclosed by the 70°C isotherm was considered the steam chamber limits.

6.3 Heat Balance

Knowledge of where does the heat injected went is crucial in analyzing the economic feasibility of any thermal recovery project. Heat balance calculations help to determine the heat distribution inside the model along with the heat lost to the overburden and the underburden, as well as the heat carried out of the model in the produced fluids. The overall heat balance equation at any time, t, is given by:

$$Q_{inj} = Q_{production} + Q_{loss} + Q_{form} \quad \text{.....(6.1)}$$

Q_{inj} = Amount of Energy Injected, (kJ)

$Q_{production}$ = Amount of Energy Pr oduced, (kJ)

Q_{loss} = Amount of Energy Lost to the Overburden and the Underburden, (kJ)

Q_{form} = Amount of energy accumulated in the mod el; the matrix and reservoir fluids, (kJ)

Run 115 (a base case run) was chosen for sample heat balance calculations. An instant in time during the experiment was chosen for the heat balance calculations. The instant chosen was at 1.00 PV of steam (CWE) injected. This time was chosen on purpose, because it was prior to the steam breakthrough time. It is hard to apply the heat

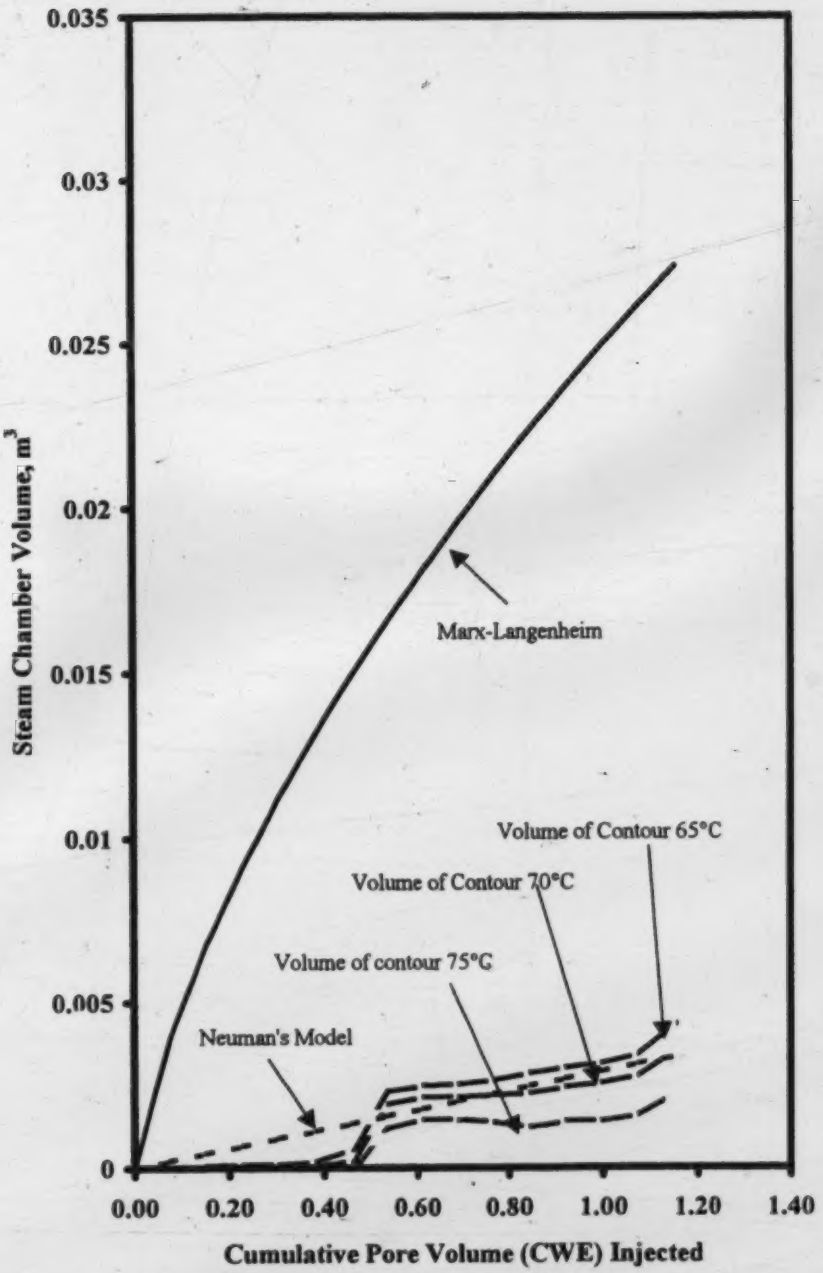

Figure 6.2 -The Steam Zone Volume Obtained from Neuman's Override Model, Marx-Langenhiem Model, and the Experimental results.

balance calculations after steam breakthrough, due to the difficulty of determining the energy produced. A detailed illustration of the heat balance calculations is presented in Appendix A. The following results of the heat calculations were obtained,

$$Q_{produced} = 3495 \text{ kJ}$$
$$Q_{loss} = 2078 \text{ kJ}$$
$$Q_{form} = 4618 \text{ kJ}$$
$$Q_{inj} = Q_{produced} + Q_{loss} + Q_{form}$$
$$= 3495 + 2078 + 4527 = 10{,}191 \text{ kJ}$$

This value of 10,191 kJ of injected heat compared favorably with the value of 9761.5 kJ, calculated using equation A1 (Appendix A). It can be seen that the percentage of the heat lost to the overburden and underburden was 20% of the total heat injected, this is much lower than had been expected (50%).

6.4 Base Case Experiments

Runs 107, 108, and 115 were the base case experiments in this study. In these experiments, 10% quality steam was injected at a rate of 180 cc/min for the whole duration of the run, unlike the other experiments in which a hot waterflood had been implemented either at the beginning of the run or toward the end. These runs were conducted to examine the performance of the different well configurations of SAGD, and to serve as base case for the other experiments. The only major difference between these runs was the well configurations (the positions of the producer and the injector.) In Run 107, the injector was in the upper position and the producer in the middle position. In Run 108; the injector was in the upper position and the producer in the lower position. In Run 115, the injector was in the middle position and the producer was in the lower position.

6.4.1 A Base Case Experiment

Because the general trend of the production performance of the base case experiments was similar, the results of only one run are discussed in detail. A comparison between the base case experiments will be presented later in this chapter. The base case run (Run 115) was chosen to be discussed in detail. The porosity of the pack was 37.2%, and the initial oil saturation was 91.9%. Figure 6.3 shows the production history of this run and Table 6.2 presents the production and the injection data. The oil cut in the production sample started at a relatively high value (41%), dropped to 23% at about 0.15 PV of steam (CWE) injected. It then, started to increase and reached the 30% range at about 0.23 PV of steam (CWE) injected. It remained fluctuating at this range up to the steam breakthrough time (at about 1.48 PV of steam (CWE) injected), at this point it started to decline, and was 14% at the end of the experiment (about 2.0 PV of steam CWE injected). The relatively high oil production at the beginning of the experiment was probably due to the more contact the steam had with the reservoir. Once the steam chamber had formed, it started to grow side ways, consistent advancing of the

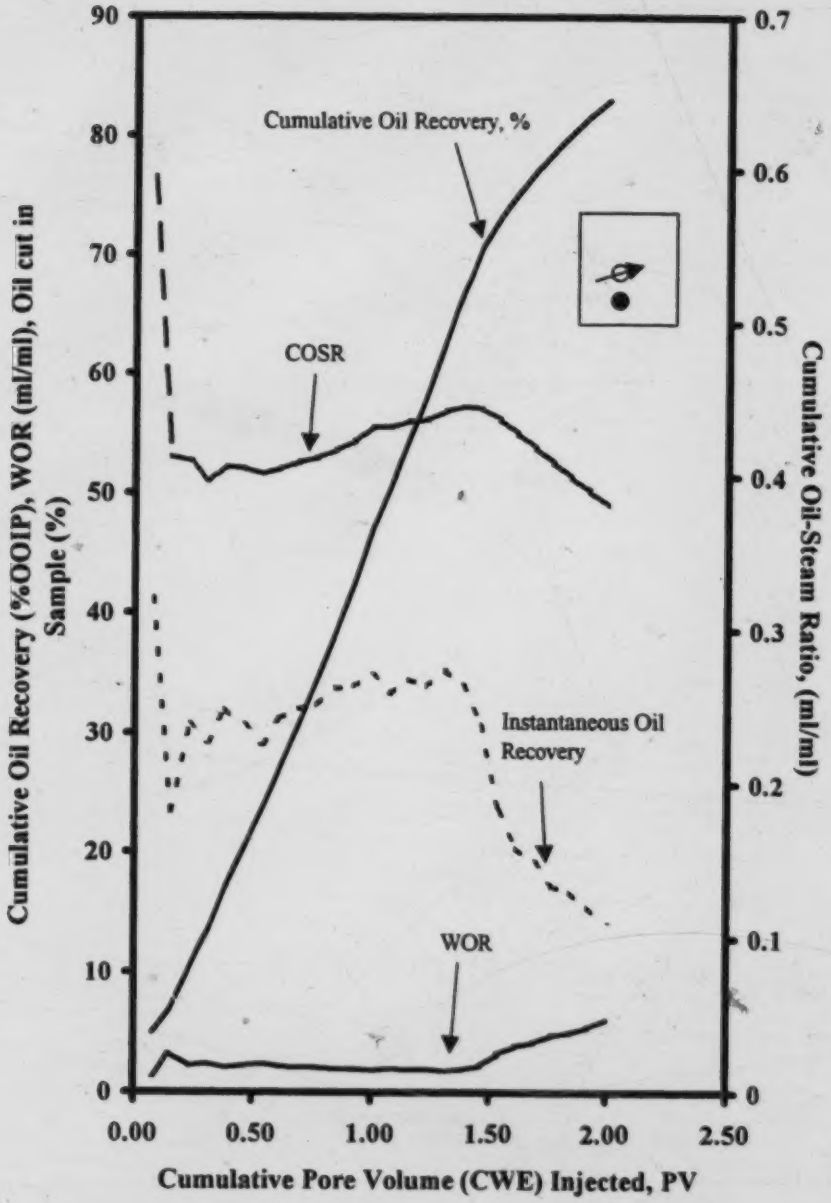

Figure 6.3 - Production History of a Base Case Experiment (Run 115); SAGD Experiment; Injector/Producer in Middle/Lower Position.

Table 6.2-Run 115: SAGD Process, the Injector in the Middle Position and the Producer in the Lower Position.

Experiment Date:	Feb. 16, 1999		
Bulk Volume:	44,042ml		
Pore Volume:	16,380ml	Type of Oil Used:	Faxam 100
HC Pore Volume:	15,050ml	Initial Model Temperature:	3.0C
Porosity:	37.2%	Steam Flow Rate:	180ml/min.
Initial Oil Saturation:	91.9%	Steam Quality:	0.1
Initial Water Saturation:	8.1%	Total Steam Volume Injected:	32,760
Net Oil Recovery:	**83.02**	**Final Oil Saturation:**	**15.5%**

Cylinder No.	Total Vol. Produced (ml)	Instantaneous Oil Prod. (ml)	Cum. Oil Recovery (ml)	Cum. Oil Rec. % OOIP	Instantaneous Produced WOR	% Sample Oleic Phase	Cum. PV Injected
1	1820	750	750	4.98	1.43	41.21	0.08
2	1240	290	1040	6.91	3.28	23.39	0.15
3	1660	510	1550	10.30	2.25	30.72	0.23
4	1540	450	2000	13.29	2.42	29.22	0.31
5	1750	560	2560	17.01	2.13	32.00	0.38
6	1630	500	3060	20.33	2.26	30.67	0.46
7	1650	480	3540	23.52	2.44	29.09	0.54
8	1730	540	4080	27.11	2.20	31.21	0.62
9	1750	560	4640	30.83	2.13	32.00	0.69
10	1700	550	5190	34.49	2.09	32.35	0.77
11	1750	590	5780	38.41	1.97	33.71	0.85
12	1800	610	6390	42.46	1.95	33.89	0.92
13	1980	690	7080	47.04	1.87	34.85	1.00
14	1620	540	7620	50.63	2.00	33.33	1.08
15	1800	620	8240	54.75	1.90	34.44	1.15
16	1680	570	8810	58.54	1.95	33.93	1.23
17	1900	670	9480	62.99	1.84	35.26	1.31
18	1820	620	10100	67.11	1.94	34.07	1.38
19	1760	540	10640	70.70	2.26	30.68	1.46
20	1620	380	11020	73.22	3.26	23.46	1.54
21	1520	310	11330	75.28	3.90	20.39	1.62
22	1460	280	11610	77.14	4.21	19.18	1.69
23	1425	245	11855	78.77	4.82	17.19	1.77
24	1380	230	12085	80.30	5.00	16.67	1.85
25	1420	220	12305	81.76	5.45	15.49	1.92
26	1350	190	12495	83.02	6.11	14.07	2.00

chamber occurred; as consequence, almost constant oil production rate took place up to the time of the steam breakthrough. Once steam breakthrough occurred, the oil rate declined due to the escape of the steam.

The cumulative oil-steam ratio (COSR) started at about 0.6, declined to 0.4 at about 0.15 PV of steam (CWE) injected. It stabilized around this value until about 0.7 PV of steam (CWE) injected. It then started to rise, reached 0.44 at about 1.48 PV of steam (CWE) injected. At that time the steam breakthrough occurred and the COSR started to decline and was 0.38 at the end of the experiment. It was noticed that the drop in the COSR after the steam breakthrough was not as sharp as the drop in the oil rate; this was due to the relatively high production rate prior to the happening of the steam breakthrough. The water-oil ratio started at 1.43, rose to 3.28 at about 0.15 PV of steam (CWE) injected. It remained around 2.0 until steam breakthrough, when it started to increase and reached 6.0 by the end of the run.

Figure 6.4 shows the production and injection temperatures (on the left axis) and the production and the injection pressures (on the right axis) vs. the cumulative pore volume (CWE) injected. The injection pressure started at a relatively high pressure of 96.5 kPa, then the pressure dropped to 52 kPa, this happened at 0.06 PV of steam (CWE) injected, because once the fluid created its path through the reservoir, there was less resistance to the fluid injectivty. The injection pressure remained at this level up to the steam breakthrough time (1.48 PV of steam (CWE) injected) when it declined to 48 kPa and remained around that value to the end of the experiment. The production pressure has a similar trend to the injection pressure, it started relatively high at 90.3 kPa, then at 0.06 PV of steam (CWE) injected, it dropped to 42 kPa. At steam breakthrough it dropped to 37 kPa and stayed there to the end of the run. The behavior of the injection and the production pressures indicated that, once the steam chamber had reached the sideways growth stage, the pressures tend to stabilize.

The injection temperature was 85.4°C at the very beginning of the run, then dropped to 83°C and continued at this temperature to the breakthrough time. At the breakthrough time, it dropped to 78°C and remained at this value to the end of the experiment. The production temperature started at 12°C at the beginning of the experiment and then rose gradually. It reached 40°C after 0.1 PV of steam (CWE) injected and reached 53°C at steam breakthrough and remained there to the end of the run. It was noted that although steam breakthrough had occurred, the produced fluid temperature was still below the steam temperature. This is due to the mixing of the live steam with colder fluids.

6.4.2 Comparison of the Base Case Experiments

Figure 6.5 shows the cumulative oil recovery profile for the three base case experiments (Run 107, Run108, and Run 115). Figures 6.6 and 6.7 illustrate the production history of Runs 107 and 108; Tables 6.3 and 6.4, present the production data of the same runs, are provided here for comparison. It can be seen that Run 108 had the highest oil recovery (85%), followed by Run 115 with 83% recovery, while Run 107 had the lowest recovery (61%). The low oil recovery in Run 107 was due to the smaller res-

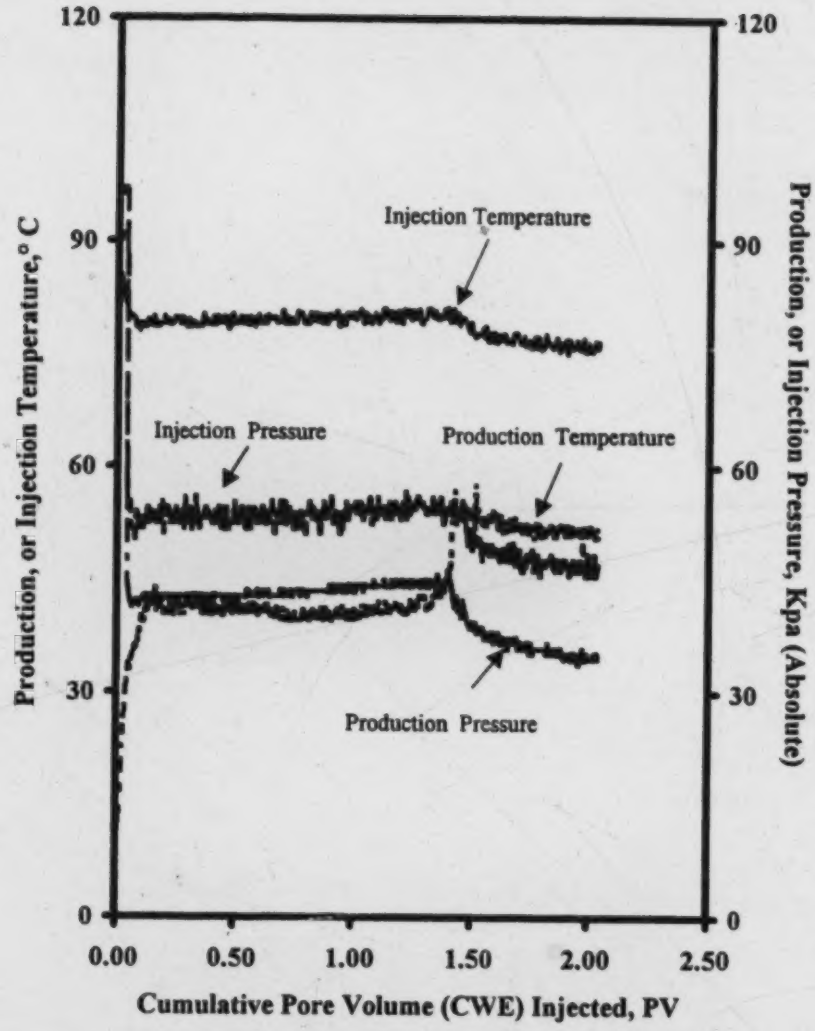

Figure 6.4 - Production History of a Base Case Experiment Run115); Injection and Production Pressure/Temperature vs. Cumulative PV CWE Injected; Injector in the Middle Position and Producer in the Lower Position.

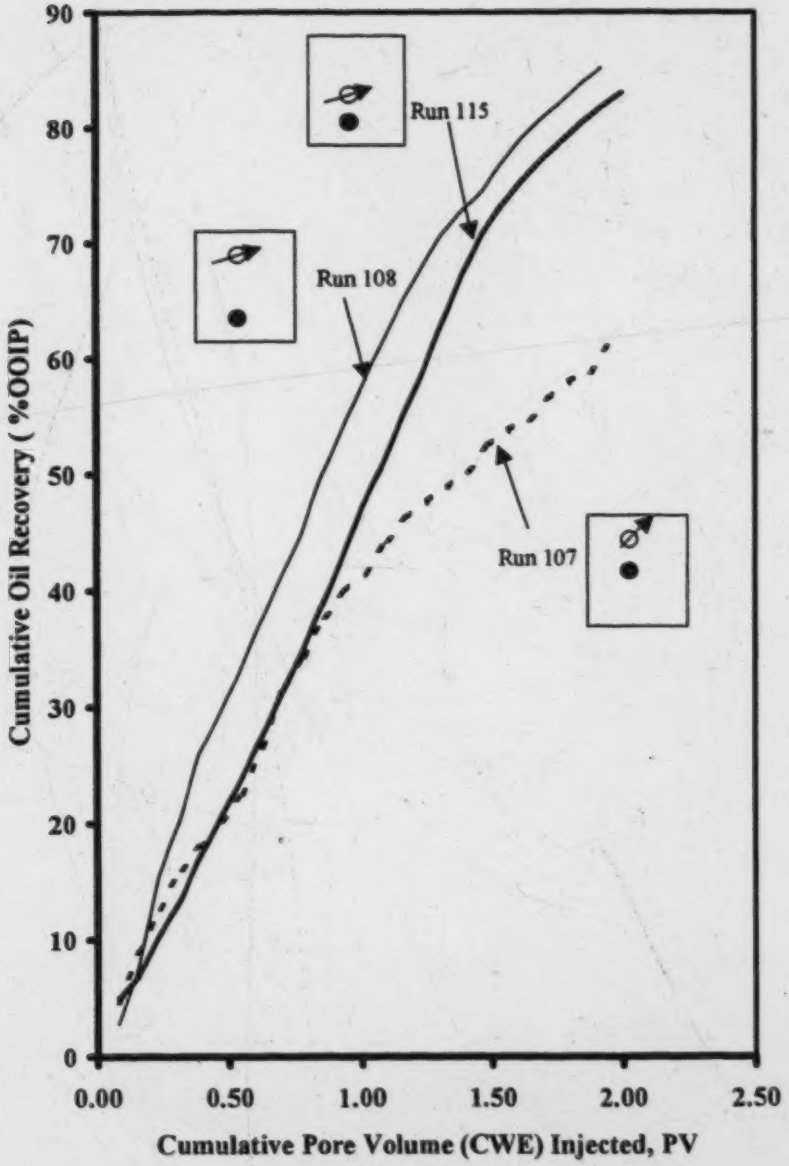

Figure 6.5 - Cumulative Oil Recovery vs. Cumulative PV Injected; the Base Case Experiments, Runs 107, 108, and 115.

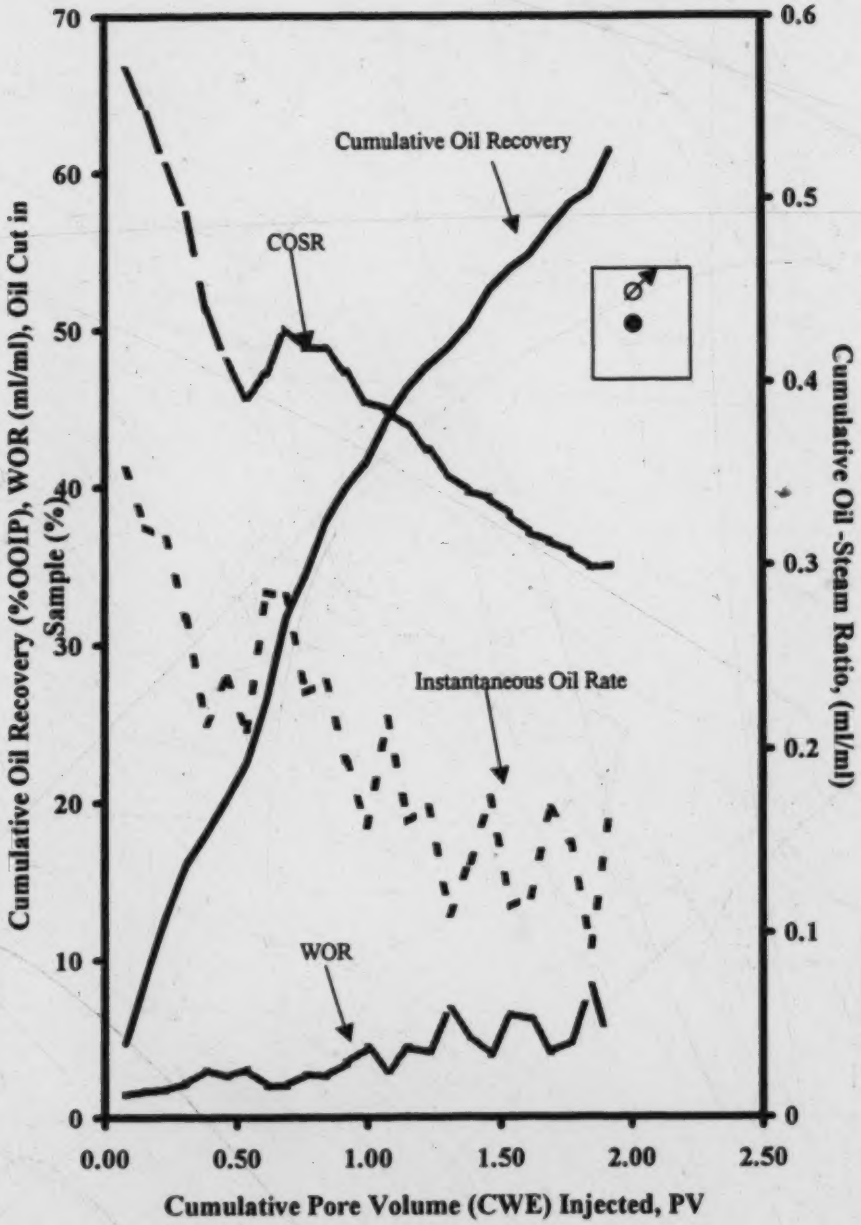

Figure 6.6 - Production History of a Base Case Experiment (Run 107); SAGD, Injector in Upper position and Producer in Middle Position.

Table 6.3-Run 107: SAGD, Producer in the Middle Position, Injector in the Upper Position.

Experiment Date: Oct 27, 1998
Bulk Volume: 44042 ml
Pore Volume: 16,100 ml
HC Pore Volume: 15350 ml
Porosity: 36.60%
Initial Oil Saturation: 95.30%

Type of Oil Used: Faxam 100
Initial Model Temperature: 3.0C
Steam Flow Rate: 180ml/min.
Steam Quality: 10%
Total Steam Volume Injected: 31,500ml

Net Oil Recovery: 60.07%

Final Oil Saturation: 37%

Cylinder No.	Total Vol. Produced (ml)	Instantaneous Oil Prod. (ml)	Cum. Oil Recovery (ml)	Cum. Oil Rec. % OOIP	Instantaneous Produced WOR	% Sample Oleic Phase	Cum. PV Injected
1	1750	720	720	4.69	1.43	41.14	0.08
2	1760	660	1380	8.99	1.67	37.50	0.16
3	1580	580	1960	12.77	1.72	36.71	0.23
4	1640	520	2480	16.16	2.15	31.71	0.31
5	1160	290	2770	18.05	3.00	25.00	0.39
6	1220	340	3110	20.26	2.59	27.87	0.47
7	1420	350	3460	22.54	3.06	24.65	0.55
8	1860	620	4080	26.58	2.00	33.33	0.63
9	2390	790	4870	31.73	2.03	33.05	0.70
10	1520	410	5280	34.40	2.71	26.97	0.78
11	1880	520	5800	37.79	2.62	27.66	0.86
12	1460	330	6130	39.93	3.42	22.60	0.94
13	1350	250	6380	41.56	4.40	18.52	1.02
14	1660	420	6800	44.30	2.95	25.30	1.10
15	1600	300	7100	46.25	4.33	18.75	1.17
16	1120	220	7320	47.69	4.09	19.64	1.25
17	1400	180	7500	48.86	6.78	12.86	1.33
18	1360	220	7720	50.29	5.18	16.18	1.41
19	1680	340	8060	52.51	3.94	20.24	1.49
20	1500	200	8260	53.81	6.50	13.33	1.57
21	1000	140	8400	54.72	6.14	14.00	1.64
22	1380	270	8670	56.48	4.11	19.57	1.72
23	1320	230	8900	57.98	4.74	17.42	1.80
24	1200	130	9030	58.83	8.23	10.83	1.88
25	2000	400	9430	61.43	4.00	20.0C	1.96

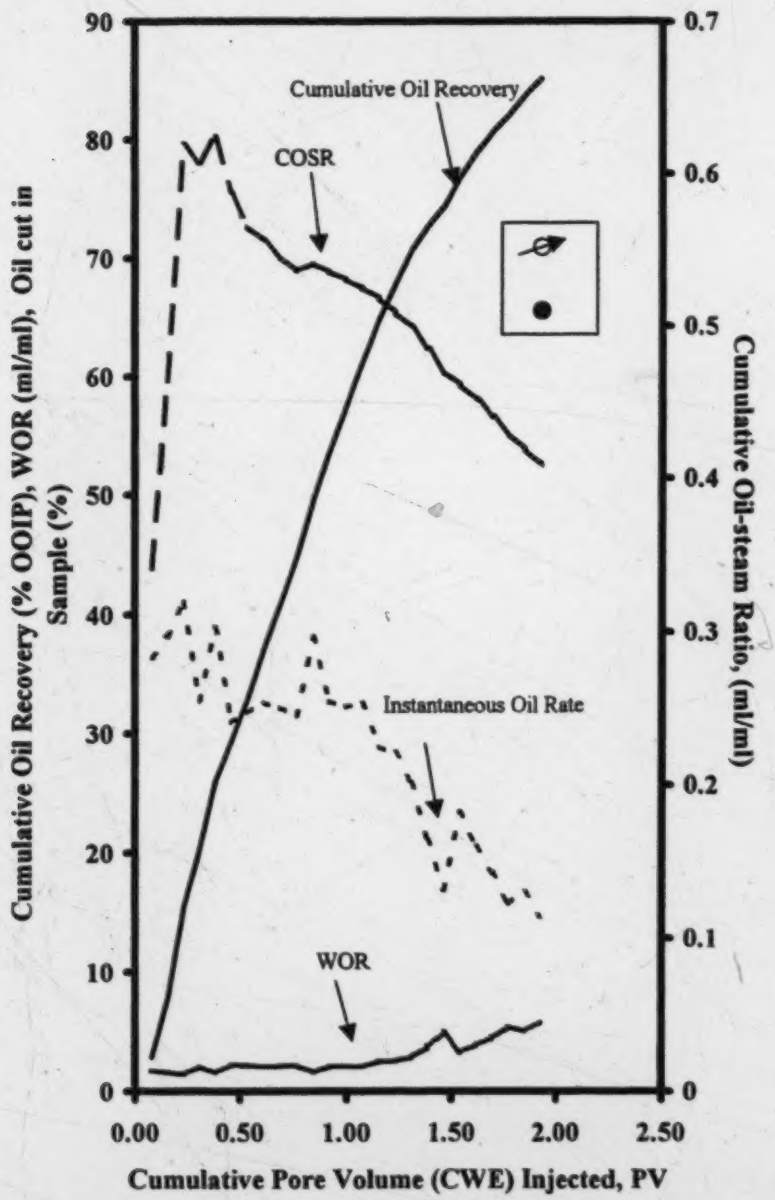

Figure 6.7- Production History of a Base Case Experiment (Run 108); SAGD, Injector /Producer in Upper/Lower Position.

Table 6.4-Run 108: SAGD, Producer in the Lower Position, Injector in the Upper Position.

Experiment Date: Oct.10, 1998
Bulk Volume: 44,042ml
Pore Volume: 16,000ml
HC Pore Volume: 15,120ml
Porosity: 36.3%
Initial Oil Saturation: 94.5%
Initial Water Saturation: 5.5%.

Type of Oil Used: Faxam 100
Initial Model Temperature: 3.0C
Steam Flow Rate: 180ml/min.
Steam Quality: 11%
Total Steam Volume Injected: 31,500ml

Net Oil Recovery: 85.2%

Final Oil Saturation: 14%

Cylinder No.	Total Vol. Produced (ml)	Instantaneous Oil Prod. (ml)	Cum. Oil Recovery (ml)	Cum. Oil Rec. % OOIP	Instantaneous Produced WOR	% Sample Oleic Phase	Cum. PV Injected
1	1180	430	430	2.84	1.74	36.44	0.08
2	1940	740	1170	7.74	1.62	38.14	0.16
3	2850	1170	2340	15.48	1.44	41.05	0.24
4	2200	720	3060	20.24	2.06	32.73	0.32
5	2250	875	3935	26.03	1.57	38.89	0.39
6	1650	510	4445	29.40	2.24	30.91	0.47
7	1700	540	4985	32.97	2.15	31.76	0.55
8	1900	620	5605	37.07	2.06	32.63	0.63
9	1800	580	6185	40.91	2.10	32.22	0.71
10	1810	570	6755	44.68	2.18	31.49	0.79
11	1940	740	7495	49.57	1.62	38.14	0.87
12	1835	600	8095	53.54	2.06	32.70	0.95
13	1830	590	8685	57.44	2.10	32.24	1.02
14	1750	570	9255	61.21	2.07	32.57	1.10
15	1870	540	9795	64.78	2.46	28.88	1.18
16	1620	460	10255	67.82	2.52	28.40	1.26
17	1700	440	10695	70.73	2.86	25.88	1.34
18	1420	300	10995	72.72	3.73	21.13	1.42
19	1480	250	11245	74.37	4.92	16.89	1.50
20	1620	380	11625	76.88	3.26	23.46	1.58
21	1560	320	11945	79.00	3.88	20.51	1.65
22	1420	260	12205	80.72	4.46	18.31	1.73
23	1400	220	12425	82.18	5.36	15.71	1.81
24	1440	240	12665	83.76	5.00	16.67	1.89
25	1430	210	12875	85.15	5.81	14.69	1.97

ervoir volume lying above the horizontal producer; as a result the area available for steam chamber growth prior to reaching the producer, was reduced leading to an early breakthrough and as consequence, a low production rate after breakthrough.

Figure 6.8 shows the cumulative oil-steam ratio (COSR) vs. cumulative pore volume (CWE) injected for the base case runs. It can be seen that Run 108 had COSR around 0.6 at the beginning of the experiment and then started to decline gradually and it was about 0.4 by the end of the run. In Run 107, the COSR started around 0.6 and then begun to decline up to the end of the experiment when it was around 0.3. The COSR of Run 115 started at 0.6 and then declined to around 0.4 and remained at that range up to the steam breakthrough time. At that time it started to drop slightly.

It can be concluded that steam breakthrough time in conventional heavy oil reservoirs undergoing a SAGD process is a function of the amount of the volume of the reservoir above the producer; the smaller the volume, the earlier the breakthrough. It could be concluded that the wells configuration of Run 108 gave the highest oil recovery and best performance, of the cumulative oil-steam ratio.

6.5 A Hot Waterflood Prior to the SAGD Process

In Runs 110 and 116, a hot waterflood was implemented prior to SAGD. In these runs, the hot waterflood had been implemented for the first 0.50 PV of steam (CWE) injected; after this time the SAGD process began and continued to the end of the experiment. The steam quality (10%) and the injection rate (180 cc/min) were the same as those used in the base case experiments. Run 110 corresponded to the base case Run 108, i.e., the injector in the upper position and the producer in the middle position. In Run 110, the porosity of the pack was 36.3%, and the initial oil saturation was 96.6%. Figure 6.9 shows the production history of Run 110, and Table 6.5 presents the production data. In this run the oil percent in the production sample started at 32%, then dropped gradually to the 15% range at about 0.32 PV of steam (CWE) injected. This was probably due to the availability of the oil around the producer at the beginning of the experiment. As the oil becomes less available around the producer the rate declines. The oil percentage in the production sample remained at the 15% range up to the end of the hot waterflood (at 0.50 PV of steam (CWE) injected.) After the start of the SAGD process the oil percentage remained around the 15% range up to the time of 0.87 PV of steam (CWE) injected. Then it rose up to the 30% range and remained there to the end of the experiment (at about 1.58 PV of steam (CWE) injected). The oil percent in the production sample did not rise immediately after the start of the SAGD, because the steam generator took time to reach the required steam temperature. The oil recovery due to the hot waterflood was 12% and that due to the SAGD was 43%. Figure 6.10 shows the production profile of Run 110 and the corresponding base case run (Run 108). In comparing their production performance, it was noticed that the cumulative oil recovery of Run 110 at 1.58 PV of steam (CWE) injected (the end of the experiment) was 56%, while in Run 108 was 77% at the same time. This was due to the low oil rate during the hot waterflood period in Run 110. Up to the end of Run 110, steam breakthrough did not occur, while in Run 108 the steam breakthrough occurred at about 1.2

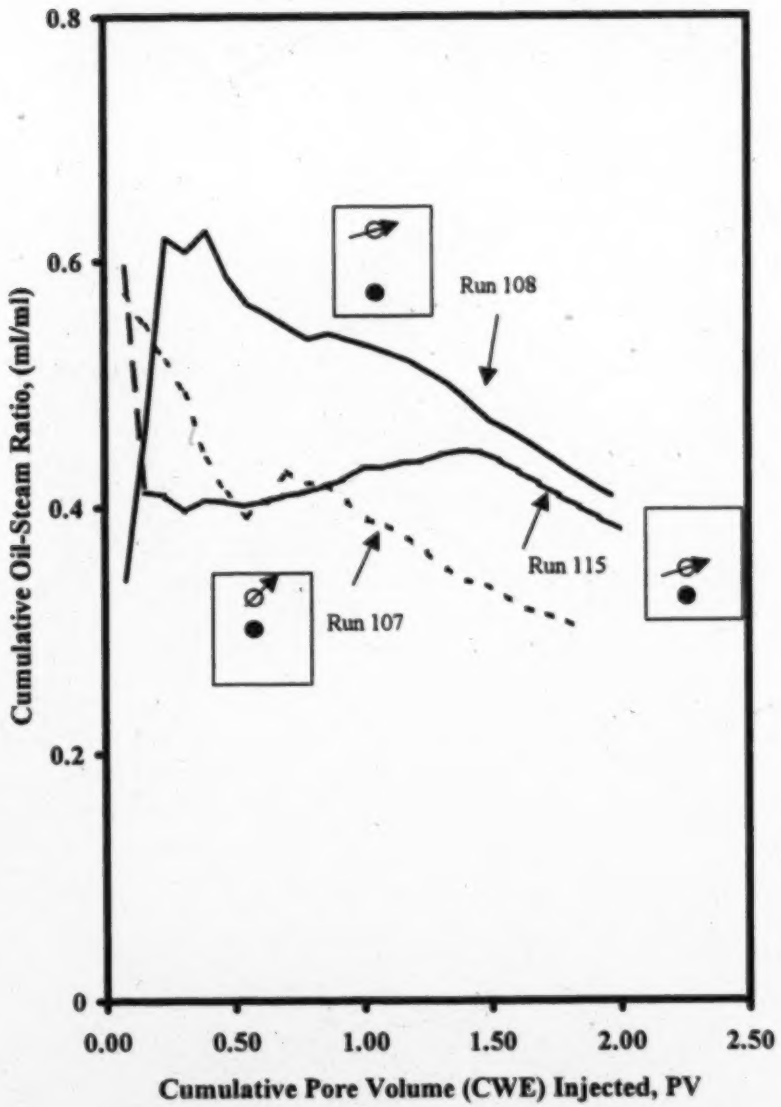

Figure 6.8-Cumulative Oil-Steam Ratio vs. Cumulative PV Injected; the Base Case Experiments, Runs 107, 108, and 115.

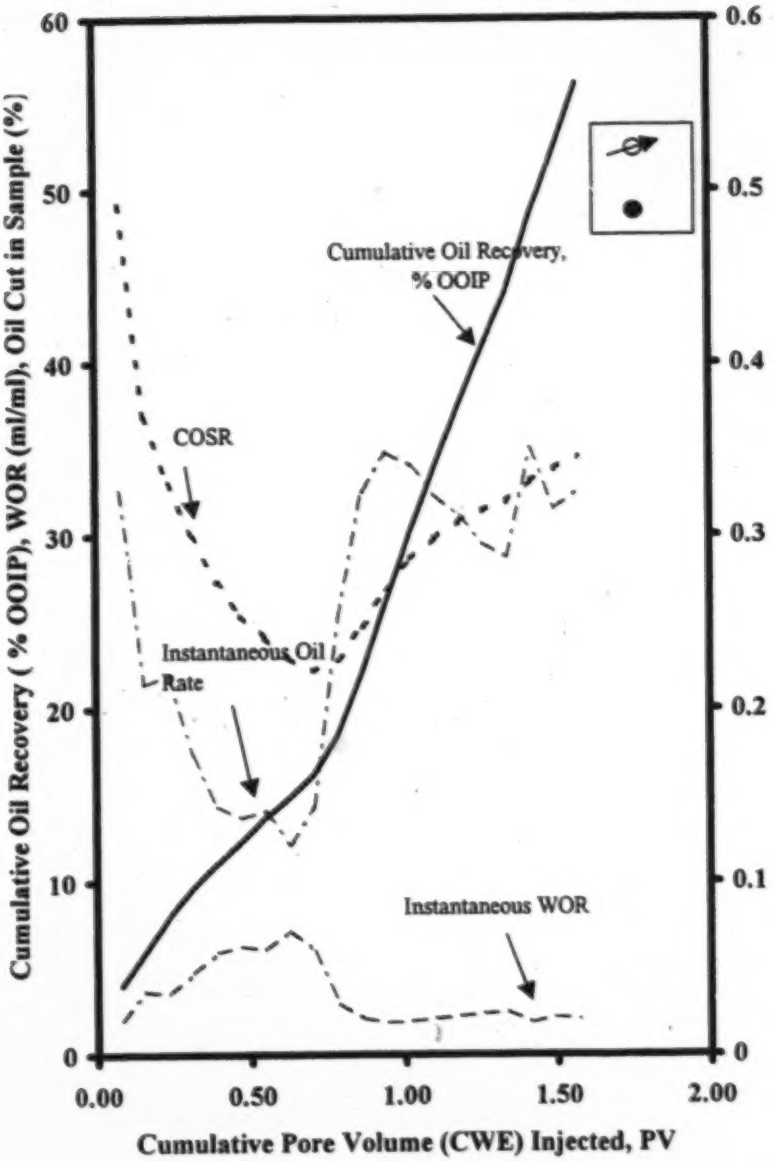

Figure 6.9-Production History of Run 110; Hot Waterflood Followed by SAGD; Injector in Upper Position and Producer in Middle Positions.

Table 6.5-Run 110: Hot Waterflood followed by SAGD, Producer in the Lower Position, Injector in the Upper Position

Experiment Date: DEC.3, 1998
Bulk Volume: 44,042ml
Pore Volume: 16,000ml
HC Pore Volume: 15,500ml
Porosity: 36.3%
Initial Oil Saturation: 96.9%
Initial Water Saturation: 3.1%

Type of Oil Used: Faxam 100
Initial Model Temperature: 3.0C
Steam Flow Rate: 180ml/min.
Steam Quality: 0.1
Total Steam Volume Injected: 25,200

Net Oil Recovery: 56.19

Final Oil Saturation: 42.4%

Cylinder No.	Total Vol. Produced (ml)	Instantaneous Oil Prod. (ml)	Cum. Oil Recovery (ml)	Cum. Oil Rec. % OOIP	Instantaneous Produced WOR	% Sample Oleic Phase	Cum. PV Injected
1	1900	620	620	4.00	2.06	32.63	0.08
2	1450	310	930	6.00	3.68	21.38	0.16
3	1460	320	1250	8.06	3.56	21.92	0.24
4	1500	260	1510	9.74	4.77	17.33	0.32
5	1460	210	1720	11.10	5.95	14.38	0.39
6	1460	200	1920	12.39	6.30	13.70	0.47
7	1490	210	2130	13.74	6.10	14.09	0.55
8	1480	180	2310	14.90	7.22	12.16	0.63
9	1400	200	2510	16.19	6.00	14.29	0.71
10	1470	370	2880	18.58	2.97	25.17	0.79
11	1690	550	3430	22.13	2.07	32.54	0.87
12	1840	640	4070	26.26	1.88	34.78	0.95
13	1820	620	4690	30.26	1.94	34.07	1.02
14	1760	570	5260	33.94	2.09	32.39	1.10
15	1800	560	5820	37.55	2.21	31.11	1.18
16	1760	520	6340	40.90	2.38	29.55	1.26
17	1740	500	6840	44.13	2.48	28.74	1.34
18	1940	680	7520	48.52	1.85	35.05	1.42
19	1840	580	8100	52.26	2.17	31.52	1.50
20	1870	610	8710	56.19	2.07	32.62	1.58

* Line inducates the end of the Hot Waterflood

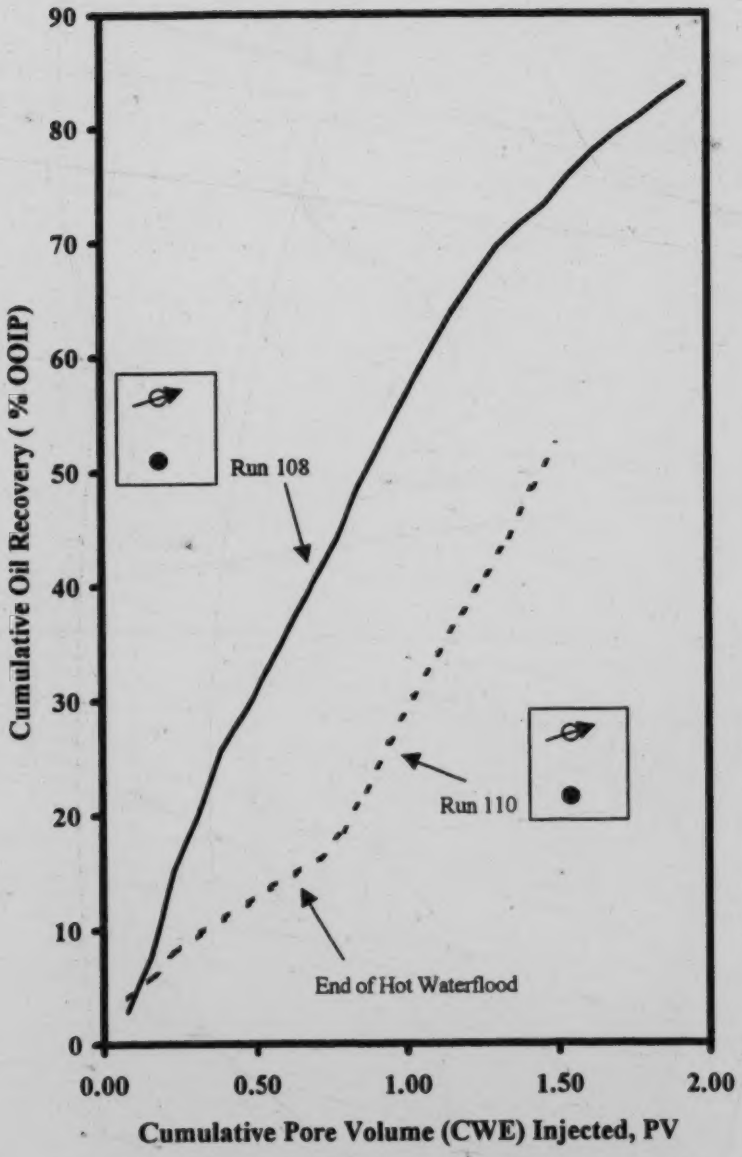

Figure 6.10-Cumulative Oil Recovery vs. Cumulative PV (CWE) Injected; for Runs 108 (SAGD), 110 (Hot Waterflood/SAGD); Injector/Producer in Upper/Lower Position.

PV of steam (CWE) injected. It was not possible to confirm that the steam breakthrough had been delayed in Run 110, because the oil recovery at the steam breakthrough time of Run 108 (about 65%) was higher than the oil recovery at the end of Run 110 (about 56%).

The production performance of Run 116 was generally similar to that of Run 110, thus, the production performance of Run 116 will not be discussed in detail. Only a comparison of the production performance of Run 116 with the production performance of Runs 115 and 110 will be mentioned here. Figure 6.11 and Table 6.6 present the production history of Run 116. Figure 6.13 shows the production profiles of Run 116 and its corresponding base case experiment (Run 115). It can be seen from Figure 6.13 that the cumulative oil recovery as % OOIP of Run 116 was 58% at the end of the experiment (at about 1.54 PV of steam CWE injected), while it was 73% in Run 115 at the same time. The difference in recovery was due to the low oil rate during the hot waterflood. From the production history of Run 116, it was noticed that the steam breakthrough did not occur. It was difficult to say that the steam breakthrough had been delayed in Run 116, because the cumulative oil recovery at the end of Run 116 (59%) was less than the cumulative oil recovery of Run 115 at the time of steam breakthrough (71%).

Figure 6.12 shows the production profile of Runs 116 and 110, It can seen that the effect of the steam injection (SAGD) was felt earlier in Run 116 than in Run 110. In Run 116 the oil percentage in the production sample reached the 30% range at 0.69 PV of steam (CWE) injected, while in Run 110 it reached that range at 0.87 PV of steam (CWE) injected. This was attributed to the location of the injection well in both runs. In Run 116 the injector (in the middle position) was closer to the bottom of the model, i.e., it was closer to the hottest region in the model during the hot waterflood period. Thus a steam chamber was formed earlier in Run 116, as a consequence, the oil recovery was higher in Run 116 (59%) than in Run 110 (56%).

In conclusion, a hot waterflood prior to the SAGD process may have delayed the occurrence of the steam breakthrough. This could not be confirmed unless an experiment, in which oil recovery higher than the one obtained at the steam breakthrough time of the base case runs, was available. In implementing a hot waterflood prior to SAGD, the injector should be as close as possible to the bottom of the reservoir. This will ensure the early formation of the steam chamber after the start of the SAGD, and as a consequence a higher oil recovery will be obtained than in the case where the injector is high in the reservoir.

6.6 SAGD Followed by a Hot Waterflood

In Runs 114 and 117, the SAGD process was followed by a hot waterflood. In these two runs the SAGD process was implemented from the beginning of the experiment up to 1.0 PV of steam (CWE) injected, followed by a hot waterflood to the end of the experiment (about 1.50 PV of steam CWE injected). The steam quality and the rate

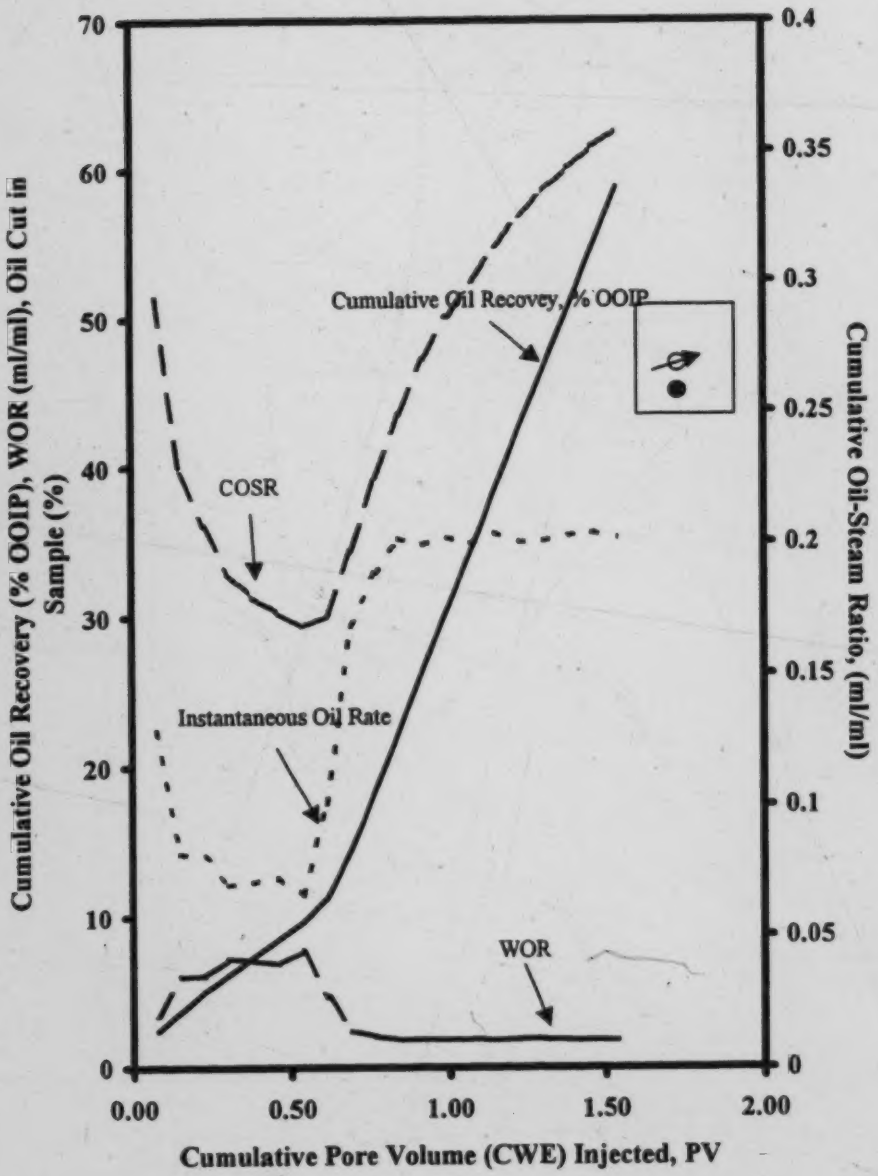

Figure 6.11- Production History of Run 116; a Hot Waterflood Followed by SAGD; Injector/Producer in Middle/Lower Positions.

Table 6.6-Run 116: Hot Waterflood followed by SAGD, Producer in the Lower Position, Injector in the Middle Position.

Experiment Date: Mar.1, 1999
Bulk Volume: 44,042ml
Pore Volume: 16,390ml
HC Pore Volume: 15,340ml
Porosity: 37.2%
Initial Oil Saturation: 93.6%
Initial Water Saturation: 5.4%

Type of Oil Used: Faxam 100
Initial Model Temperature: 3.0°C
Steam Flow Rate: 180ml/min.
Steam Quality: 0.1
Total Steam Volume Injected: 25,200

Net Oil Recovery: 58.8

Final Oil Saturation: 38.6%

Cylinder No.	Total Vol. Produced (ml)	Instantaneous Oil Prod. (ml)	Cum. Oil Recovery (ml)	Cum. Oil Rec. % OOIP	Instantaneous Produced WOR	% Sample Oleic Phase	Cum. PV Injected
1	1650	370	370	2.41	3.46	22.42	0.08
2	1400	200	570	3.72	6.00	14.29	0.15
3	1490	210	780	5.08	6.10	14.09	0.23
4	1400	170	950	6.19	7.24	12.14	0.31
5	1460	180	1130	7.37	7.11	12.33	0.38
6	1420	180	1310	8.54	6.89	12.68	0.46
7	1480	170	1480	9.65	7.71	11.49	0.54
8	1420	250	1730	11.28	4.68	17.61	0.62
9	1700	500	2230	14.54	2.40	29.41	0.69
10	1820	600	2830	18.45	2.03	32.97	0.77
11	1760	620	3450	22.49	1.84	35.23	0.85
12	1810	630	4080	26.60	1.87	34.81	0.92
13	1730	610	4690	30.57	1.84	35.26	1.00
14	1720	600	5290	34.49	1.87	34.88	1.08
15	1770	630	5920	38.59	1.81	35.59	1.15
16	1800	630	6550	42.70	1.86	35.00	1.23
17	1740	610	7160	46.68	1.85	35.06	1.31
18	1750	620	7780	50.72	1.82	35.43	1.38
19	1770	630	8410	54.82	1.81	35.59	1.46
20	1730	610	9020	58.80	1.84	35.26	1.54

* Line indicates the end of the Hot waterflood

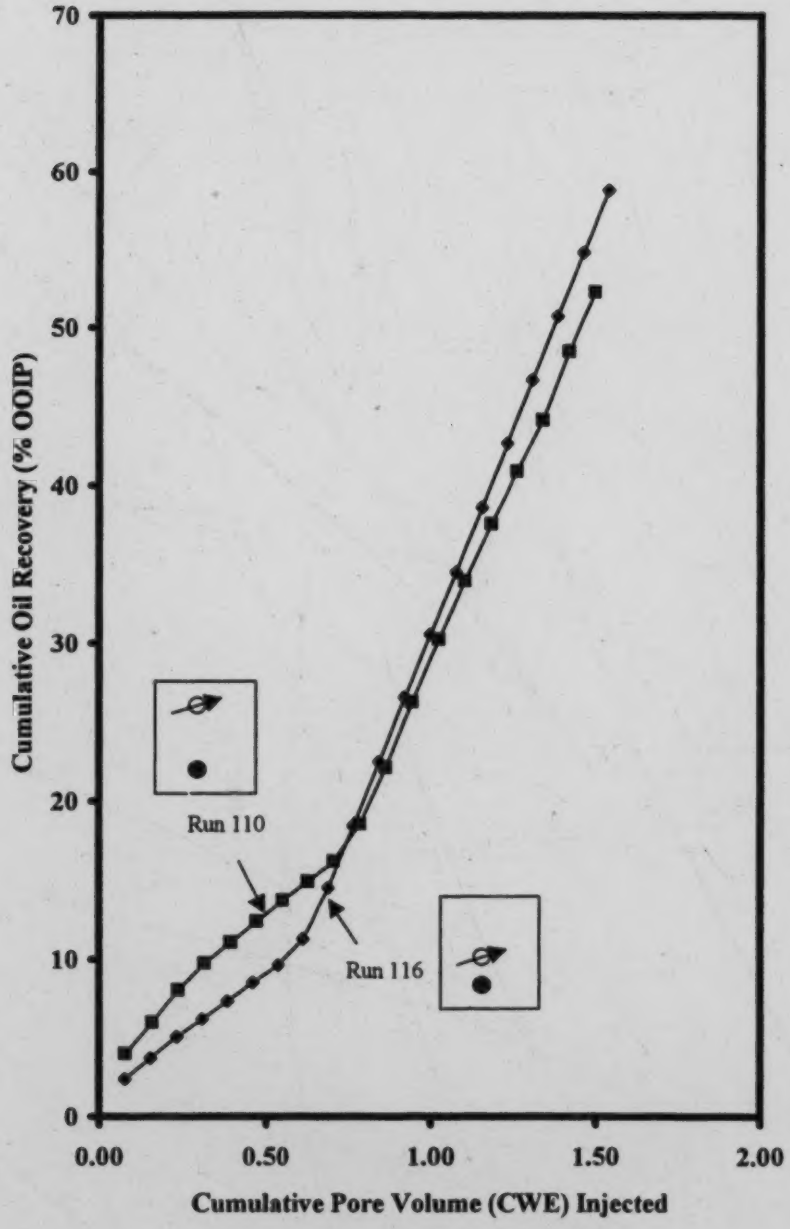

Figure 6.12 - Cumulative Oil Recovery vs. Cumulative Pore Volume (CWE) Injected; Run 110; Injector/Producer in Upper/Lower Position, and Run 116; Injector/Producer in Middle/Lower Position; Hot Waterflood Followed by SAGD.

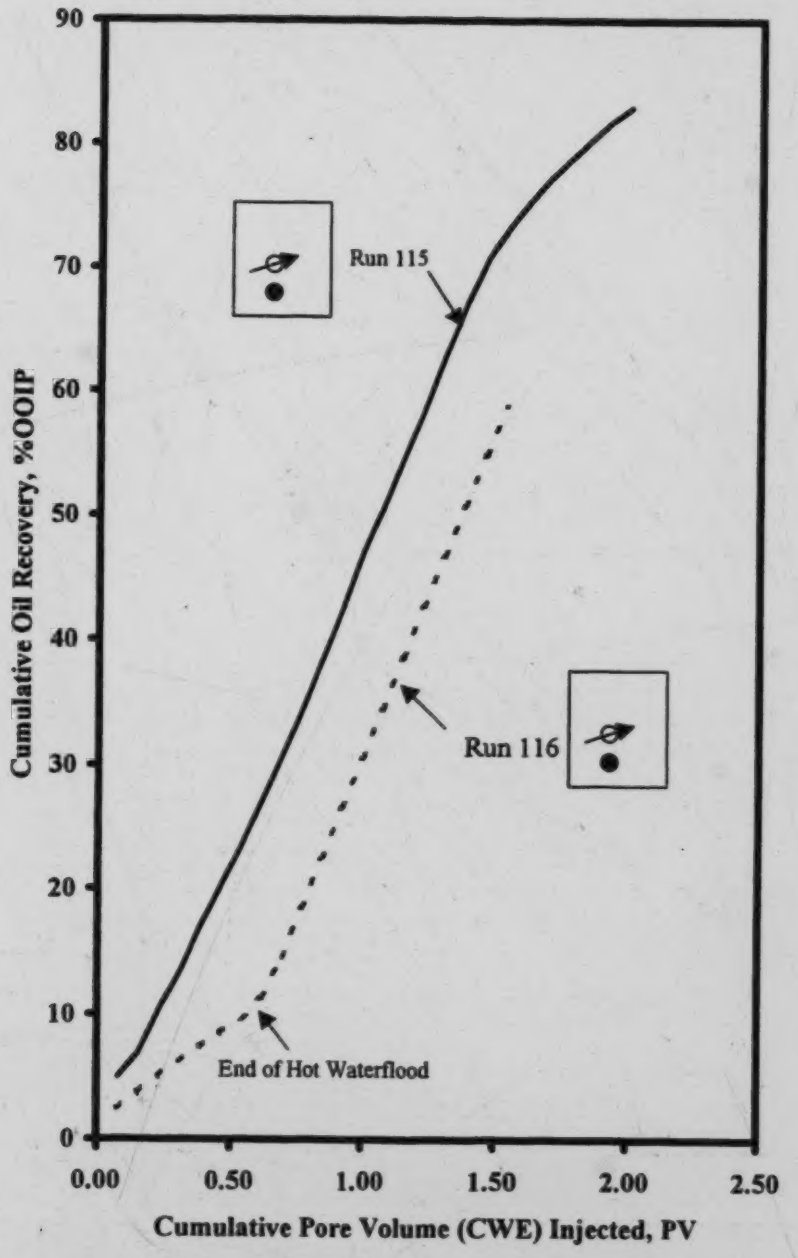

Figure 6.13-Cumulative Oil Recovery % OOIP vs. Cumulative PV of Steam (CWE) Injected; Runs 115 (SAGD), and 116 (Hot waterflood/SAGD), Injector/Producer in Middle/Lower Positions.

were the same as those used in the base case experiment (10% steam quality and 180 cc/min).

Run 114 corresponded to the base case Run 108. The porosity was 37.1%, and the initial oil saturation was 92%. Figure 6.14 and Table 6.7 present the production history of Run 114, the oil percentage in the production sample started at 46%, then it dropped to the 30% range at about 0.23 PV of steam (CWE) injected. It remained at the 30% range to the end of the SAGD process. Once the hot waterflood started, the oil percentage in the production sample declined and it was 12% by the end of the experiment. The cumulative oil recovery was 64% by the end of the run, with 54% due to the SAGD process and 10% due to the hot waterflood. Figure 6.15 shows the production profile of Run 114 and its corresponding base case run (Run 108). The cumulative oil recovery of Run 114 was 64% at 1.62 PV of steam (CWE) injected, while that for Run 108 was 79% for the same time. The lower recovery in Run 114 was due to the low production rate during the hot waterflood period.

Because the production performance of Run 117 is generally similar to the production performance of Run 114, thus only a comparison between this run and Runs 115 and 114 will be mentioned here. Run 117 corresponded to the base case of Run 115, i.e., the injector was in the middle position and the producer was in the lower position. In Run 117, porosity was 36%, and initial oil saturation was 92.9%. It can be seen from Figure 6.16 and Table 6.8 that Run 117 started with 35% oil in the production sample, then dropped to the 30% range and remained there to the end of the SAGD period. Once the hot waterflood started, the percentage of oil in the production sample declined to 12%, and remained in that range to the end of the experiment (about 1.59 PV of steam (CWE) injected). The cumulative oil recovery due to SAGD process was 53% and that due to the hot waterflood was 8%.

Figure 6.17 shows the production profile of Run 117 and its corresponding base case run (Run 115). In Run 117 the cumulative oil recovery was 61% at the end of the experiment (at 1.59 PV of steam (CWE) injected), while in Run 115 was 74.5% for the same time. This difference was due to the low production rate during the hot waterflood period. The oil production rate may have been higher during the hot waterflood period if it had been implemented directly after the SAGD, thus most of the heat available would have been scavenged instead of being lost to the overburden and the underburden. This was not possible, because the steam generator had to be cooled to the hot waterflood temperature (this cooling down of the steam generator took about half an hour).

Runs 117 and 114 both had a hot waterflood after the SAGD process. The position of the injector was in the middle position in Run 117, while it was in the upper position in Run 114. From Figure 6.18, it can be seen that Run 117 had a slightly lower oil recovery, 61% at 1.59 PV of steam (CWE) injected (the end of the run) than Run 114, 63%, although the oil recovery was the same up to the end of the SAGD process period. The difference in the oil recovery happened during the hot waterflood period, this was probably due to the larger area that could be swept by the hot water in Run 114

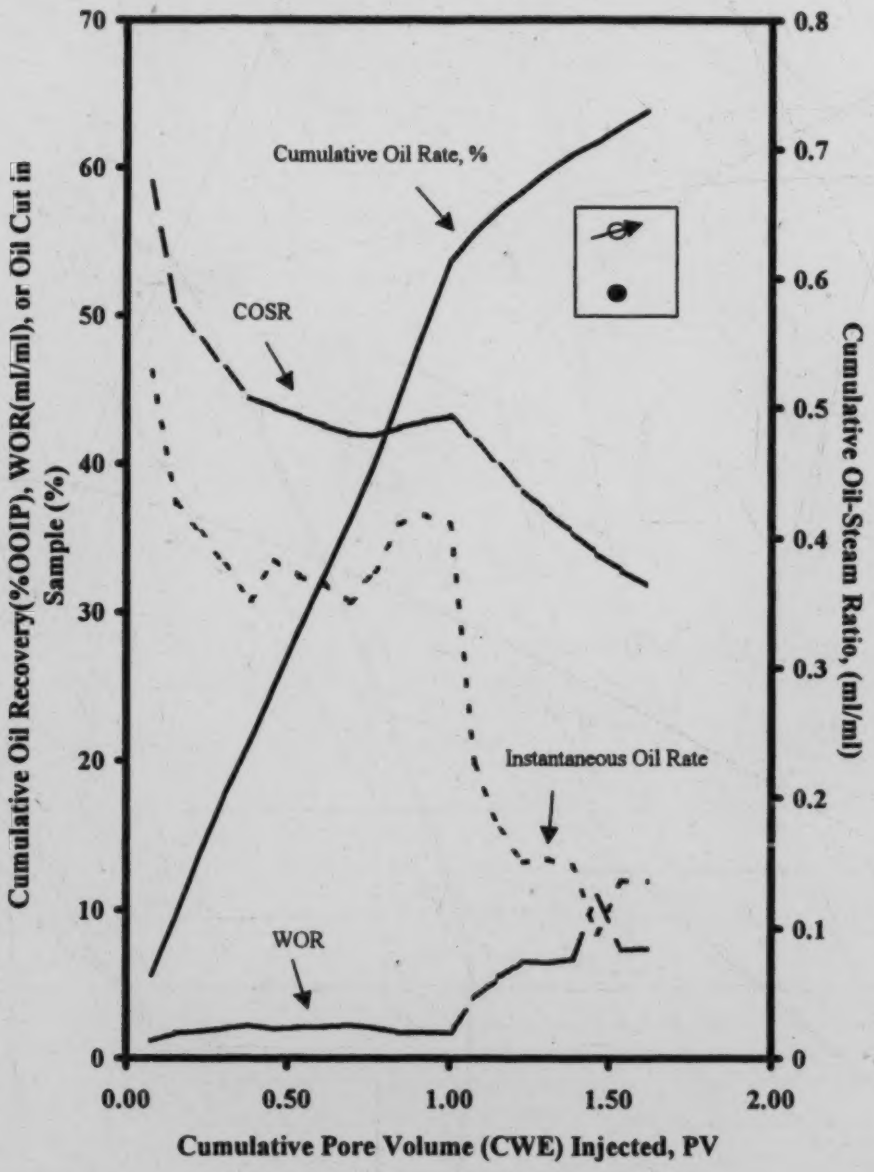

Figure 6.14 - Production History of Run 114; SAGD Followed by a Hot Waterflood; Injector/Producer in Upper/Lower Position.

Table 6.7 - Run 114: SAGD followed by a Hot Waterflood, Producer in the Lower Position, Injector in the Upper Position.

Experiment Date:	Feb.13, 1999		
Bulk Volume:	44,042ml	Type of Oil Used:	Faxam 100
Pore Volume:	16,350ml	Initial Model Temperature:	3.0C
HC Pore Volume:	15,050ml	Steam Flow Rate:	180ml/min.
Porosity:	37.1%	Steam Quality:	0.1
Initial Oil Saturation:	92.0%	Total Steam Volume Injected:	26,460
Initial Water Saturation:	8.0%		
Net Oil Recovery:	**63.6%**	**Final Oil Saturation:**	**33.3%**

Cylinder No.	Total Vol. Produced (ml)	Instantaneous Oil Prod. (ml)	Cum. Oil Recovery (ml)	Cum. Oil Rec. % OOIP	Instantaneous Produced WOR	% Sample Oleic Phase	Cum. PV Injected
1	1840	850	850	5.65	1.16	0.46	0.08
2	1610	600	1450	9.63	1.68	0.37	0.15
3	1810	640	2090	13.89	1.83	0.35	0.23
4	1750	580	2670	17.74	2.02	0.33	0.31
5	1720	530	3200	21.26	2.25	0.31	0.39
6	1730	580	3780	25.12	1.98	0.34	0.46
7	1760	570	4350	28.90	2.09	0.32	0.54
8	1720	550	4900	32.56	2.13	0.32	0.62
9	1760	540	5440	36.15	2.26	0.31	0.69
10	1800	590	6030	40.07	2.05	0.33	0.77
11	1920	690	6720	44.65	1.78	0.36	0.85
12	1860	680	7400	49.17	1.74	0.37	0.92
13	1890	680	8080	53.69	1.78	0.36	1.00
14	1470	290	8370	55.61	4.07	0.20	1.08
15	1560	240	8610	57.21	5.50	0.15	1.16
16	1440	190	8800	58.47	6.58	0.13	1.23
17	1490	200	9000	59.80	6.45	0.13	1.31
18	1310	170	9170	60.93	6.71	0.13	1.39
19	1430	120	9290	61.73	10.92	0.08	1.46
20	1420	170	9460	62.86	7.35	0.12	1.54
21	1260	150	9610	63.85	7.40	0.12	1.62

* Line indicates the end of the SAGD Process.

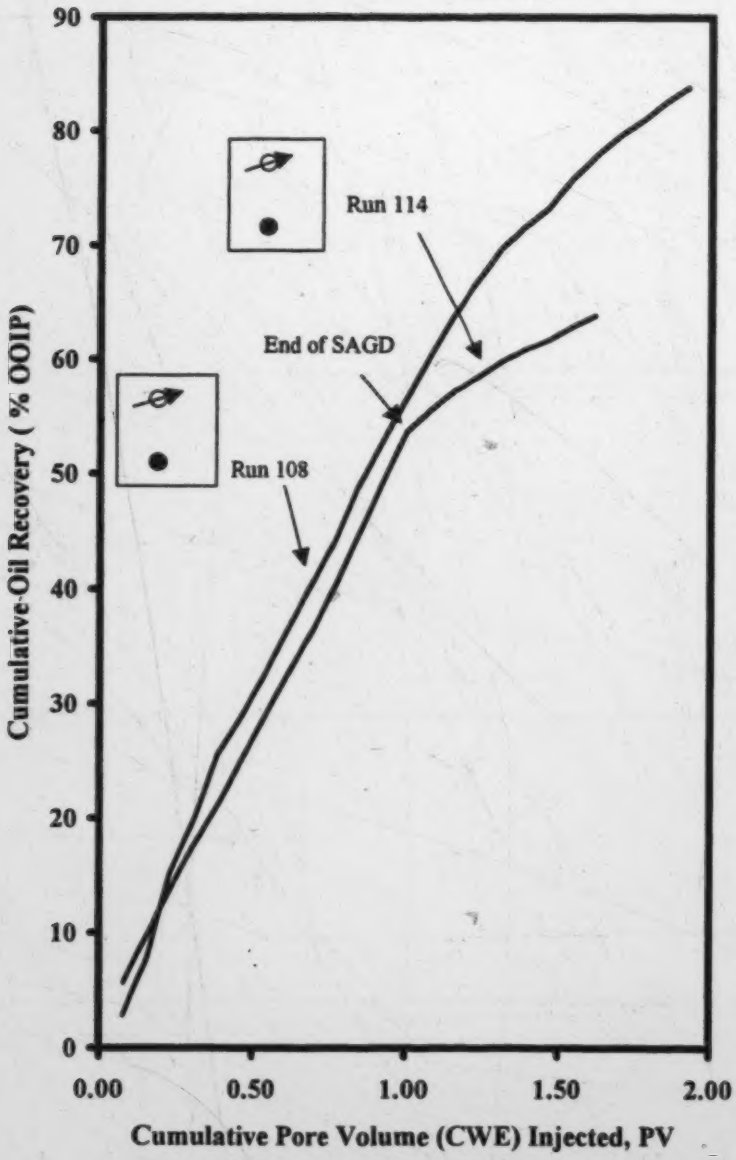

Figure 6.15-Cumulative Oil Recovery vs. Cumulative PV (CWE) Injected; for Runs 108 (SAGD), 114 (SAGD/Hot Waterflood); Injector/Producer in Upper/Lower Position.

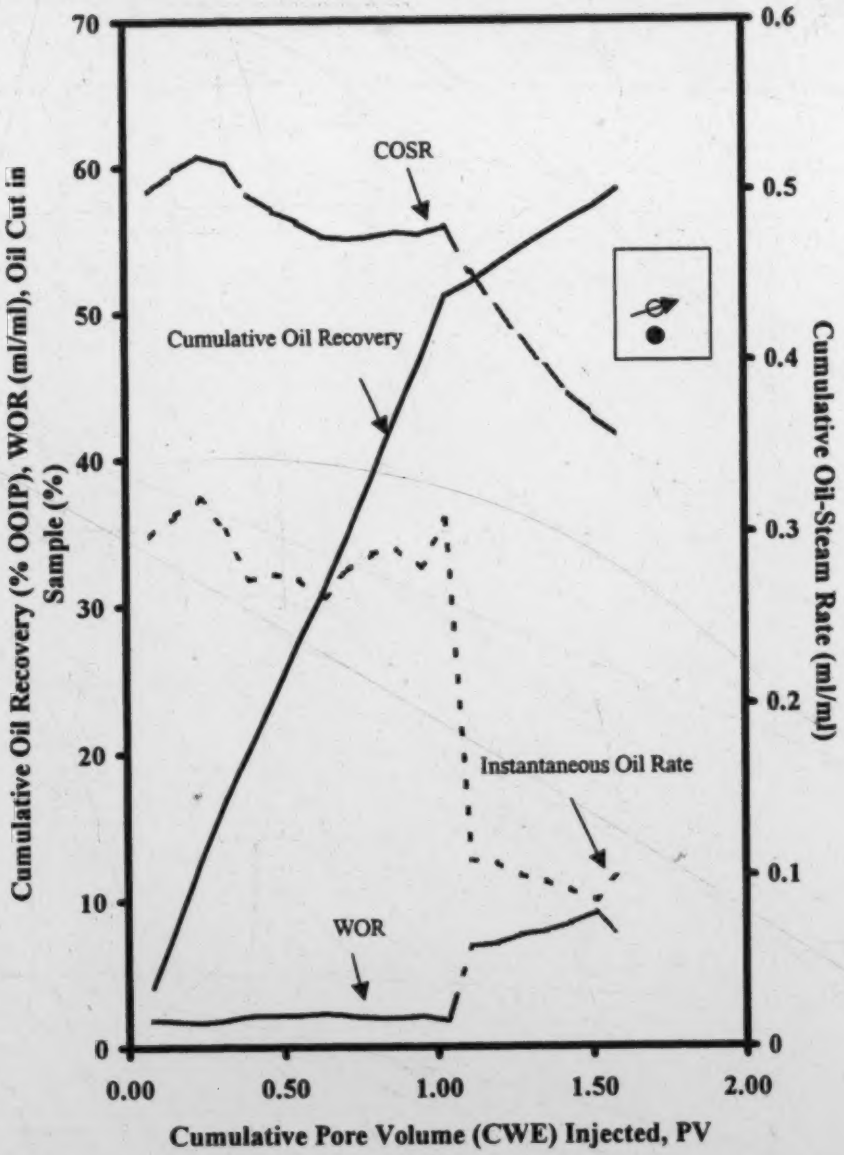

Figure 6.16-Production History of Run 117; SAGD Followed by a Hot Waterflood; Injector/Producer in Middle/Lower Position.

Table 6.8-Run 117: SAGD followed by a Hot Waterflood, Producer in the Lower Position, Injector in the Middle Position.

Experiment Date: Mar.11, 1999
Bulk Volume: 44,042ml
Pore Volume: 15,883ml
HC Pore Volume: 14,760ml
Porosity: 36.1%
Initial Oil Saturation: 92.9%
Initial Water Saturation: 7.1%

Type of Oil Used: Faxam 100
Initial Model Temperature: 3.0°C
Steam Flow Rate: 180ml/min.
Steam Quality: 0.1
Total Steam Volume Injected: 25,200

Net Oil Recovery: 60.7%

Final Oil Saturation: 36.5

Cylinder No.	Total Vol. Produced (ml)	Instantaneous Oil Prod. (ml)	Cum. Oil Recovery (ml)	Cum. Oil Rec. % OOIP	Instantaneous Produced WOR	% Sample Oleic Phase	Cum. PV Injected
1	1810	630	630	4.27	1.87	34.81	0.08
2	1820	660	1290	8.74	1.76	36.26	0.16
3	1820	680	1970	13.35	1.68	37.36	0.24
4	1790	630	2600	17.62	1.84	35.20	0.32
5	1700	540	3140	21.27	2.15	31.76	0.40
6	1710	550	3690	25.00	2.11	32.16	0.48
7	1760	560	4250	28.79	2.14	31.82	0.56
8	1700	520	4770	32.32	2.27	30.59	0.63
9	1790	580	5350	36.25	2.09	32.40	0.71
10	1820	610	5960	40.38	1.98	33.52	0.79
11	1860	630	6590	44.65	1.95	33.87	0.87
12	1780	580	7170	48.58	2.07	32.58	0.95
13	1870	670	7840	53.12	1.79	35.83	1.03
14	1100	140	7980	54.07	6.86	12.73	1.11
15	1440	180	8160	55.28	7.00	12.50	1.19
16	1460	170	8330	56.44	7.59	11.64	1.27
17	1420	160	8490	57.52	7.88	11.27	1.35
18	1410	150	8640	58.54	8.40	10.64	1.43
19	1410	140	8780	59.49	9.07	9.93	1.51
20	1520	180	8960	60.70	7.44	11.84	1.59

* Line indicates the end of the SAGD Process.

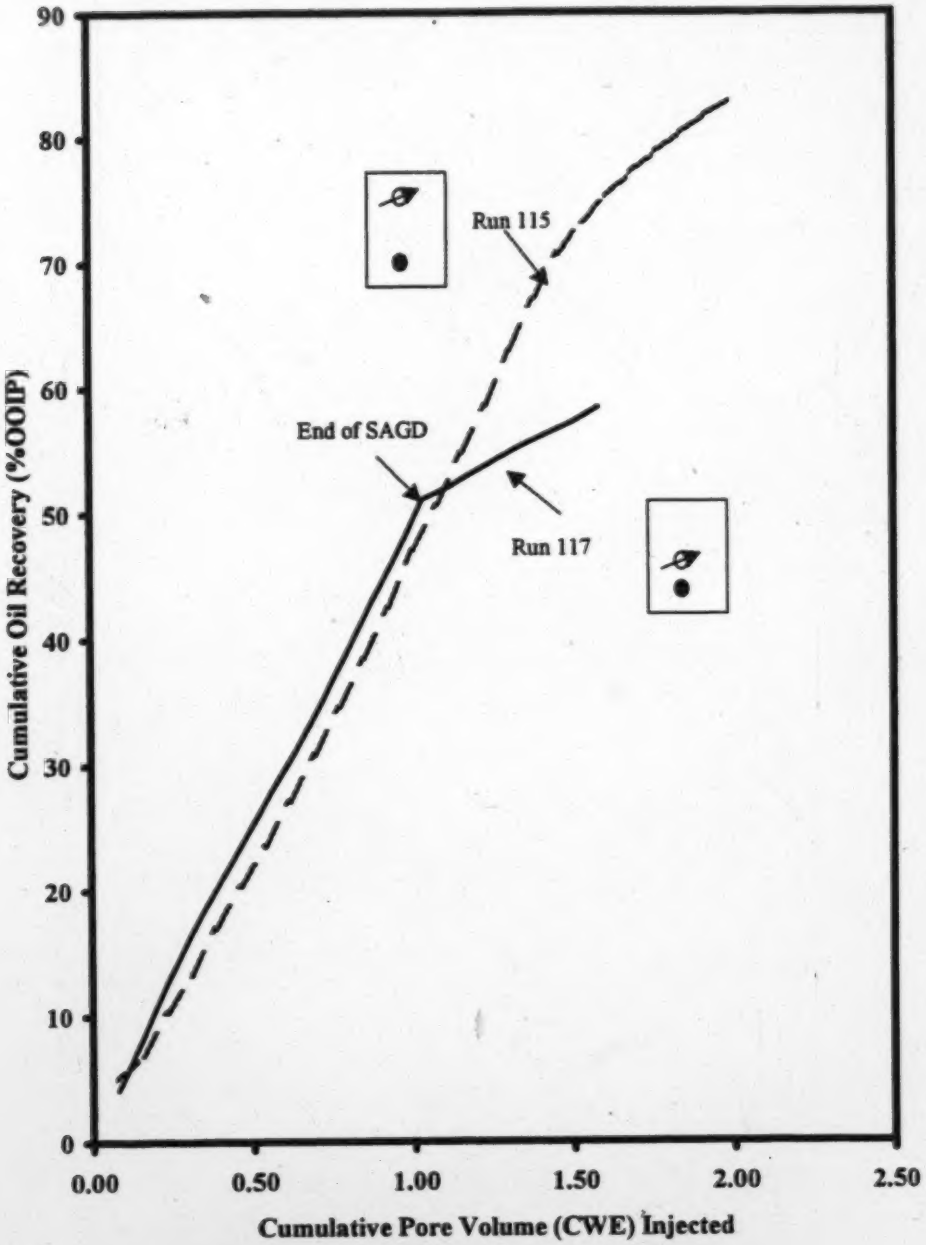

Figure 6.17 - Cumulative Oil Recovery vs. Cumulative Pore Volume (CWE) Injected; Run 115 (SAGD), and Run 117 (SAGD/Hot Waterflood), Injector/Producer in Middle/Lower Position.

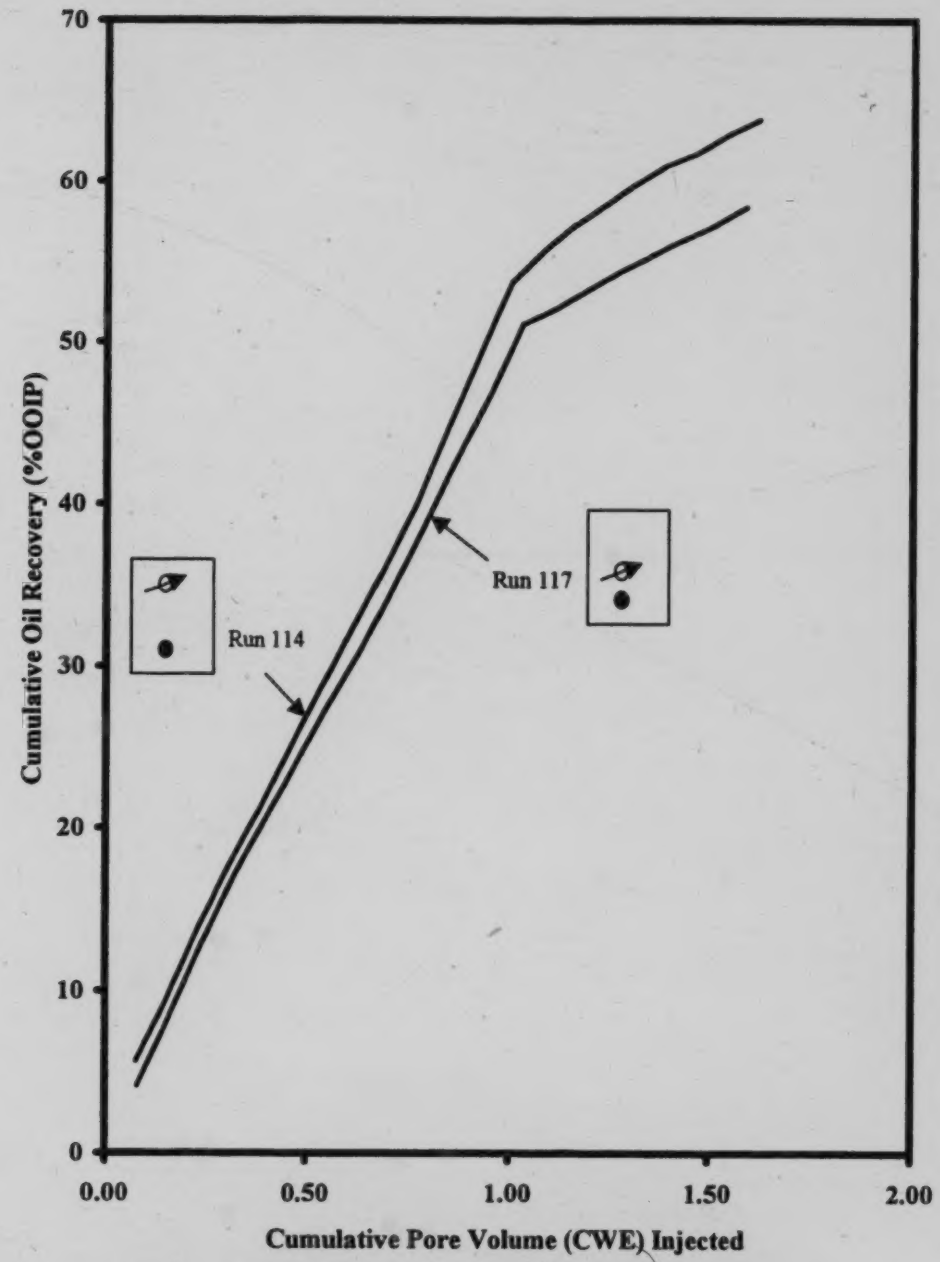

Figure 6.18 - Cumulative Oil Recovery vs. Cumulative Pore Volume (CWE) Injected; Run 114, Injector/Producer in Upper/Lower Position, and Run 117, Injector/Producer in Middle/Lower Position, Hot Waterflood Followed by SAGD.

and to the injector being in the hottest region in the model (the injector was in the upper position).

In conclusion, although the hot waterflood did not started immediately after the SAGD process, the cumulative oil recovery of a SAGD process followed by a hot waterflood was comparable to the base case runs. Taking into account the amount of heat that had been scavenged, this production scheme could become attractive. Implementation of the wells configuration of Run 114 (i.e., having the injector high in the reservoir, in a SAGD process followed by a hot waterflood gave higher oil recovery than the configuration of Run 117 (injector in the middle position). This was due to the larger area that could be swept by the hot waterflood and also due to the injector being in the upper position (i.e., in the region of the highest temperature.)

6.7 The Visual Model Experiments

Three experiments were conducted in the visual model for the purpose of visualizing the steam chamber growth and the oil displacement mechanism. In the first and the last experiments, Faxam-100 oil, which has a viscosity of 270 mPa.s at 23°C was used. In the second experiment Wainwright crude, which has a viscosity of 975 mPa.s at 23°C was used. Oils having different viscosities were used for the purpose of seeing the effect of oil viscosity on the development of the steam chamber. In the first run there was a good contrast due to the adding of a dye to the oil. In the second run no dye was added to the oil, because it was thought that the dark color of Wainwright crude oil would have given a good contrast. In the third run a dye was added to the oil but it did not provide a good contrast, because the added amount was not the right proportion. In all these experiments steam at the atmospheric pressure and 100°C was used. These experiments were recorded using an 8-mm video camera.

The good contrast between the oil and the steam in the first run was helpful in visualizing the development of the steam chamber. At the beginning of the experiment, the steam was rising to the top of the model as fingers. Once the steam reached the top, it continued to accumulate there, forming a steam zone. Because in this run the injector was in the upper position, the steam zone was like a gas cap in an oil reservoir rather than a steam chamber, which had a mushroom-like shape. Once the steam had spread across the top of the model, then it started moving down until it reached the producer. Once the steam had reached the producer, the steam breakthrough occurred, and the movement of the steam toward the bottom of the reservoir proceeded very slowly due to the escape of the steam through the producer.

In the second run, Wainwright crude was used, which had a higher viscosity than Faxam-100 oil. Although there was not much contrast between the crude oil and the steam, it was possible to monitor (to a certain extent) the growth of the steam chamber. It was noted that it took the steam chamber a longer time to reach the top of the model and to expand side ways than in the first run. This was due to the higher viscosity of Wainwright crude.

In the third run the contrast was poor, as a consequence, it was difficult to distinguish between the oil and the steam.

6.8 The Development of the Steam Chamber

Figures 6.19A, 6.20A, 6.21A present the contour maps of the first half of the model for the base case runs (107,108,115). The contour maps were drawn at 0.25, 0.50, 1.00, and 1.50 PV of steam (CWE) injected. At the begging of the three the steam chamber started as steam fingers, with some of them travelling up toward the ceiling of the reservoir and some travelling down due to the pulling force of the vacuum through the producer. These fingers will form two separate steam chambers on at the top of the reservoir and the other just above the horizontal well. This is clear from the contour map of the temperature distribution of the three runs at 0.25 PV of steam (CWE) injected. From the contour maps of the temperature distribution at 0.50 PV of steam (CWE) injected of the three runs, it was noticed that there was a difference between the temperature distributions of Runs 107 and 108 and Run 115. In Runs 107 and 108 the upper steam chamber has expanded and formed a steam zone similar to a gas cap in conventional oil reservoirs, while the lower steam chamber did not expand. On the other hand the in Run 115 the situation were different, the upper and lower steam chambers have expanded the same size. This difference is attributable to the position of the injector in these runs. In Runs 107 and 108 the injector was in the upper position which cause the steam to travel fast to the top of the reservoir forming steam zone. In Run 115 the injector was in the middle position, as a consequence it took the steam more time to travel to the top of the reservoir, causing the lower steam chamber to expand almost the same size as the upper one. From the contour maps of the temperature distribution of the three runs at 1.00 PV of steam (CWE) injected, it can be noticed that the two steam chambers joined together and formed one steam chamber, which extended from the top to the middle of the reservoir. Once steam breakthrough had happened, the pressure inside the model declined, as a consequence, more hot water flashed into steam. This clear from the contour maps of the temperature distribution of the three runs at 1.50 PV of steam (CWE) injected.

Comparing the contour maps of the temperature distribution of the first and the second half of the model of Run 107 (Figures 6.19A and 6.19B), it was noticed that the growth rate of the steam chamber was faster in the first half of the model than in the second half. This is applicable to Runs 108 and 115 too. This difference in size was as a result of the variability of the steam quality along the horizontal injector. This had happened because most of the steam found its way out of the perforations of the first half of the horizontal injector, as a consequence, a smaller amount of the steam reached the second half of the model. This phenomenon needed to be studied in detail to determine the effective well length.

6.9 The Dominant Driving Force in the Reservoir

It is very important to know the dominant driving force in the reservoir in order to improve its efficiency in driving the oil toward the producers, thus maximizing the

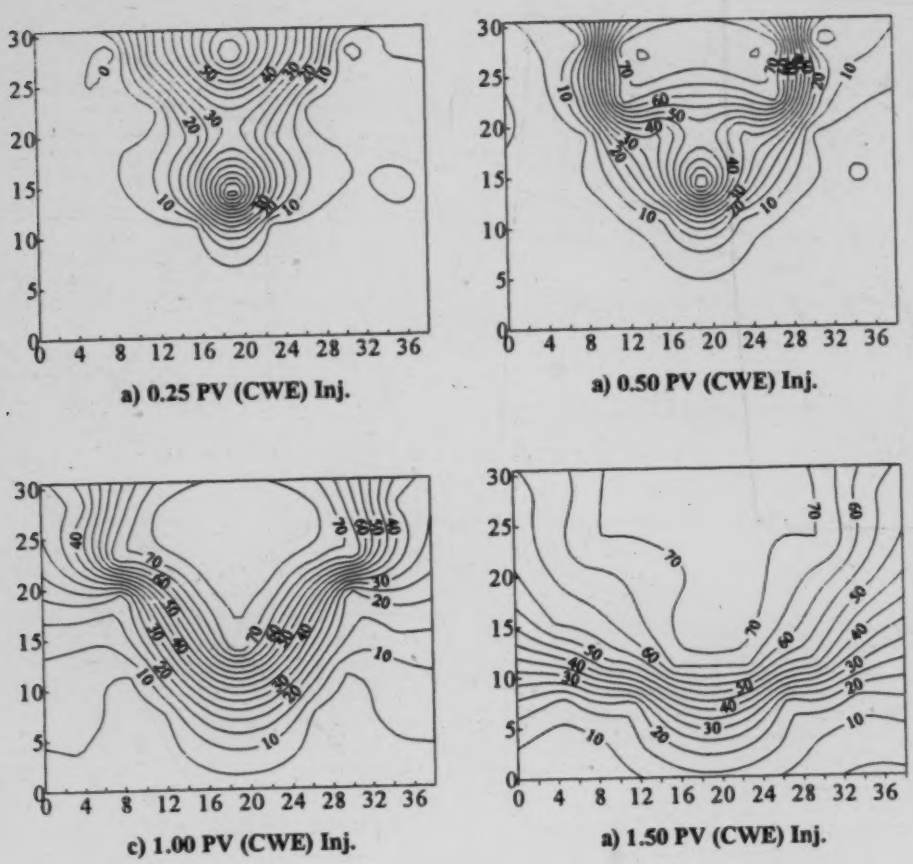

Figure 6.19 A- Front View of the Temperature Distribution for the First Half of the Model after the Injection of: a) 0.25, b) 0.50, c) 1.00, and d) 1.50 PV CWE of Steam, Run 107: SAGD, the Injector in the Upper Position and the Producer in the Middle Position.

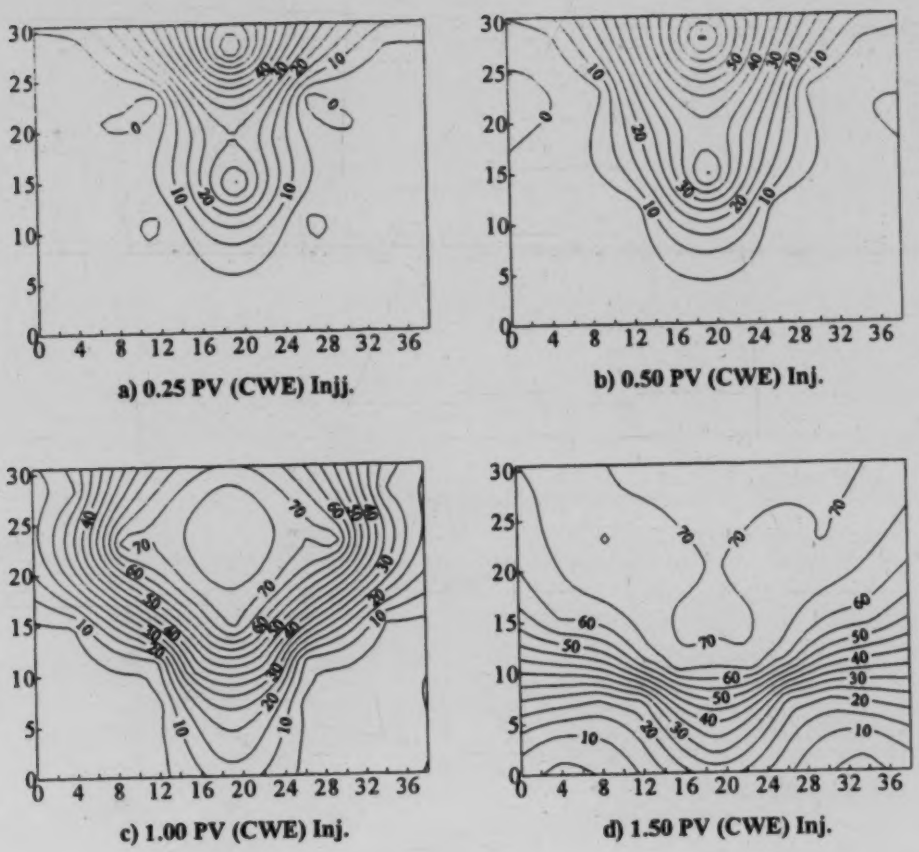

Figure 6.19B- Front View of the Temperature Distribution for the Second Half of the Model after the Injection of: a) 0.25, b) 0.50, c) 1.00, d) 1.50 PV CWE of Steam, Run 107:SAGD, the Injector in the Upper Position and the Producer in the Middle Position.

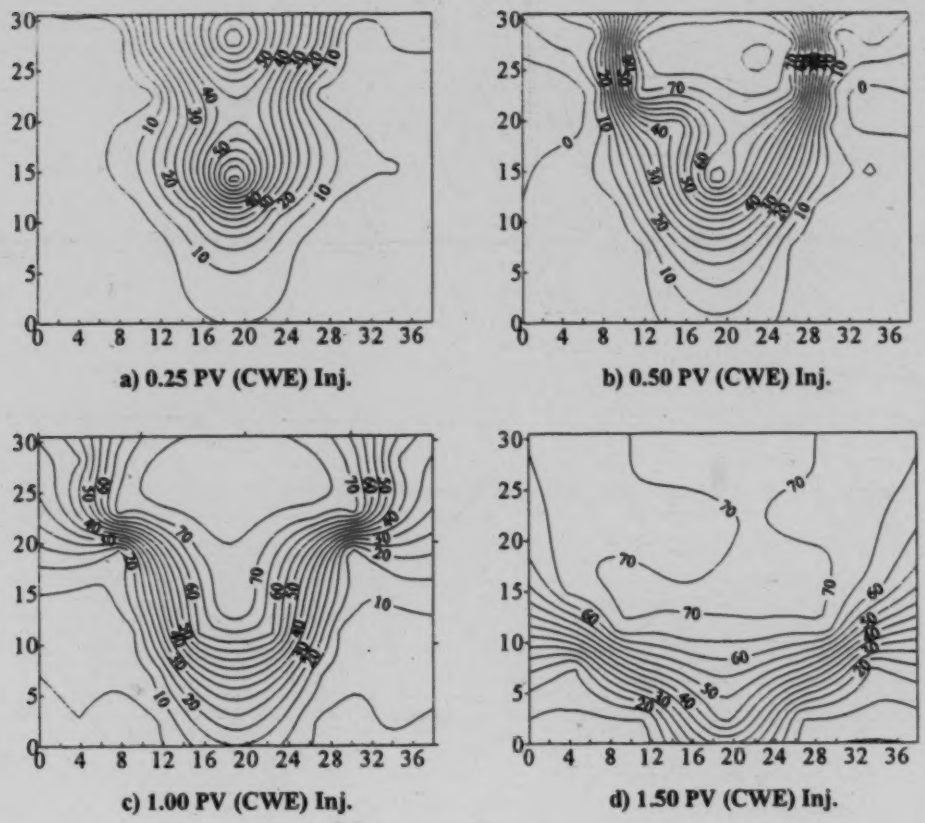

Figure 6.20A - Front View of the Temperature Distribution for the First Half of the Model after the Injection of: a) 0.25, b) 0.50, c)1.00, and d) 1.50 PV CWE of Steam, Run 108: SAGD, the Injector in the Upper Position and the Producer in the lower Position.

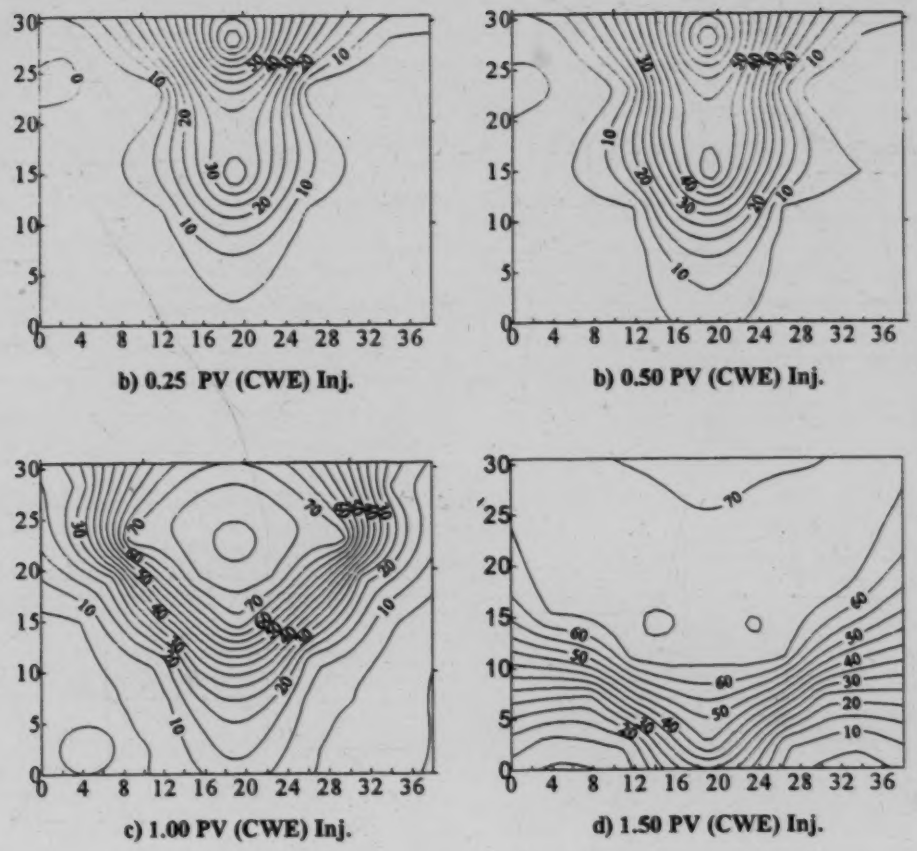

Figure 20B- Front View of the Temperature Distribution for the Second Half of the Model after the Injection of: a) 0.25, b) 0.50, c) 1.00, d) 1.50 PV CWE of Steam, Run 108: SAGD, the Injector in the Upper Position and the Producer in the Lower Position.

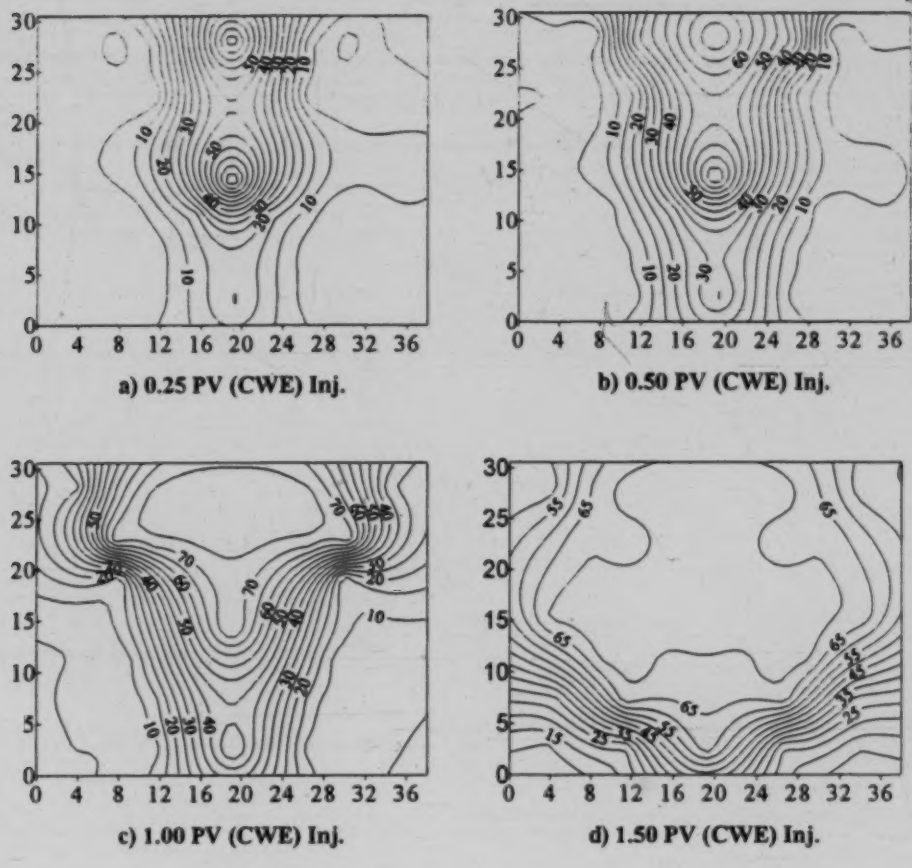

Figure 6.21A- Front View of the Temperature Distribution for the First Half of the Model after the Injection of: a) 0.25, b) 0.50, c)1.00, and d) 1.50 PV CWE of Steam, Run 115; SAGD, the Injector in the Middle Position amd the Producer in the Lower Position.

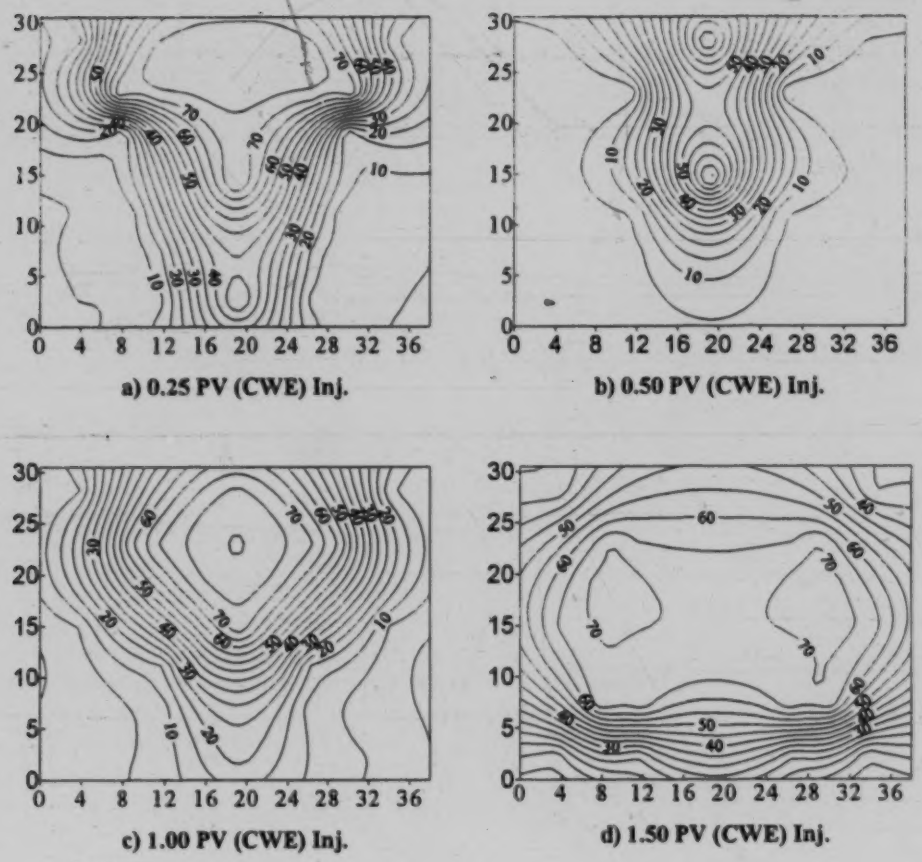

Figure 6.21B- Front View of the Temperature Distribution for the Second Half of the Model after the Injection of: a) 0.25, b) 0.50, c) 1.00, and d) 1.50 PV CWE of Steam, Run 115: SAGD, the Injector in the Middle Position and the Producer in the Lower Position.

recovery. Run 115 was chosen to investigate the dominant driving force behind the oil production. In order to do that, the step thing was to calculate the pressure gradient for the consecutive times of the experiment by dividing the difference in pressure between the injection and the production pressure by the distance separating them. Then calculating the gravity gradient by multiplying the difference in density of the steam and the oil by the gravity. Figure 22 shows the pressure gradient and the gravity gradient as a function of the PV of steam (CWE) injected, it can be seen that the average pressure gradient is 10 times the gravity gradient, thus the pressure gradient was the dominant driving force behind the oil production.

6.10 Scaling Up of the Experimental Results to the Prototype

In order to apply the experimental results to the prototype reservoir, these results have to be scaled up. Because Run 115 was the one that have been chosen to be discussed in detail out of the base case experiments, thus the results of this run were chosen to be scaled up to the prototype reservoir. The experimental oil rate was scaled up to the oil rate of the prototype reservoir using Equation 4.37, then the cumulative oil production of the prototype reservoir was calculated and plotted as function of the cumulative pore volume (CWE) injected (Figure 23.) From Figure 23 it can be noticed that the rate of increase of the cumulative oil production as percent of the OOIP of the prototype reservoir at 0.74 PV of steam (CWE) injected started to slowdown to the rate of 2% per 0.1 PV of steam (CWE) injected. After this time the rate of increase of the cumulative oil production will probably either slowdown more or at the best continue to increase at the same rate. Therefore the expected cumulative oil production of the prototype reservoir after 2.00 PV of Steam (CWE) injected will be between 50 to 60% of the OOIP.

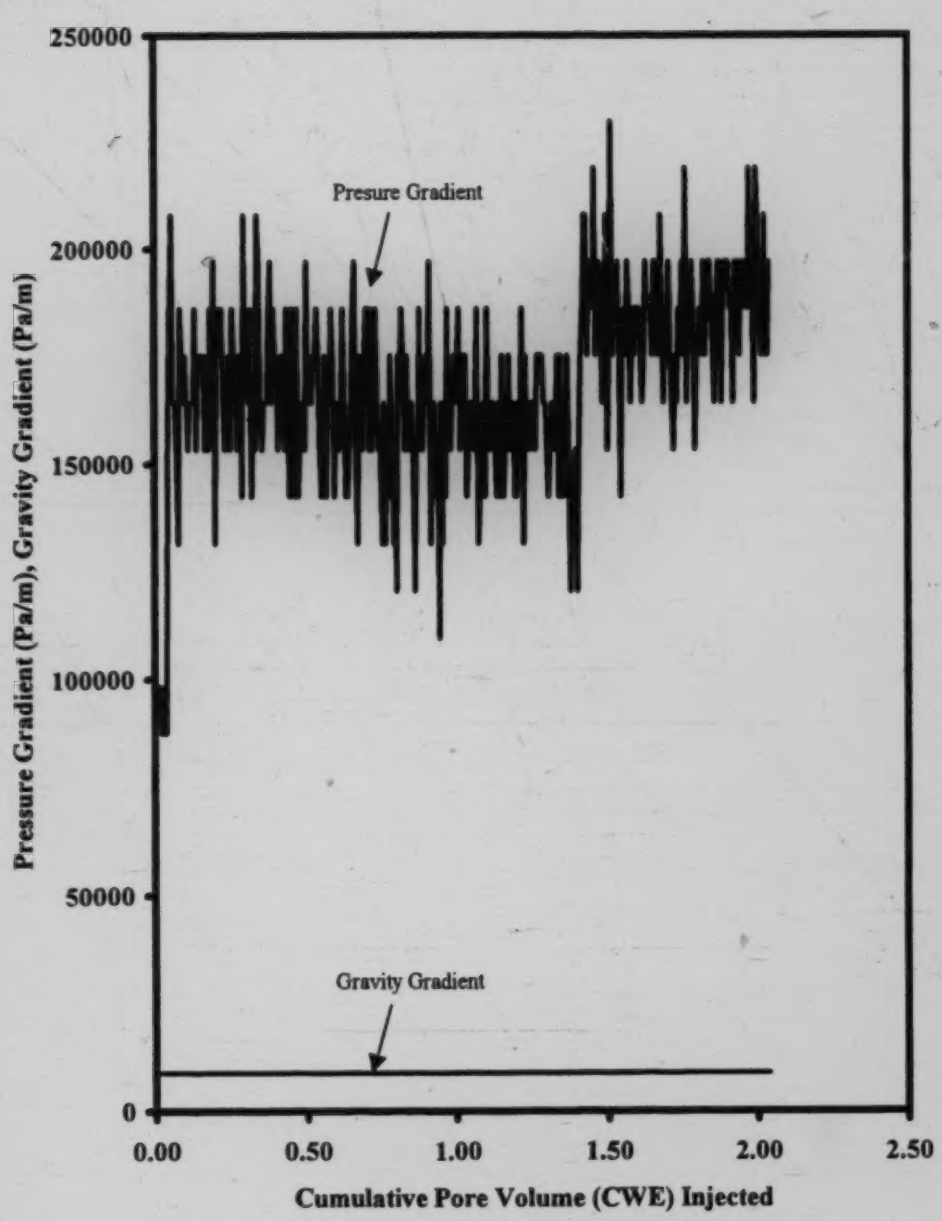

Figure 22 - A Comparison Between the Pressure Gradient and the Gravity Gradient; Run 115, Base Case Experiment, Injector in the Middle Position and Producer in the Lower Position.

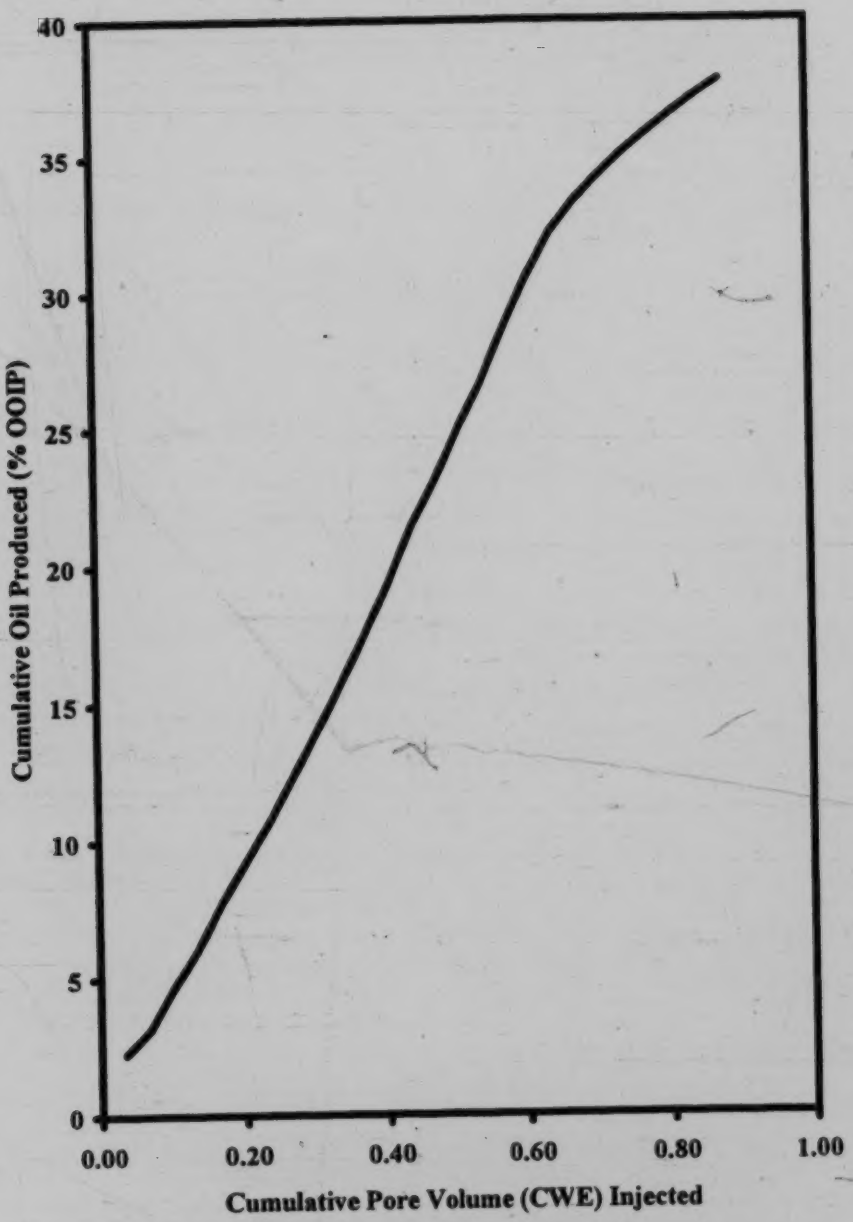

Figure 6.23 - Scaling-Up of the Model Oil Rate to the Prototype Oil Rate; Run 115, Base Case Experiment; Injector in the Middle Position and Producer in the Lower Position.

7. Conclusions

In this study, a number of experimental as well as theoretical studies were conducted. Based on the analysis of the results of these studies, the following conclusions were reached:

1. The well configuration of injector in the upper position and producer in the lower position gave the highest recovery (85%), and highest cumulative oil-steam ratio of the various tested well configurations.

2 Based on the scaling-up of the experimental results, it was found that the ultimate oil recovery for the prototype reservoir would be around 50% of the OOIP.

3 The breakthrough time was a function of the volume of the reservoir lying above the horizontal producer; the larger the volume, the later the breakthrough time. It is also a function of the pressure drawdown.

4 Based on the heat balance calculations, it was found that the heat lost to the over-burden and the underburden was much less than had been thought, and represents only 20% of the total heat injected.

5 In implementing a hot waterflood prior to the SAGD process, the injector should be as close as possible to the bottom of the reservoir.

6 In implementing a hot waterflood after the SAGD process, the injector should be as high as possible in reservoir.

7 There was a variation in the steam quality along the horizontal injector this has led to a variation in the size of the steam chamber along the horizontal injector.

8. Recommendations

1) The phenomena of the variation in the steam chamber growth along the horizontal injector should be studied in order to determine the effective well length.

2) An experimental study should be conducted to test the performance of SAGD in dip reservoirs, this is can be accomplished with the available apparatus.

3) A study of the effect of varying steam quality on the oil recovery in SAGD should be conducted.

References

Boberg, Thomas C.:Thermal Methods of Oil Recovery, An Exxon Monograph, John Wiley &Sons, 1988.

Butler, R.M., Stephens, D. J. and Weiss, M.: "The Vertical Growth of Steam Chambers in the In-Situ Thermal Recovery of Heavy Oils", Proceedings of the 30th Canadian Chemical Engineers Conference, October 19-22, 1980, Vol. 4, pp. 1152-1160.

Butler, R.M. and Stephens, D.J.: "The Gravity Drainage of Steam-Heated Heavy Oil to Parallel Horizontal Wells", *JCPT*, April-June, 1981, pp. 90-96.

Butler, R.M., McNab, G.S. and Lo, H.Y.: "Theoretical Studies on the Gravity Drainage of Heavy Oil During In-Situ Steam Heating", *JCPT*, Vol. 59, August 1981, pp 455-460.

Butler, R.M.: "A New Approach to the Modeling of Steam-Assisted Gravity Drainage", *JCPT*, May-June, 1985.

Butler R.M.: "Rise of Interfering Steam Chambers", *JCPT*, June-May, 1987.

Butler, R.M.: "Thermal Recovery of Oil and Bitumen", First Edition, Prentice Hall, 1991.

Butler, R.M.: "Horizontal Wells for the Recovery of Oil, Gas and Bitumen", Petroleum Society Monograph No. 2, 1994.

Butler, R.: "Steam and Gas Push (SAGP)", Paper 97-137, Presented at the 48th Annual Technical Meeting of The Petroleum Society, Calgary, Alberta, June 8-11,1997.

Chu, C. and Trimple, A.E.: "Numerical Simulation of Steam Displacement- Field Performance Applications", *JPT*, June 1975, pp. 765-776.

Chung, K.H. and Butler R.M.: "Geometrical Effect of Steam Injection on the Formation of Emulsions in the Steam-Assisted Gravity Drainage Process", *JCPT*, January-February 1988, pp. 36-42.

Dwight C. Look, Jr and Harry J. Sauer,Jr.: "Engineering Thermodynamics", SI Edition, Van Nostrand Reinhold (International), 1988.

Edmunds, N.R. and Gittins, S.D.: "Effective Application of Steam Assisted Gravity Drainage of Bitumen to long Horizontal Well Pairs", *JCPT*, Vol. 32, No. 6, June 1993.

Edmunds, N.R., Kovalsky, J.A., Gittins, S.D. and Pennacchioli, E.D.: "Review of Phase A Steam-Assisted Gravity Drainage Test", *SPE Reservoir Engineering Journal*, May 1994, pp.119-124.

Ferguson, F.R. Scott and Butler R.M.: "Steam-Assisted Gravity Drainage Model Incorporating Energy Recovery from a Cooling Steam Chamber", *JCPT*, Vol. 27, No.5, September-October 1988.

Farouq Ali, S.M.: Heavy Oil Recovery, March 1976.

Griffin, P.J. and Trofimenkoff, P.N.: "Laboratory Studies of the Steam-Assisted Gravity Drainage Process", presented at the AOSTRA Advances in Petroleum Recovery and Upgrading Technology Conference", Calgary, Alberta, June 14-15, 1984.

Haung, W.S. and Hight, M.A.: "Evaluation of Steamflood Process Using Horizontal Wells", SPE 14130, International Meeting on Petroleum Engineering, Beijing, China, March 17-20, 1986.

Ito Y. and Suzuki, S.: "Numerical Simulation of the SAGD Process in the Hangingstone Oil Sands Reservoir", CIM 96-57, presented at the 47th Annual Technical Meeting of the Petroleum Society, Calgary, Alberta, June 10-12, 1996.

Joshi, S. D. and Threlkeld, C.B.: " Laboratory Studies of Thermally Aided Gravity Drainage Using Horizontal Wells", *AOSTRA Journal of Research*, Vol. 2, No. 1, 1985.

Kamath, V.A., Sinha Sandeep and Hatzignatiou, D.G.: "Simulation Study of Steam-Assisted Gravity Drainage Process in Ungu Tar Sand Reservoir", SPE 26075, presented at the Western Regional Meeting, Anchorage, Alaska, May 26-28, 1993.

Kisman, K.E. and Yeung, K.C.: "Numerical Study of the SAGD Process in Burnt Lake Oil Sand Lease", SPE 30276, presented at the International Heavy Oil Symposium, Calgary, Alberta, June 19-21, 1995.

Matthias, R.C.M.: "Scaled Experiments of Heavy Oil Recovery Strategies in a Low Pressure Physical Model", M.Sc. Thesis, University of Alberta (Spring 93).

Mukherjee, N.J., Gittins, S.D., Edmunds, N.R. and Kisman, K.E.: "A Comparison of Field Versus Forcast Performance for Phase B of the UTF SAGD Project in the Athabasca Oil Sands", Unitar International Conference on Heavy Crude and Tar Sands, Houston, TX, February 12-17, 1995.

Nasr, T.N., Golbeck, H. and Lorimer, S.: "Analysis of the Steam Assisted Gravity Drainage (SAGD) Process Using Experimental/Numerical Tools", SPE 37116, presented at the SPE International Conference on Horizontal Well Technology, Calgary, Alberta, November 18-20, 1996.

Reis, John C.: "A Steam-Assisted Gravity Drainage Model for Tar Sands: Linear Geometry", *JCPT*, Vol. 31, No. 10, December 1992, pp. 14-20.

Sasaki, K., Akibayashi, S., Kosukegawa, H. and Kato, M.: "Experimental Study on the Initial Stage of SAGD Process Using 2-Dimensional Scaled Model for Heavy Oil Recovery", SPE 37089, presented at the SPE International Conference on Horizontal Well Technology, Calgary, Alberta, November 18-20, 1996.

Stegemeier G.L., Laumbach, D.D. and Volek, C.W.: "Reoresenting Steam Process with Vacuum Models", *SPEJ*, June 1980, pp. 151-174.

Sugianto, S. and Butler, R.M.: "The Production of Conventional Heavy Oil Reservoir with Bottom Water Using Steam-Assisted Gravity Drainage":, *JCPT*, Vol. 29, No. 2, March-April 1990.

Tortike, W.S. and Farouq Ali, S.M.: "Saturated-Steam-Property Functional Correlations for Fully Implicit Thermal Reservoir Simulation", *SPE Res. Eng.*, November 1989, pp.471-474.

Vikas, S. and Kamath, V.A.: "Analytical Model for Steam-Assisted Gravity Drainage in Horizontal Wells", presented at a Symposium on Exploration, Characterization and Utilization of California Heavy Fossil Fuel Resources, San Francisco, California, April 5-10, 1992.

Appendix A: Steam Zone Volume Calculations

Steam Zone Volumes – Marx-Langenheim Model

Marx and Langenheim considered the situation where steam is introduced at a constant rate into a steam zone that is spreading laterally and covering the whole thickness of the reservoir. Marx and Langenheim assumed that the whole steam zone is at T_s, steam temperature, and it extends to the point where the temperature abruptly changes from T_s to the reservoir temperature, T_R. This assumption means that there is no heat transferred ahead of the condensation front; this is usually not valid unless the injected latent heat is sufficient to supply all the losses. Marx and Langenheim arrived at the following equation for determining the steam zone volume:

$$V_s = \frac{Q_i M_s h_t^2 F_1}{4 k_{hob} M_{ob} (T_s - T_R)} \quad \text{..... (A1)}$$

In calculating the steam zone volume using equation A1, the following procedure was applied:

1) Calculate the dimensionless time, t_D, using the following equation,

$$t_D = \frac{4 k_{hob} M_{ob} t}{M_s^2 h_t^2} \quad \text{..... (A2)}$$

2) Determine the function F_1, where F_1 is defined as follows:

$$F_1 = e^{t_D} \operatorname{erfc}\sqrt{t_D} + 2\sqrt{\frac{t_D}{\pi}} - 1 \quad \text{..... (A3)}$$

F_1 can be determined from the plot of F_1 vs. t_D or can be calculated using the following approximation:

$$F_1 = \frac{t_D}{1 + 0.85\sqrt{t_D}} \quad \text{..... (A4)}$$

Once F_1 had been calculated, the values of the variables of equation A1 are inserted to find the steam zone volume.

In this study, the Marx-Langenheim model was used to calculate the steam zone volumes at consecutive times of the base case Run 115. The steam zone volumes were calculated since the beginning of the run and up to 1.20 PV of steam injected at a time interval of 420 sec, which was the same time interval used for the collection of the pro-

duction samples. This was done because at those intervals the fluids volumes inside the model are known. Table A1 contains the steam zone volumes predicted using Marx-Langenheim model for the times of the run.

Steam Zone Volume – Neuman's Model

Unlike Marx-Langenheim model, Neuman's model considers the steam override due to the density difference between the steam and the oil, i.e., it does not assume that steam covers the whole thickness of the reservoir. The assumptions underlying Neuman's model are: 1) the injected steam rise to the top of the reservoir in a negligible time compared to the time needed to heat the whole reservoir. 2) oil and water saturations are constant throughout the steam zone. 3) the pressure gradient in the horizontal direction is much smaller than the pressure gradient in the vertical direction (Neumans, 1985). Neuman derived the following equation for describing the volume of the steam zone:

$$V_s = \frac{f_d(1-f_p)i\rho_w C_w t}{M_s} \qquad \text{(A5)}$$

where:

f_d = the downhole steam quality, (dimensionless)

f_p = the fraction of injected heat that is produced, (dimensionless)

i = the steam (CWE) injection rate, (m^3/sec)

ρ_w = the density of water, (kg/m^3)

C_w = the specific heat capacity of water, (kJ/kg K)

M_s = the heat capacity of the formation, (kJ/kg K)

$= (1-\phi)\rho_{matrix}C_{matrix} + \phi\rho_w S_{wi} C_w + \phi\rho_o S_{oi} C_o$

t = injection time, sec

Equation A5 was used to calculate the theoretical steam zone volumes for the consecutive times of Run 115; these volumes were calculated at time interval of 420 seconds, as has been done with the volumes calculated using the Marx-Langenheim model. Table A1 shows the steam zone volumes calculated using Neuman's model.

Because the pressure inside the model was not known with a high degree of certainty, thus there was a necessity to compare the theoretical volumes calculated us-

ing Marx-Langenheim model and Neuman's model with the experimental volumes enclosed by the isotherms. These isotherms were the 75°C isotherm, the 70°C isotherm, and the 65°C isotherm. The experimental volumes were calculated using the volume menu in the SURFER™, these volumes are listed in Table A1. Figure A1 shows a comparison between the theoretical volumes calculated using Max-Langenheim model and Neuman's model with the experimental volumes of the three above mentioned isotherms. It can be seen that there is a discrepancy between the volumes calculated using Marx-Langenheim's model and the experimental model, this is probably because Marx-Langenheim's model assumes that the steam zone covers the whole thickness of the reservoir and does not consider the effect of the steam override. On the other hand, the steam zone volumes calculated using Neuman's model are comparable with the experimental volumes; this is because Neuman's model takes in consideration the steam override effect. The volumes enclosed by the isotherm 70°C gave the best match to the steam zone volumes calculated using Neuman's model. Therefore the contour of the 70°C isotherm was considered the boundary of the steam chamber.

Table A1: The Steam Zone Volumes Calculated from Marx-Langenheim Model, Neuman's Model, and Experimental Data.

Time Sec.	PV Injected	Vs (m3) Neuman's Model	Vs (m3) Volume enclosed by 75 °C Contour	Vs (m3) Volume enclosed by 70 °C Contour	Vs Volume enclosed by 65°C Contour	Vs (m3) Marx-Langenheim Model
0	0	0	0	0	0	0
420	0.076923	0.000223	0	0.000007	0.000022	0.003972
840	0.153846	0.000446	0	0.000016	0.000065	0.006793
1260	0.230769	0.000669	0	0.000017	0.000094	0.009169
1680	0.307692	0.000892	0	0.000016	0.000098	0.011274
2100	0.384615	0.001115	0	0.000047	0.000182	0.013189
2520	0.461538	0.001338	0.000009	0.000225	0.000568	0.014959
2940	0.538462	0.001561	0.001178	0.001905	0.002291	0.016615
3360	0.615385	0.001784	0.001464	0.002126	0.002471	0.018177
3780	0.692308	0.002007	0.001449	0.002132	0.002511	0.019659
4200	0.769232	0.002229	0.001374	0.002191	0.002651	0.021074
4620	0.846154	0.002453	0.001221	0.002243	0.002842	0.022429
5040	0.923077	0.002676	0.001388	0.002424	0.003012	0.023734
5460	1	0.002899	0.001389	0.002546	0.003149	0.024991
5880	1.076923	0.003121	0.001577	0.002758	0.003405	0.026207
6300	1.153846	0.003344	0.002241	0.003555	0.004357	0.027386

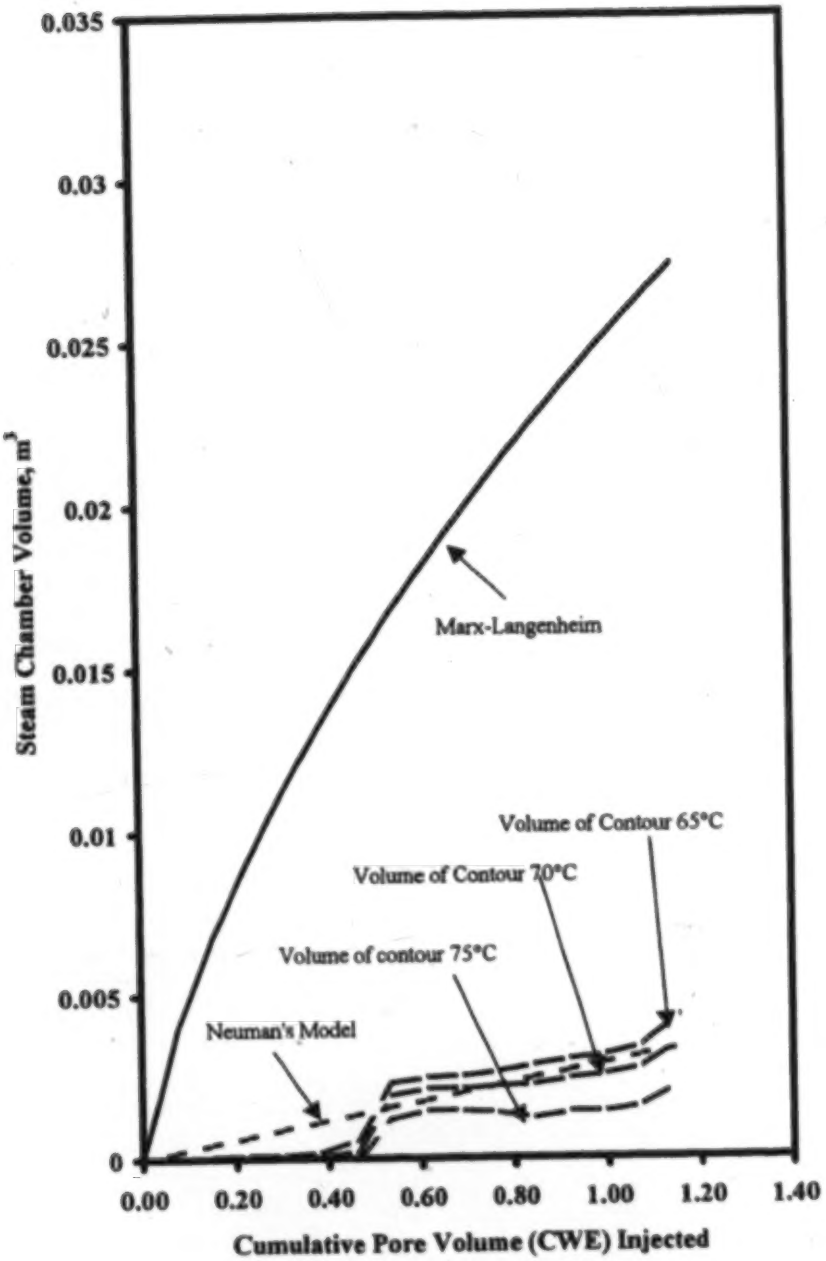

FigureA1-The Steam Zone Volume Obtained from Neuman's Override Model, Marx-Langenhiem Model, and the Experimental results.

Appendix B: Heat Balance

This appendix examines the distribution of the heat injected into the model. Assuming that there is no heat flows out of the model, thus part of the heat injected is produced with the fluids, flowing out of the model, part is lost to the overburden and the underburden, and part is accumulated in the model. Knowing the amount of each part to a high degree of certainty is a crucial factor in determining the economic viability of the thermal projects.

$$Q_{inj} = Q_{production} + Q_{loss} + Q_{formation} \quad \text{.....(B1)}$$

where:

Q_{inj} = energy injected int o the reservoir, kJ

$Q_{production}$ = energy carried out of the reservoir by produced fluids, kJ

Q_{loss} = energy lost to the overburden and the underburden, kJ

$Q_{formation}$ = energy accumulated in the reservoir fluids and reservoir matrix, kJ

A base case run was selected to apply the heat balance calculations on, and this was Run 115. The cumulative heat balance is determined at the time of 1.00 PV of steam (CWE) injected.

Cumulative Heat Injected, $Q_{inj.}$

The experiments performed in this study had a constant steam (CWE) injection rate. Assuming that the situation was ideal, i.e., the pump kept the same rate (180 cc/min) throughout the whole experiment and the steam quality (10%) was also constant from the beginning to the end of the run. As such the cumulative heat injected at any time is:

$$Q_{inj} = i_{st}\left(h_{inj} - h_{res} + f_{st}L_v\right) * t \quad \text{.....(B2)}$$

where:

Q_{inj} = energy injected int o the reservoir, kJ

i_{st} = massflow rate of the steam, (kg / sec)

h_{inj} = the enthalpy of saturated water, (kJ / kg)

h_{res} = the enthalpy of water at the reservoir temperature, (kJ / kg)

f_{st} = the quality of the steam, (ratio)

L_v = the latent heat of vaporization, (kJ / kg)

t = the cumulative injection time, (sec)

Therefore at 1.00 PV of steam (CWE) injected, the cumulative heat injected is:

$$Q_{inj} = 0.03[343.922 - 12.68 + 0.1 * 2646.988] * 5460 = 9,761.5\,kJ$$

Heat Lost to the Overburden and the Underburden, (Q_{loss})

Calculating the amount of the heat lost to the overburden and the underburden starts with the mapping of the temperature distribution in the neighbourhood of the cap and base rock at the time of 1.00 PV of steam (CWE) injected. For simplicity, it was assumed that the distribution of the temperature at 1.00 PV of steam (CWE) injected had prevailed since the beginning of the experiment. Once the contour maps of the temperature distributions were created, the area of each contour was determined using the volume menu in the contouring package (SURFER). Then the heat lost through each contour is calculated using the following equation:

$$Q = \frac{2k_h \Delta T \sqrt{t}}{\sqrt{\alpha \pi}} \qquad \text{(B3)}$$

where:

Q :Heat lost through the overburden or the underburden, kJ

k_h :Heat conductivity, kW/m.sec.K

ΔT :Temperature difference between the upper and the lower surfaces of the graniteblocks, K

t :Time elapsed, sec.

α :Thermal diffusivity, m^3/sec

Equation B3 is for an infinite cap rock that has its lower boundary temperature raised an amount, ΔT. Tables B1 and B2 present the heat lost through each isothermal area and the total heat lost through the overburden and the underburden.

Cumulative Heat Produced, $Q_{produced}$

The accuracy of the calculations of the cumulative heat produced is depending on the accuracy of the gathered data of the produced fluids volumes and their temperatures. It was fortunate that the temperature of the produced fluids prior to the steam breakthrough in the steam injection (SAGD process) experiments was constant except that of the fluids of the first two samples, which had fluctuated slightly during the collecting period of these samples. Thus the calculations of the produced heat were divided into four stages. The first three stages were chosen on the basis; that the temperature of the produced fluids do not vary that much during that period, thus an average temperature would be representative of the actual temperature. In the fourth stage the temperature was constant at 40°C. The following equation was used for the calculations of the heat produced.

Table B1: Heat Lost Through the Overburden After the Injection of 1.00 PV of Steam (CWE) , Run 115.

Contour Temp. (°C)	Contour Area (m2)	Heat Lost (kJ)
15	0.00089	2.262
20	0.0054	19.496
25	0.00588	27.468
30	0.00749	42.906
35	0.00758	51.474
40	0.01141	89.611
45	0.01211	107.923
50	0.01134	113.131
55	0.01122	123.795
60	0.01195	144.541
65	0.01409	185.432
70	0.01731	246.155
75	0.02293	350.367
80	0.00482	78.819

Total Heat Lost to the Overburden = 1583 kJ

Table B2: Heat Lost Through the Underburden After the Injection of 1.00 PV of Steam (CWE), Run 115.

Contour Temp. (°C)	Contour Area (m2)	Heat Lost (kJ)
5	0.01139	4.8337
10	0.04357	64.7426
15	0.02519	64.1706
20	0.01765	63.6826
25	0.01393	65.0573
30	0.01004	57.5183
35	0.01014	68.8627
40	0.00687	53.9246
45	0.00367	32.6831
50	0.00168	16.8004
55	0.00028	3.0906

Total Heat Lost to the Underburden = 495 kJ

$$Q_{prod} = \sum_{i=1}^{n} \left[\left(V_{w,i} \times C_{w,i} \times \rho_{w,i} + V_{o,i} \times C_{o,i} \times \rho_{o,i} \right) \times \Delta T \right] \quad \text{.....(B4)}$$

where:

i = any production sample
N = the total number of production samples
ΔT = the difference between the temperature of the production sample and the initial reservoir temperature
C_w = the specific heat capacity of water, (kJ/kg K)
= 4.3245-3.696 E-3 T+2.482 E-5 T^2
C_o = the specific heat capacity of oil, (kJ/kg K)
= 1.7915+0.00361T
ρ_w = the density of water, kg/m^3

$$= \frac{1}{\left[0.001 + 1.436E-6\left(-4.8872 + 0.134186T + 0.00212868T^2\right)\right]}$$

ρ_o = the density of oil, kg/m^3
= 879.9 kg/m^3

The specific heat and density relationships for the water were obtained from correlations introduced by Tortike and Farouq Ali (1989). The specific heat and density of oil (Faxam-100) were provided by Imperial Oil Resources Limited. Table B3 presents the heat produced during each stage and the total heat produced.

Cumulative Heat Accumulated in the Model, $Q_{formation}$

The accumulated heat in the model consisted of the heat contained in the reservoir fluids (aqueous phase, and oleic phase), and the heat contained in the matrix. The first step in determining the heat accumulated in the reservoir was to find the temperature distribution inside the model. This was done by mapping the isothermal areas at 1.00 PV of steam (CWE) injected. In order to calculate the heat in each phase, the fluid saturations in each contour had to be determined. The first step in determining the fluid saturations inside the model was to establish the boundaries of the steam chamber. Because there were no pressure measurements inside the model, the pressure distribution inside the model was not known with a high degree of certainty, as a consequence, the exact steam chamber boundaries were not known. The experimental steam zone volumes were calculated using the Volume menu in the SURFER™. Figure A1 shows a comparison between the experimental volumes and the volumes calculated using Marx-Langenhiem model and Neuman's model.

The residual oil saturation in the steam zone was taken as 6%, this was based on the results of the preliminary runs. Because the total volume of each phase inside the model was known, a spreadsheet was established taking into consideration the interdependence of the volumes of the different phases. The oil saturation and the water saturation in the other isothermal areas were assigned using the experience gained from the experiments and engineering judgment. Assuming that each volume was in thermal

Table B3: Heat Poduced after the Injection of 1.00 PV of Steam (CWE)

Production Stage	Temperature (°C)	Cw (kJ/kg K)	Co (kJ/kg K)	Heat Produced (kJ)
1	12.7	5.2956	2.823	15.257
2	22.4	5.3996	2.858	40.807
3	33.3	5.522	2.898	113.812
4	40	5.601	2.922	3323.714

Total Heat Produced = 3495 kJ

equilibrium, the following equation was used for the calculations of the heat accumulated in the model:

$$Q_{formation} = \sum_{k=1}^{m} V_{R,k} \times \{\phi S_{o,k}\rho_{o,k}C_{o,k} + \phi S_{w,k}\rho_{w,k}C_{w,k} + \phi S_{st,k}\rho_{st,k}C_{st,k} + (1-\phi)\rho_{M,k}C_{M,k}\} \quad \text{.....(B5)}$$

where

m =the number of the temperature contours.

K =the kth temperature contour

$V_{R,k}$ =the volume corresponding to the kth contour, (m^3)

ϕ =the porosity of the glass beads pack, (dimensionless)

$S_{o,w,s,k}$ =the saturation of oil, water, and steam for the kth contour,(dimensionless)

$\rho_{o,w,s,k}$ =the density of oil, water, and steam for the kth Contour, (kg/m^3)

$C_{o,w,s,k}$ =the heat capacity of oil, water, and steam of the kth contour, (kJ/kg.K)

$\rho_{M,k}$ =the density of the matrix, (kg/m^3)

$C_{M,k}$ =the heat capacity of the matrix, (kJ/kg.K)

Table B4 presents the calculated heat accumulated in each fluid phase, the calculated heat accumulated in the glass beads as well as the total heat accumulated in the model for Run 115.

Table B4: The Total Amount of Heat Accumulated in the Model after the Injection of 1.00 PV CWE of Steam, Run 115.

Contour Temp. (°C)	First Half Volume (m3)	Second Half Volume (m3)	Oil Sat.	Oil Volume (m3)	Water Sat.	Water Volume (m3)	Steam Sat.	Steam Volume (m3)	Heat in Oil (kJ)	Heat in Water (kJ)	Heat in Steam (kJ)
0	0.000111549	0	0.919	0.0000381	0.081	0.000003	0	0	.0	0	0
5	0.002749595	0.0001145	0.919	0.0009791	0.081	0.000086	0	0	4.8168	0.8994	0
10	0.002764842	0.0034729	0.5	0.0011602	0.5	0.0011602	0	0	20.1055	42.7363	0
15	0.001673596	0.0018066	0.5	0.0006473	0.5	0.0006473	0	0	19.3531	41.2813	0
20	0.001558817	0.0013837	0.5	0.0005473	0.5	0.0005473	0	0	23.3289	49.9455	0
25	0.001393878	0.0012799	0.9	0.0008951	0.1	0.000099	0	0	49.6921	11.8663	0
30	0.001109809	0.0013862	0.9	0.0008356	0.1	0.000092	0	0	57.2891	13.7355	0
35	0.000884108	0.0012789	0.8	0.0006437	0.2	0.0001609	0	0	52.6301	28.5102	0
40	0.000807158	0.0012746	0.7	0.0005421	0.3	0.0002323	0	0	51.5658	48.0938	0
45	0.000786353	0.0010853	0.6	0.0004177	0.4	0.0002785	0	0	45.3864	66.1425	0
50	0.00078831	0.0011501	0.5	0.0003605	0.5	0.0003605	0	0	44.1039	96.8563	0
55	0.000812668	0.0008913	0.4	0.0002535	0.6	0.0003803	0	0	34.5245	114.2701	0
60	0.000881182	0.0008247	0.3	0.0001903	0.7	0.0004442	0	0	28.5874	147.9066	0
65	0.001043917	0.0008519	0.2	0.0001411	0.8	0.0005642	0	0	23.1781	206.6095	0
70	0.001568393	0.0009849	0.1	0.0000949	0.9	0.0008548	0	0	16.9668	342.0483	0
75	0.001772225	0.0016888	0.06	0.0000773	0	0	0.94	0.001210263	14.9177	0	365.6175
80	0.00131461	0.0025466	0.06	0.0000862	0	0	0.94	0.001350177	17.9034	0	436.2107

Total heat in oil = 504 kJ
Total heat in water = 1211 kJ
Total heat in glass = 2101 kJ
Total Heat in steam = 802 kJ
Total heat accumulated in the model at 1.00 PV Inj.= 4618 kJ